藥學博士學位論文

Role of Ninjurin1 during Leukocyte Trafficking in the Inflamed Central Nervous System

중추신경계 염증반응 과정에서 Ninjurin1 단백질에 의한 면역세포이동 조절기전에 관한 연구

2013 年 **2** 月

서울大學校 大學院

藥學科 醫藥生命科學專攻

安 範 柱

Role of Ninjurin1 under Leukocyte Trafficking in the Inflamed Central Nervous System

중추신경계 염증반응 과정에서 Ninjurin1 단백질에 의한 면역세포이동 조절기전에 관한 연구

指導敎授 金 奎 源

이 論文을 藥學博士學位論文으로 提出함
2013年 **2**月

서울大學校 大學院
藥學科 醫藥生命科學 專攻
安 範 柱

安 範 柱의 藥學博士學位論文을 認准함
2013 年 **2** 月

委 員 長 _____ 印

副委員長 _____ 印

委 員 _____ 印

委 員 _____ 印

委 員 _____ 印

ABSTRACT

Role of Ninjurin1 under Leukocyte Trafficking in the Inflamed Central Nervous System (CNS)

Bum Ju Ahn

Division of Pharmaceutical Bioscience

College of Pharmacy

The Graduate School

Seoul National University

Ninjurin1 (nerve injury-induced protein) is an adhesion molecule that is essential for cell-to-cell interactions. However, the pathophysiological relevance of Ninjurin1 *in vivo* and its precise regulatory mechanisms in inflamed Central Nervous System (CNS) remain largely undefined. Here, it is demonstrated that Ninjurin1 is involved in leukocyte trafficking through promigratory activity and its posttranslational modifications by using *in vivo* animal model and *in vitro* cell culture system. Ninjurin1 was dominantly expressed in myeloid cells (macrophages/monocytes and neutrophils) and

endothelial cells (ECs) in the brain of experimental autoimmune encephalomyelitis (EAE), the animal model of Multiple sclerosis (MS). Both Ninjurin1 KO and neutralized mice alleviated the severity of EAE by reducing the recruitment of leukocyte into inflamed lesions, suggesting the contribution of Ninjurin1 in leukocyte trafficking *in vivo*. With *in vitro* experiments on gain or loss of Ninjurin1 activity, we proved the dual functions of Ninjurin1, adhesive and protrusive activity, depending on the steps of leukocyte trafficking. Ninjurin1 contributes to the later crawling and transmigration stages via formation of membrane protrusion as well as to the initial rolling and adhesion stages via homophilic binding.

Next, we investigated the contribution of posttranslational modifications of Ninjurin1, proteolytic cleavage and N-glycosylation, on the leukocyte trafficking. The fragmentations of Ninjurin1 are occurred not only in a vector system *in vitro* but also in mouse tissues *in vivo*. MMP9 is responsible for the cleavage of mouse Ninjurin1 between Leu^{56} and Leu^{57} in N-terminal ectodomain. Intriguingly, the liberated ectodomain of Ninjurin1 seems to have a chemotactic activity which is supported by its secondary structure similar to well-known chemokines. We also found that Ninjurin1 is glycosylated on Asn^{60} residue of N-terminal ectodomain. Mutagenesis of Asn^{60} to Ala^{60} (N60A) decreased the formation of membrane protrusions and showed impaired

localization to plasma membrane and loss of homophilic binding activity. Additionally, leukocyte-endothelial adhesion and transendothelial migration (TEM) activity were reduced in N60A mutant transfectants. Altogether, the *in vitro* and *in vivo* studies clearly demonstrated that Ninjurin1 enhances leukocyte trafficking through adhesive and protrusive activities that are regulated via its posttranslational modifications, proteolytic cleavage or N-glycosylation.

Therefore, we strongly suggest that Ninjurin1 is a beneficial therapeutic target for modulating pathogenesis of inflamed CNS including MS.

Keywords : **Experimental autoimmune encephalomyelitis (EAE) / Leukocyte trafficking / Ninjurin1 / Membrane protrusion formation / Posttranslational modifications**

Student Number : **2007-30469**

TABLE OF CONTENTS

LIST OF FIGURES

LIST OF TABLES

LIST OF ABBREVIATIONS

Ninjurin1	;	Nerve injury induced protein 1
BMDMs	;	Bone marrow-derived macrophages
ECs	;	Endothelial cells
WT	;	Wild-type
TNFα	;	Tumor necrosis factor α
INFγ	;	Interferon γ
TEM	;	Transendothelial migration
KO	;	Knock-out
EAE	;	Experimental autoimmune encephalomyelitis
MS	;	Multiple sclerosis
CNS	;	Central nervous system
BBB	;	Blood-brain barrier
EIU	;	Endotoxin-induced uveitis
CSFE	;	Carboxyfluorescein succinimidyl ester
MMP	;	Matrix metallopeptidase
MOG	;	Myelin oligodendrocyte glycoprotein
MBP	;	Myelin basic protein
M-CSF	;	Macrophage-colony stimulating factor

PI3K	;	Phosphatidylinositol 3-kinase
CM	;	Conditioned media
GFAP	;	Glial fibrillary acidic protein

INTRODUCTION

I. Leukocyte trafficking

Leukocyte recruitment from blood to the lesion site is a leading contributor to regulate the inflammatory response (Luster et al, 2005). To reach their destination, leukocyte should confront and overcome multiple barriers, including the vascular endothelium, pericyte sheath, and the basement membrane and consequent interstitial space (Ley et al, 2007). These processes begin with interactions between circulating leukocyte and the activated vascular endothelium, which are widely considered to be a crucial step in leukocyte emigration and an important stage in the development of drugs against inflammatory diseases. Over several decades, much scientific progress on leukocyte-endothelium interactions has been made, allowing us to understand well how leukocyte can transmigrate across an inflamed endothelium (Figure 1).

The process of leukocyte diapedesis is explained as sequential adhesive events, including the tethering, rolling, arresting, firming, crawling and transmigration of leukocyte against the endothelium (Ley et al, 2007) (Figure 2). The activity of numerous effectors in each step such as adhesion molecules, chemokines and cognate receptors should be well orchestrated for the

completion of TEM. The diverse homotypic or heterotypic bindings of adhesion molecules on leukocyte and endothelial cells are responsible for the leukocyte adhesion cascade in a stage-restrictive or non-restrictive manner ; for example, Selectin/PSGL-1 (Finger et al, 1996) while rolling; LFA-1/ICAM-1 (Smith et al, 1989) and VLA4/VACM1 (Barreiro et al, 2002; Weber & Springer, 1998) while arrest and crawling; and PECAM-1/PECAM-1 (O'Brien et al, 2003), CD99/CD99 (Schenkel et al, 2002), LFA-1/ICAM-2 (Constantin et al, 2000) and LFA-1/JAM-1 (Ostermann et al, 2002) during transmigration (Figure 2).

Their binding affinity is modulated by chemokines locally presented at the inflamed endothelium, triggering leukocyte arrest and increasing the adhesion strength (Imhof & Aurrand-Lions, 2004). After firmly attached to the endothelium, leukocyte experience a morphological change from a spherical to a flattened cell body and in turn, crawl laterally on the luminal surface of the endothelium (Nourshargh et al, 2010). Simultaneously, actin-based protrusive structures known as podosomes on the ventral side of the leukocyte are formed for the probing and path-finding of permissive sites on the luminal surface of the endothelium (Carman, 2009; Carman et al, 2007). In the case of memory T cells, chemokine-induced invasive filopodia under a shear flow facilitate millipede-like crawling (Shulman et al, 2009) (Figure 2).

In the cytoplasm of moving cells, the Rho family of small GTPase,

such as RhoA, Rac1, Cdc42 meditate the signal from the plasma membrane to regulate actin reorganization during the process of leukocyte transmigration (Parsons et al, 2010; Ridley et al, 2003). Studies using a constitutive activator and dominant-negative inactivation as well as a gene-deficient model have elucidated the roles of these small GTPases in chemokine-triggered integrin-dependent adhesion, luminal crawling, invasive protrusion formation and subsequent TEM (Heasman & Ridley, 2008). In general, RhoA controls the assembly of actin stress fibers, the formation of focal adhesion sites, and myosin-based uropod contractions, whereas the Rac family promotes lamellipodium and membrane ruffle formation while Cdc42 influences the formation of finger-like filopodia (Cernuda-Morollon & Ridley, 2006).

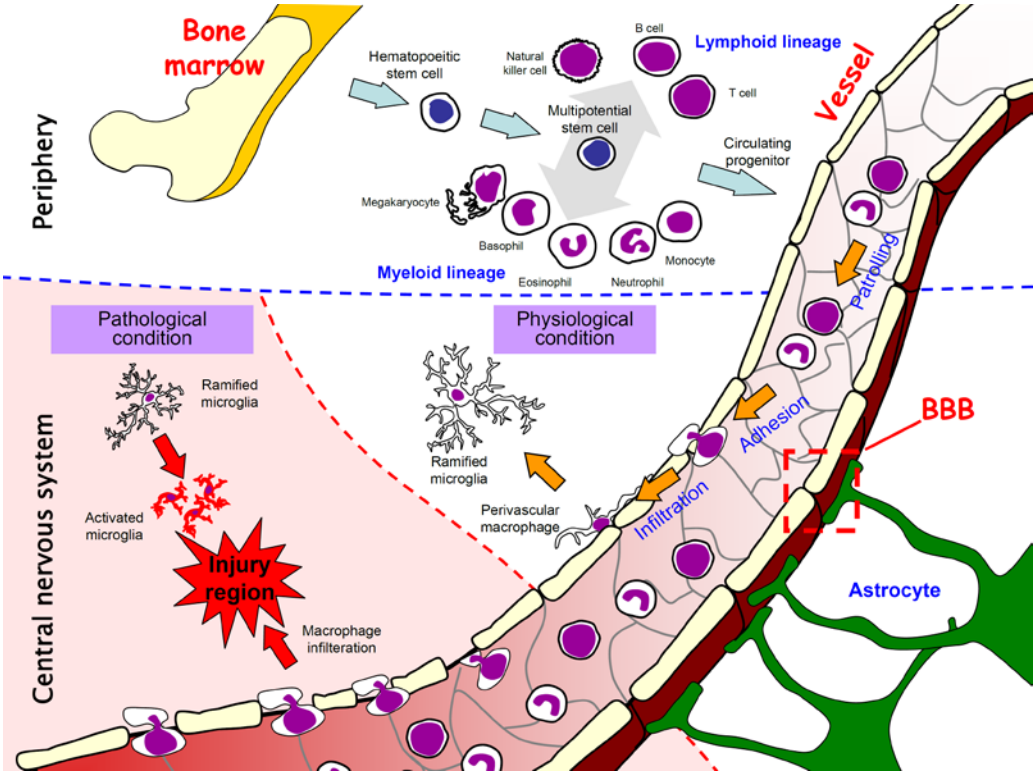

Figure 1. Leukocyte-mediated CNS inflammation. In normal physiological condition, leukocyte entry into the central nervous system (CNS) is highly restricted due to isolation by the blood-brain barrier (BBB), described as immune privilege. However, disruption of BBB by injury allows leukocyte to actively enter toward the lesion regions in the parenchymal CNS. The recruited leukocyte drive inflammatory processes to cause controversial results; protective tissue repair or harmful neurodegeneration that should be explored in the future.

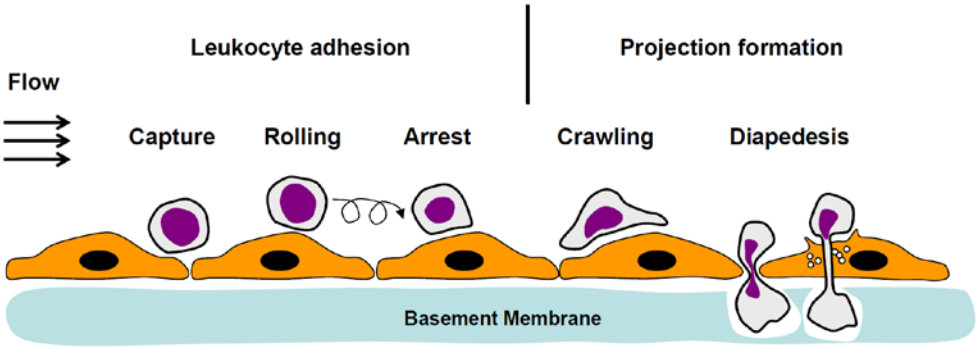

Figure 2. Five steps of leukocyte trafficking. For leukocyte trafficking, dynamic leukocyte-endothelium interactions are necessary that classified as major five stages; capture, rolling, arrest, crawling, and diapedesis. In earlier three stages, adhesive activity between leukocyte and endothelium is required and, in latter two stages, migratory and protrusive activity is necessary for leukocyte to probe the permeable sites or go directly through the monolayer of endothelial cells.

II. Multiple sclerosis

Immune responses mediated by leukocyte have a great influence on the pathogenesis of several the CNS inflammatory diseases including Multiple sclerosis (MS), stroke, Alzheimer's disease, Parkinson's disease, trauma, and epilepsy (Ousman & Kubes, 2012). The MS is caused by autoimmune T cells coordinating with monocytes, dendritic cells, and B cells recruited from the blood; it is one of the most common diseases with neuromyelitis and encephalomyelitis (Goverman, 2009). It begins with the disruption of the BBB. In particular, the remarkable accumulation of leukocyte in the plaque of the damaged region is a hallmark of MS (Figure 3) and its animal model, experimental autoimmune encephalomyelitis (EAE) which can be induced by immunization with the myelin antigen (Figure 4). Therefore, there have been active attempts to modulate leukocyte diapedesis in these CNS diseases (Lopez-Diego & Weiner, 2008).

Despite the intensive effort, clinical trials to target leukocyte diapedesis have been unsatisfactory for therapeutic applications due to several unexpected side effects. For example, Natalizumab is a monoclonal antibody approved by the Food and Drug Administration (FDA) which inhibits T lymphocyte trafficking by targeting the α4-integrin during inflammation (Kleinschmidt-DeMasters & Tyler, 2005). However, progressive multifocal

leukoencephalopathy (PML) which arises in MS patients has unfortunately led to this drug being used with much caution (Steinman, 2005). These problems are thought to have derived from the absence of the cell-type specificity of targeted molecules. Leukocyte is classified into two groups, lymphoid-lineage or myeloid-lineage cells, which play a distinct roles in the processes of adaptive immunity or innate immunity, respectively. Although these cells share the basal TEM steps, precise regulation can be spatiotemporally diverse according to the stages and types of diseases. Therefore, the most important strategy for minimizing side effects is to identify adhesion proteins contributing to cell-type-specific TEM.

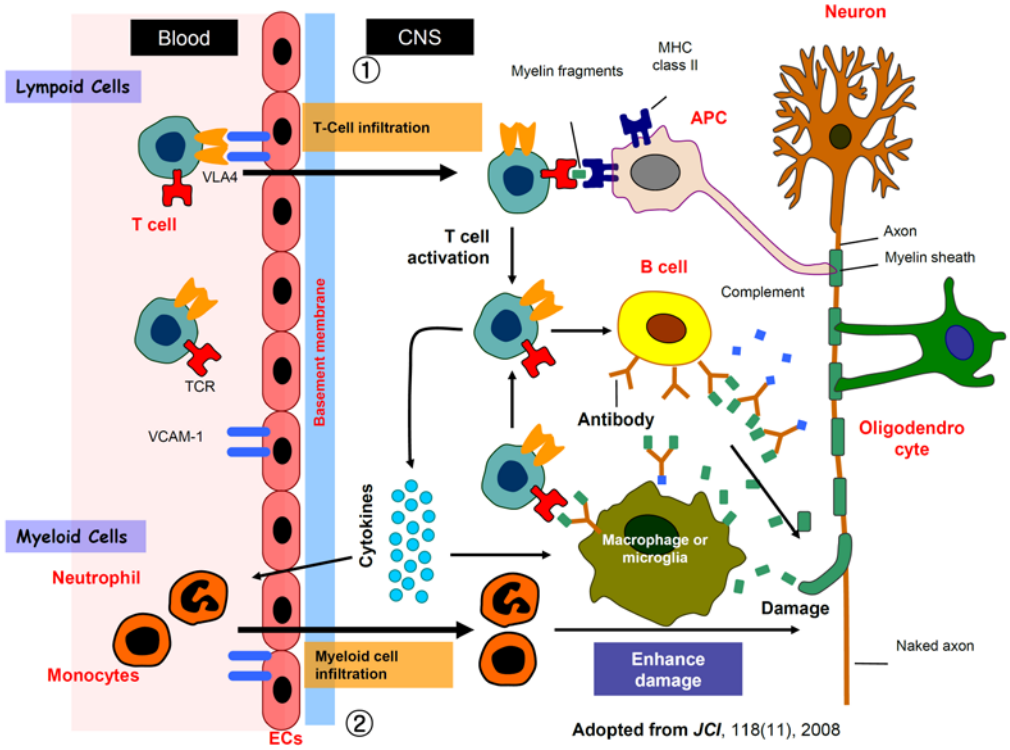

Figure 3. Molecular mechanism of MS. MS is characterized by extensive infiltration of the CNS by inflammatory cells. Initiation of MS involves the activation of myelin-specific T cells, which in turn trigger the expansion of resident macrophage/microglia, cytokine release, and the recruitment of myeloid cells like monocytes and neutrophils. These inflammatory processes facilitate demyelination and clinical symptoms of MS (Steinman, 2008).

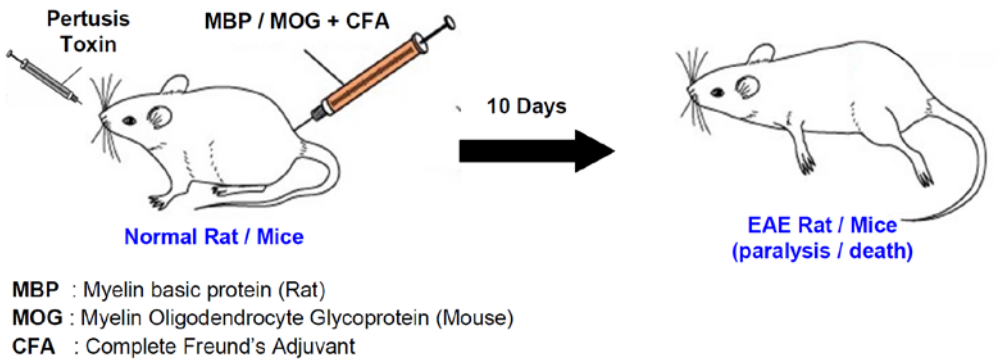

Figure 4. Experimental autoimmune encephalomyelitis (EAE). Demyelination is produced by injection of CNS proteins such as myelin basic protein (MBP, rat) or myelin glycooligodendrocyte protein (MOG, mice) emulsified in an adjuvant such as complete Freund's adjuvant (CFA). The presence of the adjuvant allows the generation of inflammatory responses to the protein/peptides. Rat/Mice are coinjected with pertussis toxin to break down the BBB and allow immune cells access to the CNS tissue. This immunization leads to multiple small disseminated lesions of demyelination in the brain and spinal cord and the onset of clinical symptoms.

III. Ninjurin1

Ninjurin1 was originally identified by Araki *et al.* as a small-size adhesion molecule with 152 amino acids (aa, ~17 kDa) consisting of an N-terminal (1-71 aa) and C-terminal (139-152 aa) ectodomain, two transmembrane domains (72-100 aa and 111-138 aa), and an intercellular region (101-110 aa) (Araki & Milbrandt, 1996). In particular, the 12 residues on the N-terminal ectodomain of Ninjurin1, from Ala^{26} to Val^{37}, is crucial for its homophilic binding activity (Araki et al, 1997), promoting neurite extension and axonal regeneration after sciatic nerve injury following transection (Araki & Milbrandt, 1996) (Figure 5).

The expression of Ninjurin1 is variable in many tissues, including those of epithelial origin, peripheral neurons, and blood cells (Araki & Milbrandt, 1996). Recently, we demonstrated that Ninjurin1 is expressed in macrophages and mediates the regression of hyaloid vessels via a close interaction between macrophages and vascular ECs during early ocular development (Lee et al, 2009b). This finding suggests that Ninjurin1 could similarly play a role in inflammatory diseases mediated by macrophages, glial cells, blood cells, and other cells. In addition, there are some reports that Ninjurin1 is involved in the adhesion and migration of several types of cells in diverse pathological conditions. For example, Ninjurin1 is upregulated in Schwann cells and dorsal

root ganglion neurons after spinal cord injury (Araki & Milbrandt, 1996), in infiltrated blood cells of leprosy patients (Cardoso et al, 2007), in $CD10^{+}/CD19^{+}$ B cells in acute lymphoblastic leukemia (Chen et al, 2001), and in all specimens from hepatocellular carcinoma patients (Kim et al, 2001a).

Furthermore, microarray studies of MS revealed that Ninjurin1 was detected in MS brain tissue, suggesting that Ninjurin1 is involved in the initiation or progression of MS (Tajouri et al, 2007). However, the biological relevance of Ninjurin1 in MS remains largely unknown.

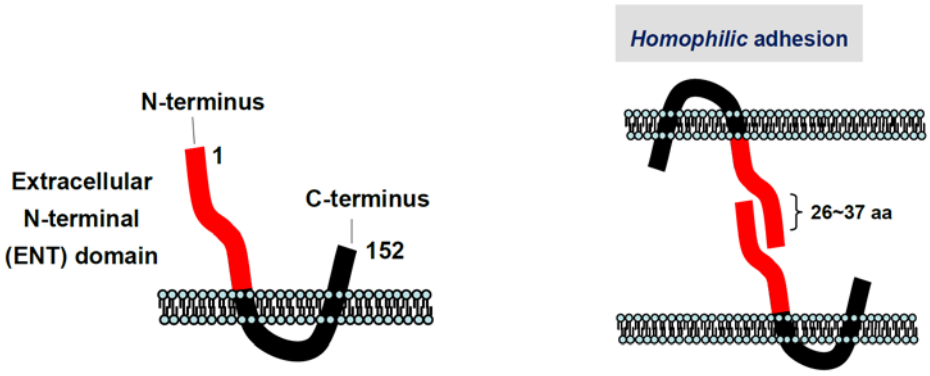

Figure 5. The structure of Ninjurin1. Ninjurin1 is an adhesion molecule with 152 amino acids (aa, 17 kDa); N-terminal (1-71 aa) and C-terminal (139-152 aa) ectodomain, two transmembrane domains (72-100 aa and 111-138 aa), and an intercellular region (101-110 aa). The 12 residues, from Pro^{26} to Asn^{37}, on the N-terminal ectodomain of Ninjurin1 are critical for homophilic binding.

PURPOSE OF THIS STUDY

Leukocyte-mediated immune responses have been considered as major regulator in the pathogenesis of inflamed CNS diseases. Several adhesion molecules on both leukocyte and endothelial cells are involved in leukocyte trafficking by enhancing leukocyte-endothelium interaction. Ninjurin1 was previously identified as an adhesion molecule to promote neuroregeneration via homotypic adhesion in trajectory peripheral nervous system (PNS) injury (Araki & Milbrandt, 1996). Recently, our group demonstrated the expression of Ninjurin1 in the macrophage of the developmetal mice retina (Lee et al, 2009a).

Based on the adhesive property and expression in macrophage as well as the lack of studies in inflamed CNS, we hypothesized that Ninjurin1 might be able to involve the inflammatory pathogenesis by regulating leukocyte trafficking in CNS diseases. In this present study, therefore, we tried to discover *in vivo* relevance of Ninjurin1 on leukocyte trafficking and to define its regulatory mechanism and the effects of posttranslational modifications, proteolytic cleavage and N-glycosylation. Ultimately, the main purpose of this study is to estimate the potential of Ninjurin1 as target molecule for modulating inflammatory responses of CNS diseases, in particular MS.

MATERIALS AND METHODS

1. Animals

Lewis rats or C57BL/6 mice were purchased from Orient Bio. Inc., Korea. Ninjurin1 KO mice (C57BL/6J background) were generated by Dr. Goo Taeg Oh at Ewha Womans University, Korea, and backcrossed with C57BL/6 for at least seven generations. The breeding colony was established and maintained under pathogen-free conditions in the animal housing facility of the College of Pharmacy, Seoul National University, for the duration of the experiments under the rule of the Committee for Care and Use of Laboratory Animals at Seoul National University (SNU-090316-9, SNU-101011-1). The primer sequences for genotyping are as follows: wild-type (Forward): 5'-GAG ATA GAG GGA GCA CGA CG-3', Neo (Forward): 5'-ACG CGT CAC CTT AAT ATG CG-3', Reverse primer: 5'-CGG GTT GTT GAG GTC ATA CTT G-3'.

2. EAE induction and clinical scoring

For rat EAE model, female Lewis rats weighing 160-200 g and aged 6-10 weeks were immunized subcutaneously with an emulsion containing 25 μg of guinea pig myelin basic protein $(MBP)_{68-86}$ in complete Freund's adjuvant

(CFA; *Mycobacterium tuberculosis* H37Ra, 4 mg/mL). Each animal was injected with 2 μg of pertussis toxin intraperitoneally at the time of immunization. For mice EAE model, sex and age (6–10 weeks) matched C57BL/6 mice were immunized subcutaneously with an emulsion containing 100 μg of MOG_{35-55} (Peptron Inc., Korea) in CFA. Each mouse was injected with 300 ng of pertussis toxin intraperitoneally at 0 and 2 day after immunization. The rats and mice were weighed and observed daily for clinical signs of EAE. The progression of EAE was graded according to the following scale: 0, no symptoms; 1, floppy tail; 2, mild paralysis of the hind limbs; 3, complete paralysis of one hind limb and partial paralysis of another one; 4, complete paralysis of both hind limbs; 5, a moribund state or death.

3. Endotoxin-induced uveitis (EIU) and quantification of retinal adherent leukocyte

Each mouse (male, 6-10 weeks) received a single intraperitoneal injection of lipopolysaccharide (LPS, Sigma-Aldrich) in PBS at the dose of 9 mg/kg body weight. 24 hr after the LPS injection, the chest cavity was opened and a 24-gauge syringe was introduced into the left ventricle under deep anesthesia. After injection of 5 mL PBS to remove erythrocytes and non-adherent leukocyte, 5 mL Rhodamine-conjugated Concanavalin A (ConA, 5

mg/kg) (Vector Lab) was perfused. After the eyes were enucleated, the retinas were flatmounted. The flatmounts were imaged with a fluorescence microscope, and the total number of ConA-positive adherent leukocyte per retina was counted.

4. Cell culture

BV2, Raw264.7, MBEC4, COS7 and HeLa cells were cultured in Dulbecco's modified Eagle's medium (DMEM, Gibco) supplemented with 10% fetal bovine serum (FBS, Invitrogen). HBMECs were grown in M199 medium with 20% FBS and maintained in an incubator with a humidified atmosphere of 95% O_2 and 5% CO_2 at 37 °C. For the bone-marrow-derived macrophage (BMDM) culture, bone marrow cells were isolated from femurs and tibias and cultured in RPMI 1640 medium supplemented with 10% FBS, 1% penicillin and streptomycin for 3 days and differentiated in RPMI 1640 containing 20 ng/ml macrophage-colony stimulating factor (M-CSF, Peprotech) for 3 days. The protrusion index of the BMDMs and the Raw264.7 cells was calculated as the ratio of x to y, where x is the longest distance across the cells (from head to tail) and y is the widest perpendicular to x. The properties (percentage, number and length) of each protrusion were quantified by Image J software (NIH Image).

5. Antibodies

For a custom-made anti-moue Ninjurin1 antibody, keyhole limpet hemocyanin (KLH)-conjugated synthetic peptide-bearing mouse Ninjurin1 residues 26-37 (Ab_{26-37}), 1-15 (Ab_{1-15}), or 139-152 (Ab_{1-139}) were immunized to rabbits following standard procedures (Peptron Inc. and Abfrontier Inc., Korea); these anti-Ninjurin1 antibodies were purified in each case with antigen-specific affinity chromatography. The isotype rabbit IgG purified using a Protein A column (Upstate) from the serum of normal rabbits were used for the *in vivo* blocking experiment in the EAE model. Each antibodies was used for immunostaining (Ab_{1-15}) and Western blotting (Ab_{1-15} and $Ab_{139-152}$). The Ab_{26-37} was used for *in vivo* blocking experiment in EAE.

6. Expression vectors

Several mouse Ninjurin1 (NM_013610) expression vectors were constructed as described previously (Lee et al, 2009b). The pCMV-Tag2B or $pCS2^{+}$-GFP was used as a backbone for the construction of N-terminus tagging vectors, Flag-mNinj1 or GFP-mNinj1, respectively. The 3xFlag tagging mouse Ninjurin1 (3xFlag-mNinj1) vector was made with the pCMV14 backbone for the C-terminus tagging system. Using the $pCS2^{+}$ GFP backbone, some

truncated vectors including GFP-mNinj1$_{1\text{-}71}$ (C-terminal region deletion) or GFP-mNinj1$_{72\text{-}152}$ (N-terminal region deletion) were constructed. The non-tagging mouse Ninjurin1 vector (pcDNA3.1^{+} myc/his) was designed by adding a stop codon at the end of the Ninjurin1 sequence.

7. Construction of stable Raw264.7 cells

For the construction of stable Ninjurin1-overexpressed Raw264.7 cells, full-length cDNA corresponding to mouse Ninjurin1 (NM_013610) was inserted into the pEGFP vector (GFP-mNinj1). The constructed GFP-mNinj1 plasmid was transfected in Raw264.7 cells and maintained in complete DMEM with G418 (500 μg/ml). After several days, the surviving colonies were selected. Purity and homogeneity (> 90%) were determined by means of fluorescence microscope observations and Western blotting.

8. Peptides

For *in vivo* neuratlization, peptides were chemically synthesized using solid phase Fmoc chemistry on PeptrEX synthesizer (Peptron Inc., Korea) and purified by high pressure liquid chromatography (> 90% purity). Cyclization was generated by cysteine covalently linked to the N-/C-terminus of the peptide. All peptides were verified by mass spectroscopy analysis. Each peptide is based

on mouse Ninjurin1 and each sequence is following. Scramble cyclic peptide$_{26-37}$ (scPEP$_{26-37}$) : CWPPNPLRRGINRC, cyclic peptide (cPEP$_{26-37}$): CPPRWGLRNRPINC, linear peptide$_{26-65}$ (lPEP$_{26-65}$) : PPRWGLRNRPINVNHYANKKSAAESMLDIALLMANASQLK,

9. Time-lapse imaging

Time-lapse series of BMDMs and Raw264.7 cells were taken at 37°C using microscopes (Carl Zeiss, Axiovert M200 and LSM 700) equipped with a computer-driven cooled CCD camera, a humidified CO_2 chamber, and an autofocus system. We used the Axiovert M200 to image cell motility and the LSM700 for the membrane dynamics.

10. Cell adhesion assay

BV2 cells and HBMECs transfected with pCS2$^+$-Ninj1 or pCS2$^+$-Mock (control) DNA were used for adhesion assays. For immunocytochemical staining, BV2 cells were incubated with Hoechst (H33342) for 5 min and washed with DMEM. Then, BV2 cells were separated with trypsin/EDTA and detached cells were added to a black flat-bottomed 96 well microtiter plate coated with a monolayer of HBMECs. The plate was incubated for 30 min, washed with PBS and the fluorescent signal was detected. For quantification, a

similar method was used, except that in the quantification experiment, a much smaller coat of HBMECs was used. Finally, the aggregation of BV2 cells and HBMECs was counted using a mixture of Ninjurin1 transfectants and non-transfected cells.

For the measurement of adhesion activity by Ab_{26-37} treatment, Raw264.7 cells activated by TNFα and IFNγ (10 ng/ml, 12 hr, Peprotech) were labeled with Carboxyfluorescein succinimidyl ester (CSFE, 5 μM, 5 min) and were pre-incubated with Ab_{26-37} for 1 hr corresponding to each concentration. CSFE-labeled Raw264.7 cells were added to a MBEC4 monolayer activated with TNFα and IFNγ (10 ng/ml, 12 hr) and were incubated for 20 min. After washing three times with PBS, the adherent cells were imaged in at least six positions by microscopy and the percentages of CSFE-labeled cells were quantified in each picture. In the case of myc-mNinjurin1-overexpressed Raw264.7 cells, the cells were added to CSFE-labeled MBEC4 monolayer which was activated with TNFα and IFNγ (10 ng/ml, 12 hr) and were incubated for 20 min. After 4% PFA fixation, samples were stained with anti-myc antbody (Santa Cruz) and visualized using the microscopy.

11. Transmigration assay

For the measurement of TEM activity by Ab_{26-37} treatment, MBEC4

was seeded in the upper chamber of each trans-well (6.5 mm diameter, 5 μm pore size; Costar) and the cells were grown to form a confluent monolayer. CSFE-labeled Raw264.7 cells pre-incubated with Ab_{26-37} for 1 hr corresponding to each concentration were added to the upper chamber and 10 ng/ml TNFα and IFNγ were used as a chemoattractant in the lower chamber. After incubation for 12 hr, the trans-well was fixed with 4% PFA and its upper side was cleaned with cotton and then mounted. The migrated cells were imaged at six positions by means of microscopy and analyzed by counting the percentages of CSFE-labeled cells which had transmigrated. For TEM activity of BMDMs, siNinjurin1 or stable Raw264.7 cells, each cell was labeled with CSFE and added to MBEC4 monolayer containing with TNFα and IFNγ (10 ng/ml, 12 hr) in lower chamber as chemoattractants and were incubated for 12 hr. The migrated cells were quantified using microscopy.

For the migration assay of Raw264.7 cells toward GFP-mNinj1 CM, Raw264.7 cells labeled with 5 μM CSFE for 5 min were added to the upper chamber of the trans-well (6.5 mm diameter, 8 μm pore size, Costar). The GFP or GFP-mNinj1 overexpressed CM was applied into the lower chamber to examine the chemotactic activity. After incubation for 8 hr, the trans-well was fixed with 4% PFA and its upper side was cleaned with cotton and mounted. Pictures were taken at 6 positions using microscopy (Axiovert M200, Carl

Zeiss) and the migrated cells were analyzed by determining the percentage of CSFE-labeled cells.

12. RNAi interference

For Ninjurin1 knock-down by RNAi interference, siRNAs (siNinjurin1) against mouse Ninjurin1 (NM_013610) were designed using design software and were purchased from Invitrogen. Negative control siRNAs (siCont) were predesigned from Bioneer Inc. (Korea). Each sequence of siRNA is as follows: siCont: 5'-CCT ACG CCA CCA AUU UCG U dTdT-3', siNinjurin1: 5'-ACC GGC CCA UCA AUG UAA ACC AUU A-3'. Each siRNA was transfected in Raw264.7 cells by Nucleofector (Amaxa) at a concentration of < 200 mol per sample. After 24 hr, the Ninjurin1 knock-down efficiency was determined by the Western blotting of anti-GFP and the custom-made anti-Ninjurin1 antibody ($Ab_{1\text{-}15}$).

13. Immunoblotting and immunoprecipitation

Tissues and cells were extracted in a cell lysis buffer containing 20 mM Tris-HCl (pH 7.5), 150 mM NaCl, 1 mM Na_2EDTA, 1 mM EGTA, 1% Triton, 2.5 mM sodium pyrophosphate, 1mM β-glycerophosphate, 1 mM Na_3VO_4, 1 μg/ml leupeptin and a protease inhibitor cocktail. Lysates were

immunoprecipitated or immunoblotted with antibodies of Ninjurin1 (Ab_{1-15}), tubulin (Biogenex), actin (Sigma), green fluorescent protein (GFP) (Abcam), and myc antibody (Santa Cruz).

14. Immunofluorescence staining and microscopy

For the study of rat, tissues were incubated with the following antibodies against Ninjurin1 (a kind gift from Dr. J. Milbrandt), GS-lectin (Molecular Probes), CD11b (Abcam), CD45 (Abcam), Iba-1 (Wako), MPO-1 (Dako), CD4 (AbD Serotec), and CD20 (Santa Cruz). For the study of mice, tissues or cells were incubated with the following antibodies against F4/80 (Serotec), CD45 (BD), CD3 (R&D), MOG (R&D), myc (Santa Cruz), and FITC- or Alexa546-phalloidin (Molecular Probes). After incubation with primary antibodies overnight at 4℃, tissues or cells were visualized with Alexa 488-conjugated IgG or Alexa 546-conjugated IgG (Molecular Probes) as secondary antibodies. Nucleus-staining was performed with Hoechst 33342 (Molecular probes). Both Axiovert M200 and LSM 700 microscope (Carl Zeiss) were used for immunofluorescence imaging.

15. Small GTPase activity and inhibitors

We analyzed the small GTPase activity of BMDMs or Raw264.7 cells

via the recommended procedure using a G-LISA Assay Biochem Kit (Cytoskeleton Inc.), the RhoA activity (BK124), the Rac activity (BK125), and the Cdc42 activity (BK127). For pharmacological inhibitory study, GFP-mNinj1 Raw264.7 cells were treated with either NSC23766 (Rac1 inhibitor, Tocris), PP2 (Src inhibitor, Tocris), LY29004 (PI3K inhibitor, Cell signaling) or their DMSO carrier for 3 hr as the indicated concentrations.

16. Measurement of cell surface GFP-mNinj1 trafficking by Flow cytometry.

HEK293T cells were cultured in 100mm dishes and transfected GFP-mNinj1(WT or N60A mutant). Myc-mNinj1 WT or N60A mutant transfected HEK293T cells were used as a GFP intensity negative control. The cells were detached from dishes by 0.25% Tripsin-EDTA and washed 3 times with ice-cold PBS and were incubated in 1% NaN_3/PBS for 10 min at 4°C. After washing with ice-cold PBS, the cells were incubated with 1:200 diluted anti-GFP or control IgG in 3% BSA/PBS for 1 h at 4°C. After 3 times washing with ice-cold PBS, the cells were incubated with 1:500 diluted APC-conjugated anti-mouse IgG in 3% BSA/PBS for 30 min at 4°C. After 3 times washing, the cells were resuspended in 10% FBS/PBS. The fluorescence of stained cells was measured using a BD FACS Calibur flow cytometer and analysed using

CellQuest Pro software. 5000 GFP-positive cells and 20000 myc-mNinj1 transfected cells gated by FSC and SSC were counted.

17. Deglycosylation assay

Deglycosylation assay by PNGase F was performed as protocols supported from the company (New England BioLabs Inc.). Briefly, 293T HEK cells lysate overexpressed with GFP-mNinj1 WT were denatured by boiling during 10 min at 100℃ and incubated with 2 units PNGase F during 1 h at 37℃, and then, were investigated by western blotting.

18. *In vitro* MMPs cleavage assay

Recombinant MMP2 (R&D), MMP9 (R&D), and the catalytic domain of MMP9 (Cat-MMP9, Peprotech) were commercially purchased. Non-tagging mouse Ninjurin1 protein was immunoprecipitated with the $Ab_{1\text{-}15}$ antibody. After 1 mM p-aminophenylmercuric acetate (APMA) activation, the concentration of MMP2 or MMP9 was determined. The APMA-activated MMPs were incubated with the immunoprecipitated mouse Ninjurin1 protein with or without GM6001 (10 μM), a pan-MMP inhibitor in a buffer solution containing 0.2 M NaCl, 5 mM $CaCl_2$, 50 mM Tris-HCl (pH 7.5), 0.005% Brij, and 0.0025% NaN_3 for 16 hr at 37 °C. Reaction products were analyzed by

Tris-glycine SDS-PAGE and western blot with the $Ab_{139-152}$ antibody.

To determine the cleavage sites of Ninjurin1, three kinds of peptides, PEP_{1-30}, PEP_{21-50}, and PEP_{41-70}, were chemically synthesized using solid phase Fmoc chemistry on a PeptrEx synthesizer (Peptron Inc.) and purified by liquid chromatography (LC) (> 90% purity). All peptides were verified by mass spectrometry (MS) analysis. Each peptide was incubated with recombinant MMP9 at an enzyme : peptide ratio of 1:10 (w/w) for 16 hr at 37 °C in a buffer solution containing 0.2 M NaCl, 5 mM $CaCl_2$, 50 mM Tris-HCl (pH 7.5), 0.005% Brij, and 0.0025% NaN_3. Reaction products were analyzed by LC-MS.

19. Photothrombosis

Female F344 rats (6weeks, 200g) were subjected to photothrombosis. Under general anesthesia, Rose Bengal (Sigma, 0.1ml/ 25g body weight of 10% solution) was injected via the tail vein, which was allowed to circulate for 5 min. After the incision of scalp, the skull was exposed to cold light source (Zeiss FL1500 LCD, 150W, 1mm diameter) for 20min. The position of optic center was 4 mm to the left and 4 mm to the back of the bregma. The scalp was sutured and rats were allowed to awake.

20. Data analysis and statistics

All data are presented as means ± s.e.m and are expressed as relative percentages and fundamental units. Statistical significance was calculated using an unpaired two-tailed Student T-test for single comparisons and an ANOVA test for multiple comparisons. * $P < 0.05$ was considered statistically significant.

RESULTS

I. Role of Ninjurin1 on leukocyte trafficking

Our group previously demonstrated that Ninjurin1 is expressed in macrophages and mediates the regression of hyaloid vessels via a close interaction between macrophages and vascular ECs during early ocular development (Lee et al, 2009a). In paticular, LPS administration in the adult rat provoked a remarkable increase in the number of Ninjurin1-expressing round-shaped macrophages in the flat mounted eye, but not in ramified resident macrophages (Lee et al, 2009a). This finding highly suggests that Ninjurin1 could similarly play a role in leukocyte-mediated inflammation in CNS diseases, particularly MS. Therefore, we investigated the contribution of Ninjurin1 in the brain and on its pathogenesis.

1. Ninjurin1 is mainly expressed in meninges, the choroid plexus, and parenchymal perivascular region of normal rat brain.

Expression of Ninjurin1 in the normal brain was examined by immunostaining of adult rat brain sections. Ninjurin1 was specifically expressed in round-shaped cells, and Ninjurin1^{+} cells were located in three

distinct regions of brain, including meninges, the choroid plexus, and the parenchymal perivascular region (Figure 6A). These regions are primary routes by which leukocyte cross the BBB and enter the CNS (Ransohoff et al, 2003), suggesting that Ninjurin1^{+} cells might be leukocyte circulating in the cerebrospinal fluid. We also observed that Ninjurin1 was weakly expressed in the cerebral cortex (Figure 6B) and in hippocampal regions (Figure 6C).

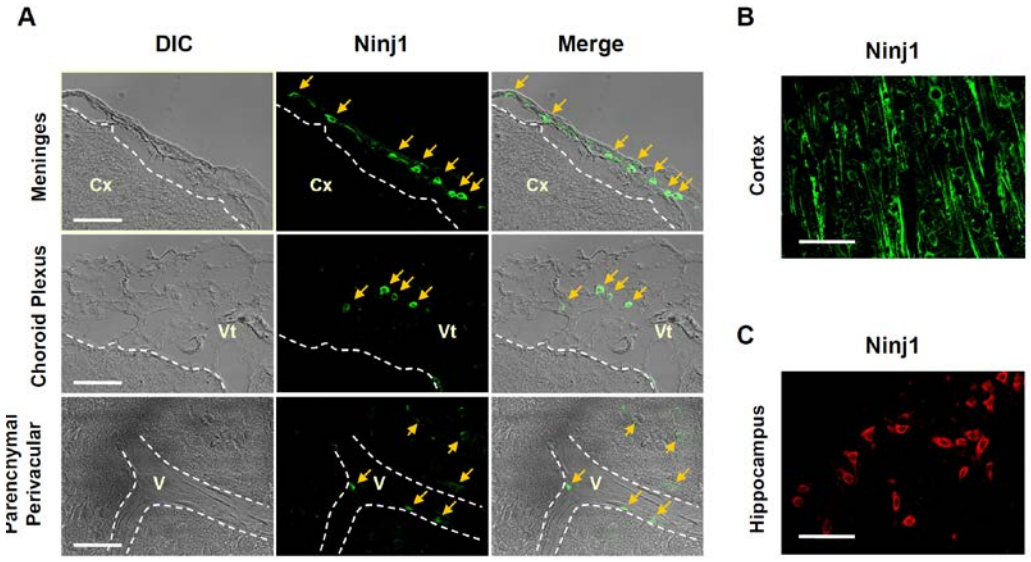

Figure 6. Expression of Ninjurin1 in the normal adult rat brain. (A) Ninjurin1^{+} cells (green) were located in three major compartments: meninges, the choroid plexus, and parenchymal perivascular space. Differential interference contrast (DIC) microscopy revealed the structure of the brain. White dotted lines indicate the boundary of the parenchymal tissue and yellow arrows denote Ninjurin1^{+} cells. Cx; cerebral cortex, Vt; ventricle, V; vessel. (B) Ninjurin1 (green) was weakly expressed in the cerebral cortex. (C) Ninjurin1 (red) expression was also detectable in the hippocampal region. Scale bar = 50 ㎛.

2. Ninjurin1 is upregulated in the brain of EAE rats.

To investigate the role of Ninjurin1 in pathological conditions, we generated EAE rats and determined the expression of Ninjurin1 in the CNS. As in normal brains, Ninjurin1^{+} round-shaped cells were detected in three compartments – meninges, the choroid plexus, and parenchymal perivascular region (Figure 7A). However, Ninjurin1^{+} cells were much more abundant than in control rat brains (Figure 7B). The Ninjurin1 mRNA level was also elevated in EAE blood, indicating that either Ninjurin1 expression or Ninjurin1^{+} cell number is upregulated in the EAE model (Figure 7C).

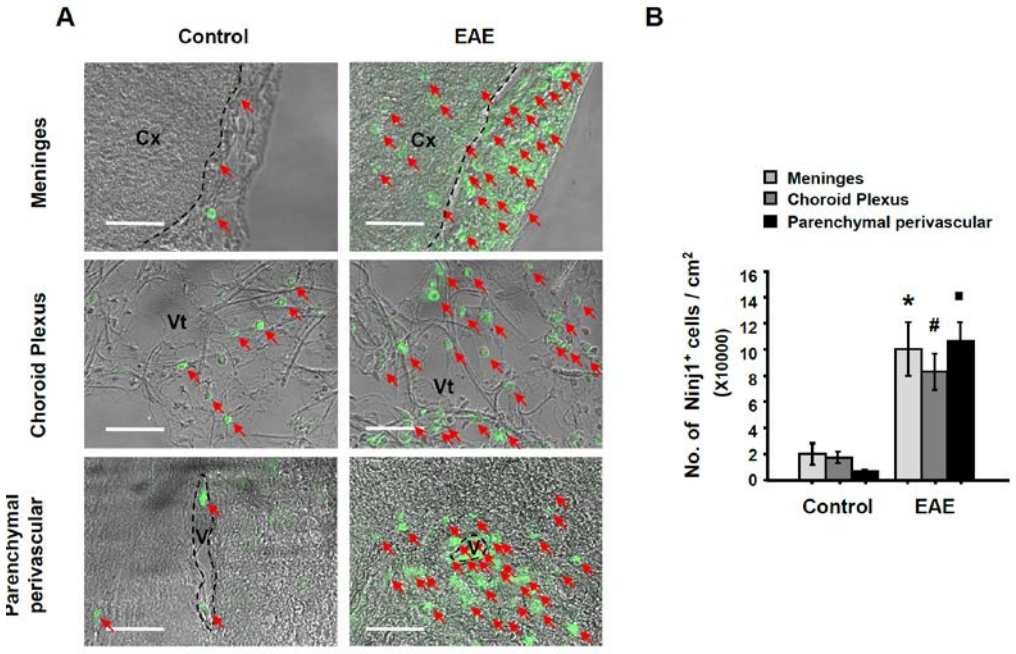

Figure. 7 Ninjurin1^{+} cells in the EAE rat brain and peripheral blood. (A) Immunistaing of Ninjurin1 (from Dr. Araki) in the EAE rat brain. Arrows indicate Ninjurin1^{+} cells and dotted lines demonstrate the boundary with parenchymal tissue. Scale bar = 50 ㎛. (B) Quantitation of Ninjurin1^{+} cells by immunostaining in control and EAE rat brains. Values were obtained by three replicates in control (n=2) and EAE (n=2) animals, and were converted to fundamental units (Ninjurin1^{+} cell number / cm^{2}). *, P<0.01 versus control for meninges; #, P<0.01 versus control for the choroid plexus; ■, P<0.01 versus control for parenchymal perivascular space; Cx, Cerebral cortex; Vt, ventricle; V, vessel and Scale bars are 50㎛.

3. Ninjurin1 is expressed in myeloid cells and endothelium, but not lymphoid cells.

To determine the identity of Ninjurin1^{+} cells in the EAE rat brain, we performed double immunostaining using specific antibodies for macrophages / endothelial cells (GS-lectin), macrophages / microglia (CD11b), pan leukocyte (CD45), macrophages/monocytes (Iba-1), neutrophils (MPO-1), T lymphocytes (CD4), B lymphocytes (CD20), and astrocytes (GFAP). Ninjurin1-expressing cells were positive for CD11b, CD45 (Figure 8A), Iba-1 and MPO-1 (Figure 8B), but negative for CD4, CD20 (Figure 8D), and GFAP (Figure 8E). These results indicate that Ninjurin1 expression is positive in myeloid cells such as macrophages / monocytes and neutrophils, but negative in lymphoid cells such as B lymphocytes and T lymphocytes, as well as for astrocytes. Interestingly, although Ninjurin1 was not detectable in the endothelium of the normal rat brain, we could detect Ninjurin1 signal in some GS lectin^{+} ECs in EAE rat brain (Figure 8C, arrow) as well as myeloid cells. Therefore, these results suggest the possibility that Ninjurin1-mediated homophilic binding exists and plays a role in cell-cell interaction between leukocyte and inflamed brain endothelium in EAE rats, resulting in the entry of leukocyte into the CNS across the BBB.

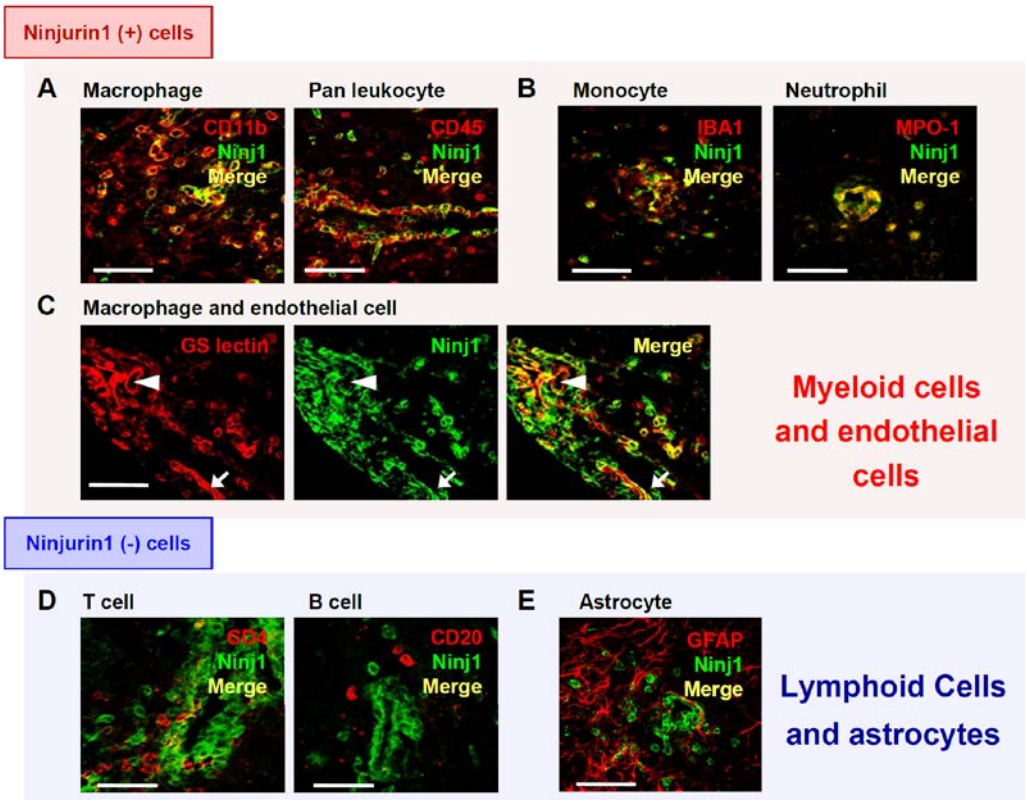

Figure 8. Ninjurin1 expression in myeloid cells and partial expression in endothelium in the brain of EAE rats. Double immunostaining of Ninjurin1 with (A) CD11b, CD45, (B) Iba-, MPO-1, (C) GS lectin, or (D) CD4, CD20, GFAP in the EAE rat brain. White arrow indicates Ninjurin1^{+} endothelium and the arrowhead denotes Ninjurin1^{-} endothelium in EAE rat brain. Scale bar = 50 ㎛.

4. Ninjurin1 expression is upregulated with treatment of INFγ in macrophage cells and endothelial cells.

To detect endogenous Ninjurin1, we made a couple of anti-mouse Ninjurin1 antibodies, $Ab_{1\text{-}15}$ and $Ab_{139\text{-}152}$ which selectively recognize N- or C-terminal region of Ninjurin1, respectively (Figure 9A). The specificity of each antibody was evaluated using two truncated GFP-mNinj1 plasmids, GFP-mNinj1$_{72\text{-}152}$ or GFP-mNinj1$_{1\text{-}71}$, which lacks of its N- or C-terminal region, respectively. As expected, the $Ab_{1\text{-}15}$ antibody recognized well the full-length and GFP-mNinj1$_{1\text{-}71,}$ but not the GFP-mNinj1$_{72\text{-}152}$ (Figure 9B, middle), whereas the $Ab_{139\text{-}152}$ antibody detected both the full-length and GFP-mNinj1$_{72\text{-}152}$, but not the GFP-mNinj1$_{1\text{-}71}$ (Figure 9B, right), indicating that the specificities of these antibodies are enough to distinguish the each domain of mouse Ninjurin1.

To check Ninjurin1 expression in the inflammatory condition, INFγ was administrated in macrophage cells such as BV2 cells, murine migralia cell line (Figure 10A), Raw264.7 cells, murine peritoneal cell line (Figure 10B), and endothelial cells such as MBEC4 cells, murine microvascular endothelial cell line (Figure 10C). Ninjurin1 expression is upregulated with treatement of INFγ in dose-dependent manner, suggesting the possibility of Ninjurin1-mediated interaction in inflammatory condition.

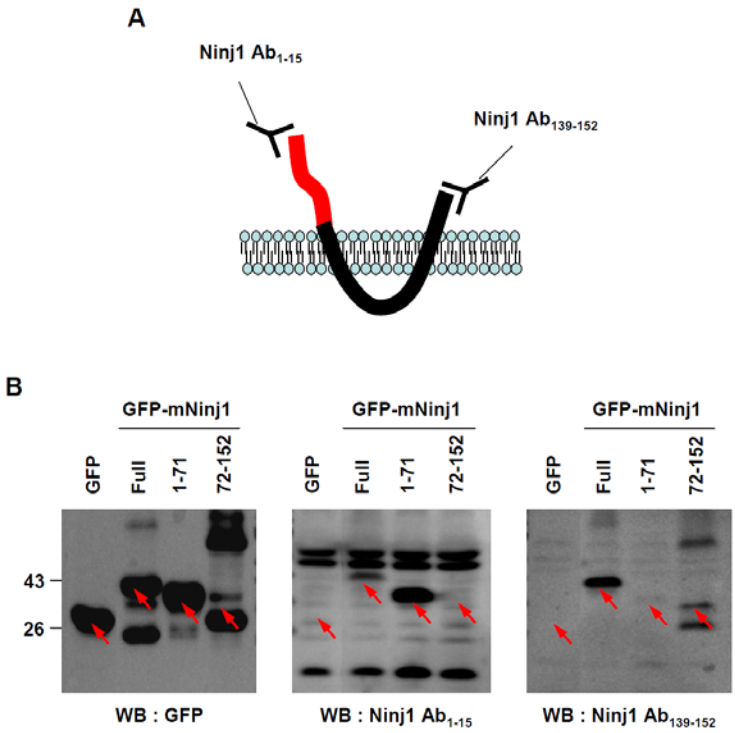

Figure 9. Two kinds of Ninjurin1 antibodies. (A) The construction of two custom-made rabbit anti-mouse Ninjurin1 antibodies which are specific to the N- or C-terminal region of mouse Ninjurin1, $Ab_{1\text{-}15}$ or $Ab_{139\text{-}152}$, respectively. A couple of plasmids truncated with the C- or N-terminal domain, GFP-mNinj$1_{1\text{-}71}$ or GFP-mNinj$1_{72\text{-}152}$, were constructed and overexpressed in HEK293T cells. After 24 hr, the lysate was blotted with anti-GFP (left) or anti-Ninjurin1 antibody, $Ab_{1\text{-}15}$ (middle) and $Ab_{139\text{-}152}$ (right). Red arrows indicate the product corresponding to the expected product of each plasmid.

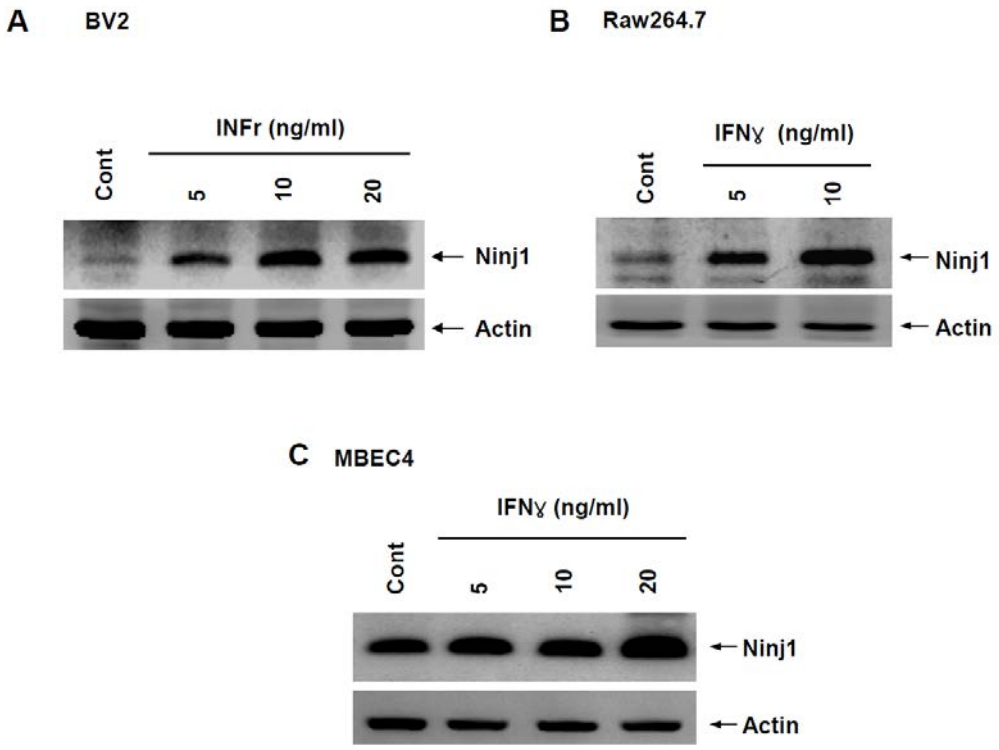

Figure 10. Upregulation of Ninjurin1 in BV2, Raw264.7 or MBEC4 cells with IFNγ treatment. (A) BV2, (B) Raw264.7 and (C) MBEC4 cells were cultured in DMEM media with 10% FBS. After starvation for 6 hr in serum-absent media, IFNγ was treated for 24 hr with indicated concentration (ng/ml). Western blot analysis was performed with anti-Ninjurin1 ($Ab_{1\text{-}15}$) antibody.

5. Ninjurin1 KO mice attenuate EAE susceptibility with reduced leukocyte infiltration.

To determine the role of Ninjurin1 during CNS inflammation *in vivo*, Ninjurin1 KO mice were generated by removing exon 1 from among a total of 4 exons of Ninjurin1 located on chromosome 13 by homologous recombination (Figure 11A) and were backcrossed with the C57BL/6 strain for at least seven generations. The Ninjurin1 KO mice were evaluated by genotyping via a genomic PCR and Western blotting (Figure 11B). Some of the Ninjurin1 KO mice showed developmental retardation and dysfunctions such as ataxia and hydrocephalus (Figure 12).

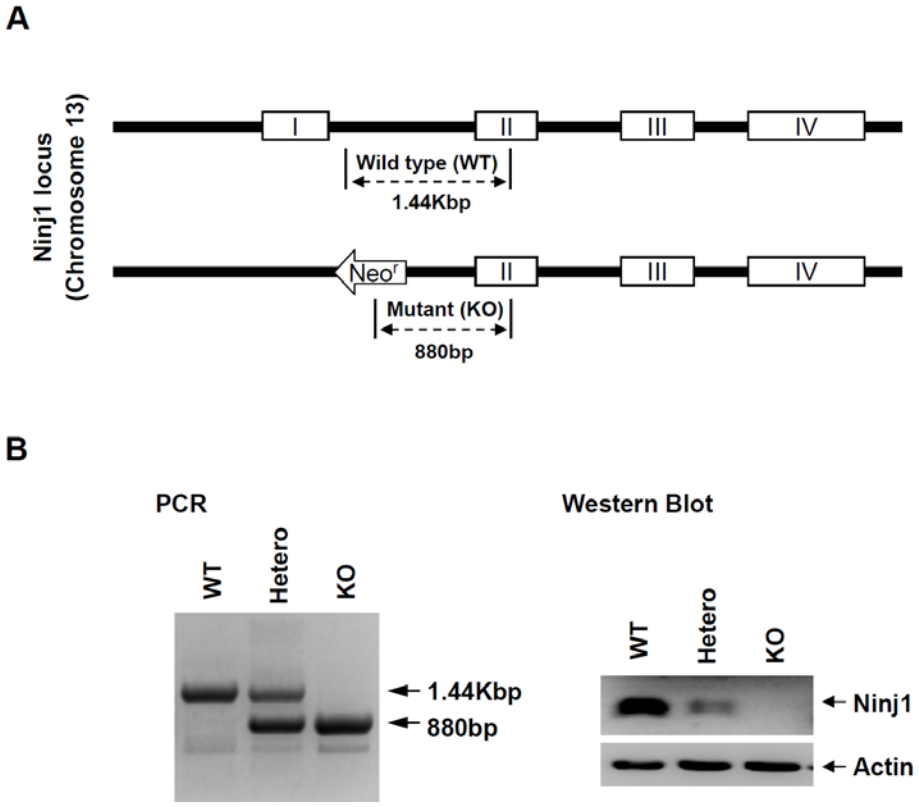

Figure 11. Construction of Ninjurin1 KO mice. (A) Schematic diagram of Ninjurin1 KO mice (upper). Targeted disruption of the Ninjurin1 gene was carried out by replacement of exon 1 among the 4 exons located on chromosome 13. (B) The wild-type (WT), heterozygotes (hetero) and homozygotes (KO) mice were identified by their PCR amplicons (WT=1.44 Kbp, KO=880bp and Hetero=1.44 Kbp and 880bp), and the Western blot analysis of the brain tissue (right).

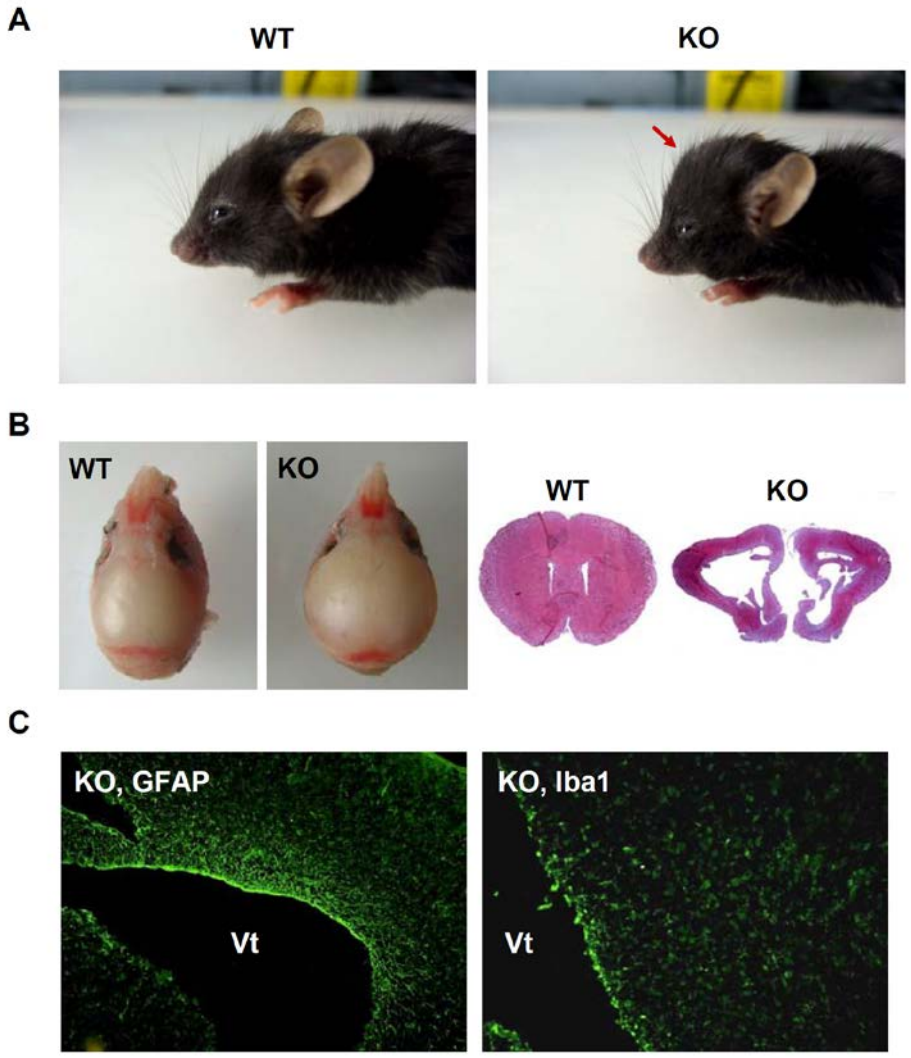

Figure 12. Hydrocephalic brian of abnormal Ninjurin1 KO mice. (A) Dorm -shape head of Ninjurin1 KO mice. Red arrow indicates dorm-shape brain. (B) Skull and H&E staining of hydrocephalic brain of Ninjurin1 KO mice. (C) Activation of astrocytes (GFAP) and microglia (IBA1) in Ninjurin1 KO mice. Vt : ventricle.

However, we used Ninjurin1 KO mice with a normal appearance and a hemogram similar to that of wild-type (WT) mice in this study (Table 1). Initially, the susceptibilities to EAE were compared between WT and Ninjurin1 KO mice for a 30-day period after myelin oligodendrocyte glycoprotein $(MOG)_{35-55}$ immunization. Interestingly, Ninjurin1 KO mice showed significantly lower EAE clinical scores from 17 to 22 days after immunization compared to WT mice (Figure 13A) with a difference in their peak scores (Figure 13B). A histological analysis of the spinal cord of mice revealed that Ninjurin1 KO mice had not only a decreased accumulation of immune cells with CD45, F4/80, and CD3 (Figure 13C and D) but also a smaller lesion area and less demyelination (Figure 13E). The expression of Ninjurin1 in the spinal cord was upregulated depending on severity of EAE symptoms (Figure 13F).

	WT		KO		
Variable	Mean	SEM	Mean	SEM	P-value
WBC (K/ul)	7.10	0.15	7.84	0.22	0.30
Neutrophils (K/ul)	0.95	0.03	1.22	0.05	0.07
Lymphocytes (K/ul)	5.87	0.12	6.29	0.17	0.44
Monocytes (K/ul)	0.21	0.01	0.28	0.01	0.15
Eosinophils (K/ul)	0.05	0.005	0.05	0.003	0.71
Basophils (K/ul)	0.02	0.002	0.02	0.001	0.40
Erythrocytes (M/ul)	8.91	0.04	8.88	0.03	0.85
Platelets (K/ul)	563.9	21.47	563.0	12.35	0.99

Table 1. Hematogram of WT and Ninjurin1 mice. Peripheral blood was collected from the retro-orbital sinus of mice 10-week old mice (WT; n=8, KO; n=6). Cell counts were performed using an automated cell counter with veterinary parameters and reagents. K, 10^3; WBC, white blood cells.

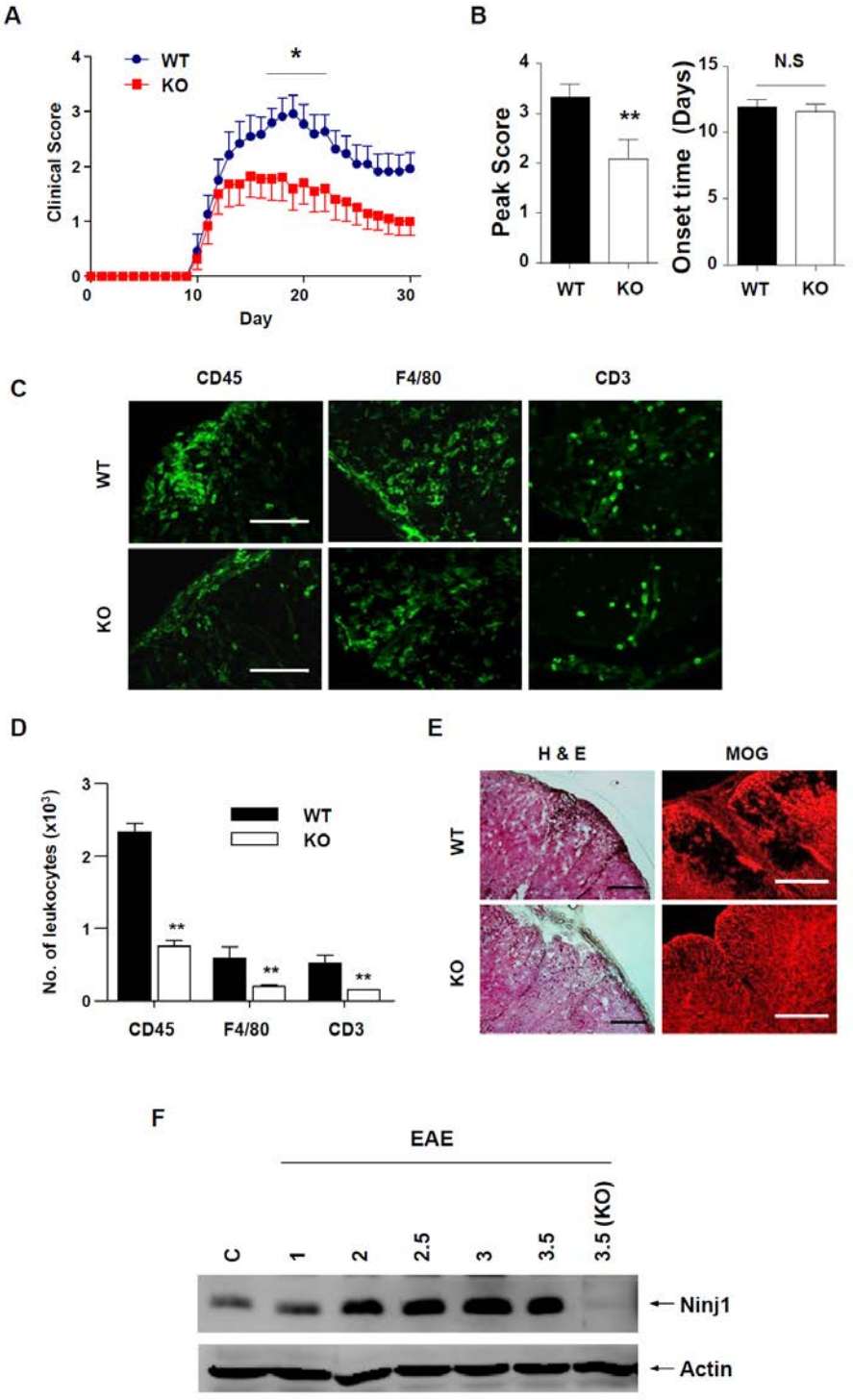
A
WT
KO
*
Clinical Score
Day
B
Peak Score
**
N.S
Onset time (Days)
WT
KO
C
CD45
F4/80
CD3
WT
KO
D
No. of leukocytes (x10³)
WT
KO
**
CD45
F4/80
CD3
E
H & E
MOG
WT
KO
F
EAE
C
1
2
2.5
3
3.5
3.5 (KO)
Ninj1
Actin

Figure 13. Ninjurin1 KO mice attenuate EAE susceptibility. (A) EAE was induced in WT (n=12) and Ninjurin1 KO mice (n=11) by immunization with 100 μg of myelin oligodendrocyte glycoprotein (MOG) $_{35-55}$ peptide per mouse: * $p < 0.05$. (B) Ninjurin1 KO mice had resistance to EAE with a difference in the peak clinical score (WT=3.33 and KO=2.09) but no difference in the onset time (WT=11.9 and KO=11.6 day after immunization). ** $p < 0.01$, N.S; no significance. (C) Representative immunostaining images with CD45 (pan leukocyte), F4/80 (macrophage), and CD3 (T lymphocyte) show the accumulation of leukocyte in the spinal cord of WT or Ninjurin1 KO mice. Scale bar = 50 μm. (D) The number of infiltrated immune cells in the spinal cord was counted in three mice per group: ** $p < 0.01$. (E) Representative images of hematoxylin eosin (H&E) staining showing a lesion area and MOG staining (red) showing demyelination in the spinal cord of WT or KO mice. (F) Ninjurin1 up-regulation in spinal cord of EAE mice. Spinal cords of EAE mice with each clinical score were extracted. Western blot analysis was performed with anti-Ninjurin1 antibody (Ab_{1-15}). Actin was used as loading control.

From these data, we identified Ninjurin1 as a potential regulator of the infiltration of leukocyte from peripheral blood into the CNS across the BBB. In normal rat brains, Ninjurin1^{+} cells were detected at a basal level in routes by which leukocyte enter the CNS, such as meninges, the choroid plexus and parenchymal perivascular regions (Ransohoff et al, 2003) (Figure 6). In EAE rat brains, Ninjurin1^{+} cells were significantly more abundant in these regions (Figure 7), and their expression was also detected in brain endothelium and in peripheral blood myeloid cells (Figure 8). Interestingly, Ninjurin1 KO mice attenuated EAE susceptibility by reducing the recruitment of leukocyte into inflamed lesions (Figure 13). Collectively, these results suggest that Ninjurin1 may have an important role in cell-cell interaction between leukocyte and ECs in EAE autoimmune disease (Figure 14).

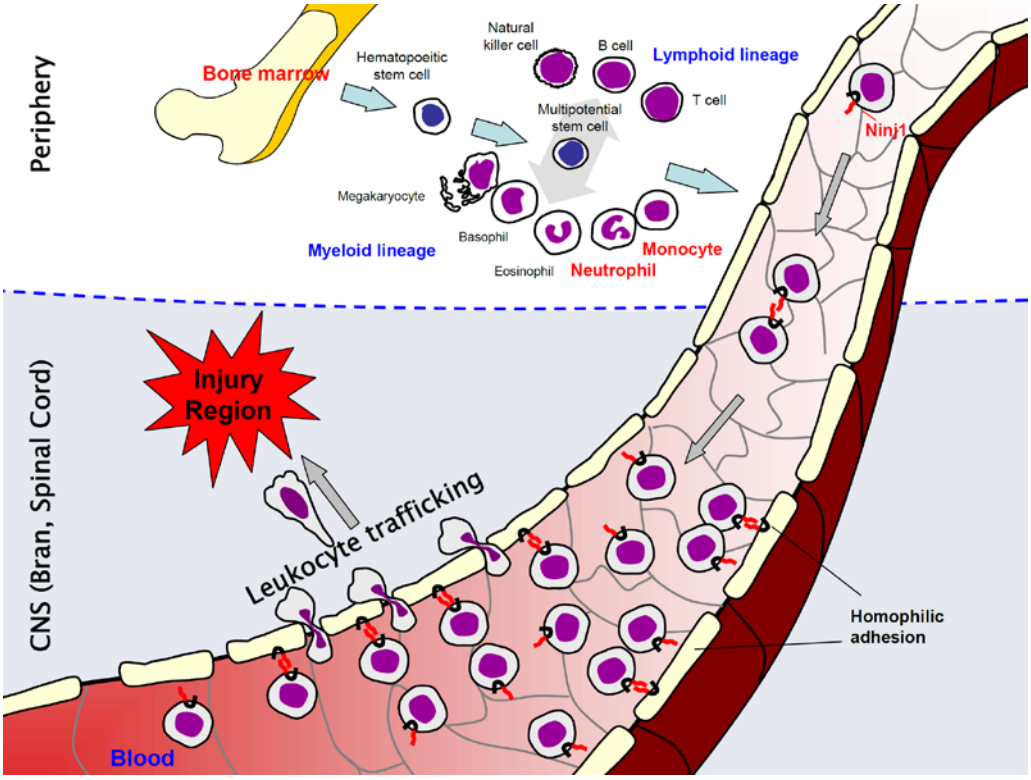

Figure 14. Potential role of Ninjurin1 on the leukocyte trafficking.

6. Ninjurin1 mediates adhesion between monocyte lineage cells and ECs *in vitro*.

To confirm the homotypic binding of Ninjurin1, GFP-tagged mouse Ninjurin1 (GFP-mNinj1) of Flag-tagged mouse Ninjurin1 (Flag-mNinj1) was overexpressed in HEK293T cells and then immunoprecipitated with anti-Flag antibody. Binding between Flag-mNinj1 and GFP-mNinj1 was observed, clarifying the homotypic binding of Ninjurin1 (Figure 15A).

Next, we investigated whether Ninjurin1 could regulate cell-cell adhesion of leukocyte and ECs using BV2 cells (murine monocyte lineage microglia) and HBMECs (human brain microvascular endothelial cells). To examine Ninjurin1-dependent binding activity, we overexpressed myc-tagged mock or myc-tagged Ninjurin1 in BV2 cells and HBMECs. We then detected the expression of Ninjurin1 in the cytosol and membrane of these cells, indicating that the transfected recombinant Ninjurin1 protein was localized normally in the host cells. In *in vitro* binding assays, Ninjurin1-transfected BV2 cells showed enhanced adhesion to HBMECs compared to the mock-transfected BV2 cells (Figure 15B). This effect was further confirmed by additional transfections of the Ninjurin1 expression vector into HBMECs and BV2 cells. Ninjurin1 overexpression in both BV2 cells and HBMECs synergistically enhanced the binding between these two types of cells (Figure 15C).

To clarify the adhesion contribution of Ninjurin1 on leukocyte-endothelium interaction *in vivo*, the endotoxin-induced uveitis (EIU) model was used, which is accompanied by acute and intense leukocyte infiltration into the vitreous in the retina within 24 hr after intraperitoneal injection of lipopolysaccharide (LPS) at a sublethal dose (Rosenbaum et al, 1980). In EIU mice, the number of adherent leukocyte on the vessel wall of the retina was lower in Ninjurin1 KO mice (Figure 15D), indicating that Ninjurin1 is directly involved in leukocyte-endothelium interaction *in vivo*. These data suggest that Ninjurin1 might mediate homophilic binding between leukocyte and endothelium, which is an initial step of leukocyte trafficking into the injury lesions.

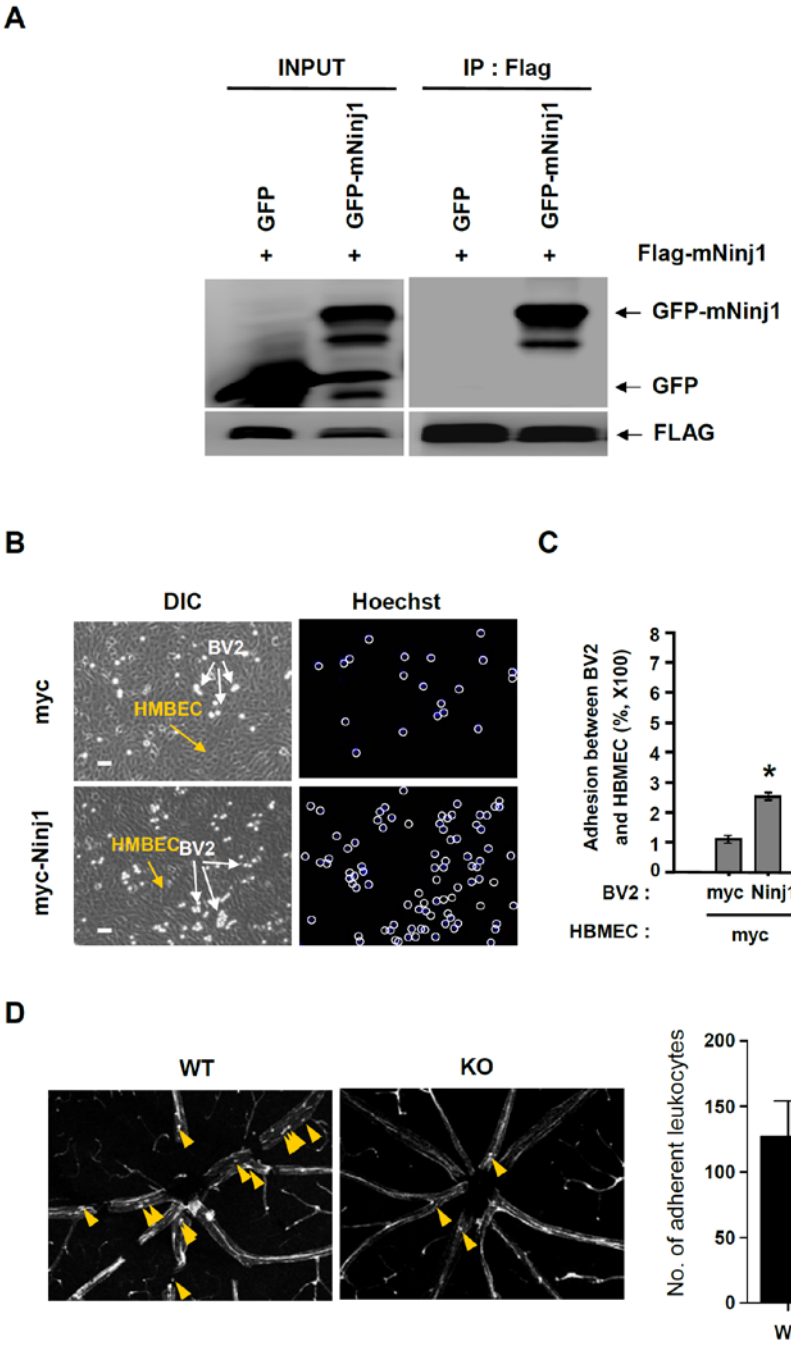
A
INPUT
IP : Flag
+ GFP
+ GFP-mNinj1
+ GFP
+ GFP-mNinj1
Flag-mNinj1
GFP-mNinj1
GFP
FLAG
B
DIC
Hoechst
myc
myc-Ninj1
BV2
HMBEC
C
Adhesion between BV2 and HBMEC (%, X100)
BV2 :
HBMEC :
myc Ninj1 myc Ninj1
myc
myc-Ninj1
D
WT
KO
No. of adherent leukocytes
WT
KO

Figure 15. Ninjurin1 increases binding between leukocyte and endothelium. (A) GFP- or GFP-mNinj1 and Flag-mNinj1 were transfected in HEK293T cells. After pull-downed with anti-Flag antibody, western blotting was performed. (B) *In vitro* cell adhesion assay between mock- or Ninjurin1-transfected BV2 cells and HBMECs. myc- or myc-mNinj1 transfected BV2 cells labeled with Hoechst (white arrow) were seeded onto HBMECs monolayer (yellow arrow) for 30 min. White circles indicate Hoechst-labeled BV2 cells binding to the HBMECs monolayer. Scale bar = 200 ㎛ (C) Quantification of adhesion between myc- or myc-mNinj1 transfected BV2 cells and myc- or myc-mNinj1 transfected HBMECs. Values were normalized using the degree of aggregation when both BV2 cells and HBMECs were transfected with mock DNA as 100%. Scale bars are 50 ㎛. (D) Endotoxin-induced uveitis (EIU) in WT (n=7) and Ninjurin1 KO mice (n=7). Mice were intraperitoneally injected with LPS at 9 mg/kg per mouse for 24 hr, and the adherent leukocyte on the vessel wall of the retina were labeled with Rhodamine-Concanavalin (Con) A. Representative images of adherent leukocyte (yellow arrowheads) are shown. Scale bar = 50 μm. The number of adherent cells per retina was counted. ** $p < 0.01$.

7. Selective blockage of the Ninjurin1 homophilic binding domain reduces leukocyte trafficking and the EAE clinical score.

Ninjurin1 can interact with itself through the homophilic binding domain, from Pro^{26} to Asn^{37}, of the N-terminal ectodomain (Araki et al, 1997), which may mediate leukocyte-endothelium adhesion and subsequent TEM under inflammation. To examine the blockage effects of the Ninjurin1 homophilic binding domain, a custom-made antibody, $Ab_{26\text{-}37}$, was generated using the peptide length from Pro^{26} to Asn^{37} of the N-terminal ectodomain of Ninjurin1 as an antigen (Figure 16A). The treatment with $Ab_{26\text{-}37}$ decreased the adhesion and TEM of Raw264.7 cells on or across the MBEC4 cell monolayer (Figure 16B and C). Moreover, the intraperitoneal administration of $Ab_{26\text{-}37}$ at 4, 6, 8, and 10 days after EAE induction attenuated its clinical symptoms (Fig 17A) and decreased leukocyte infiltration compared to an IgG control group (Figure 17B). Consistent with $Ab_{26\sim37}$, the treatment of $cPEP_{26\text{-}37}$, a cyclized peptide corresponding to Ninjurin1 homophilic binding domain (Figure 18A), decreased not only Ninjurin1-mediated cell-cell adhesion and TEM *in vitro* (Figure 18B and C) but also EAE susceptibility *in vivo* (Figure 19). Thus, the selective targeting of the Ninjurin1 homophilic binding domain effectively inhibits leukocyte trafficking and EAE susceptibility.

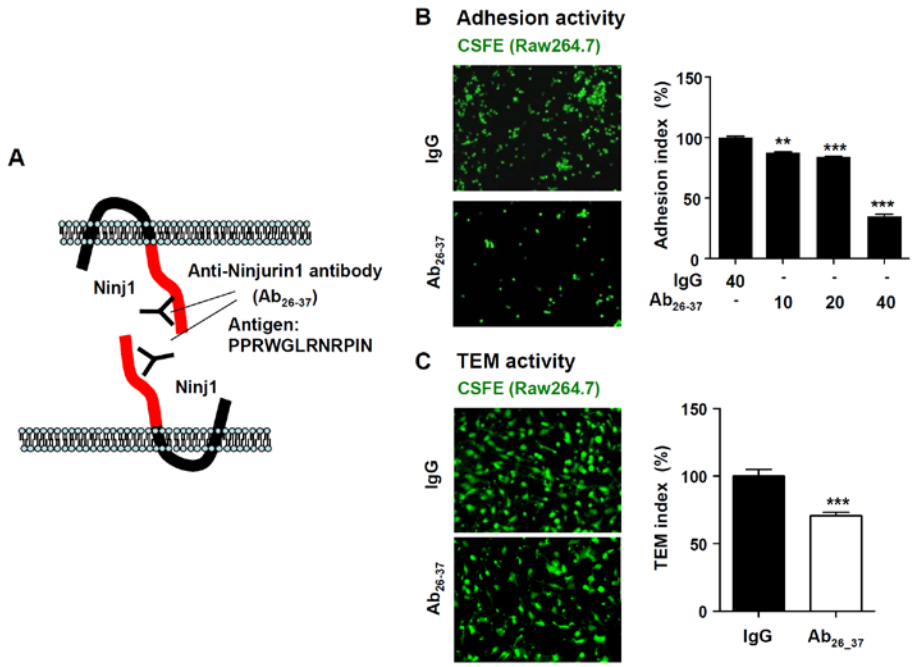

Figure 16. Functional blockage of the Ninjurin1 homophilic binding domain via $Ab_{26\text{-}37}$ reduces the adhesion activity and TEM of Raw264.7 cells. (A) Schematic diagram of a custom-made antibody ($Ab_{26\text{-}37}$). The $Ab_{26\text{-}37}$ was made by immunizing rabbits with a synthetic peptide corresponding to the homophilic binding domain of Ninjurin1 as the antigen. (B) Impaired adhesion or (C) TEM activity ($Ab_{26\text{-}37}$, 40 μg/ml) of the CSFE (5 μM, 5 min)-labeled Raw264.7 cells on the MBEC4 monolayer with pretreatment of $Ab_{26\text{-}37}$. The adhesion and transmigration index is shown as relative to the IgG normalized to 100%. ** $p < 0.01$, *** $p < 0.001$.

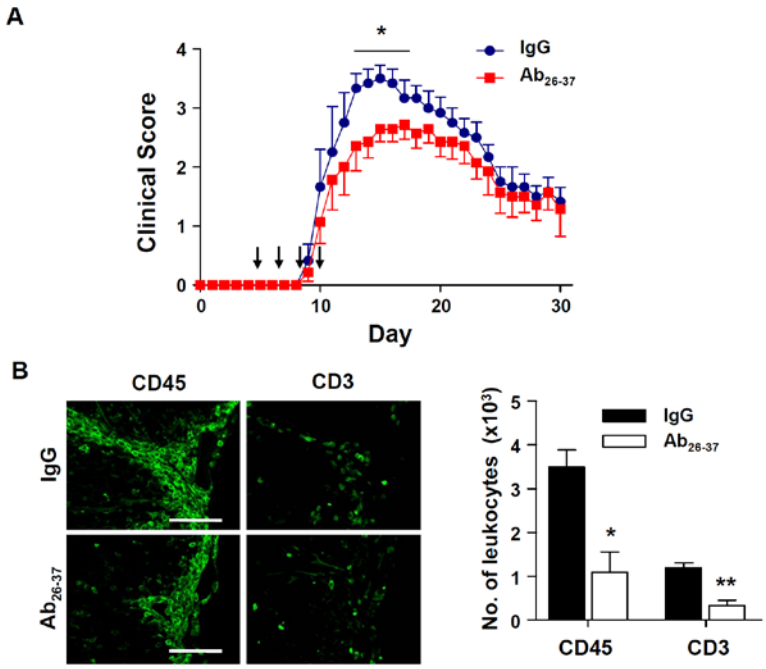

Figure 17. Functional blockage of the Ninjurin1 homophilic binding domain via Ab_{26-37} alleviates EAE susceptibility. (A) 100 µg Ab_{26-37} (n=7) per mouse was administrated intraperitoneally at days 4, 6, 8, and 10 (black arrow) after MOG_{35-55} immunization. Control mice (n=6) were injected with isotype IgG at an equivalent amount. * $p < 0.05$. (B) Representative immunostaining images with CD45 (pan leukocyte) and CD3 (T lymphocyte) show the accumulation of leukocyte in the spinal cord of IgG or Ab_{26-37}–injected mice. The number of infiltrated immune cells in the spinal cord was counted in three mice per group: * $p < 0.05$, ** $p < 0.01$.

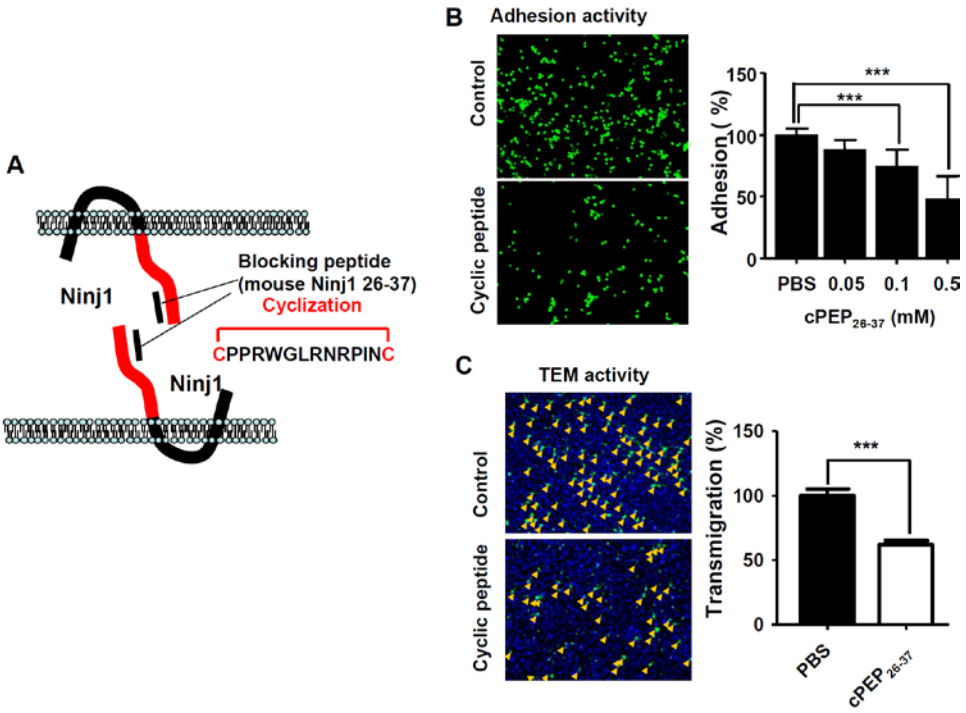

Figure 18. Functional blockage of the Ninjurin1 homophilic binding domain via cPEP$_{26\text{-}37}$ reduces the adhesion activity and TEM of Raw264.7 cells. (A) The synthesis of a cyclic peptide (cPEP$_{26\text{-}37}$) specific to the homophilic binding domain of ninjurin1 (from Pro^{26} to Asn^{37}). The cyclization was made through a disulfide bond by adding a cysteine at each end of the peptide. (B) Impairmed adhesion (left) and (C) TEM activity (right) of the CSFE-labeled Raw264.7 on the MBEC4 monolayer with treatment of cPEP$_{26\text{-}37}$, which is specific to the homophilic binding domain of ninjruin1 (from Pro^{26} to Asn^{37}), *** $p < 0.001$.

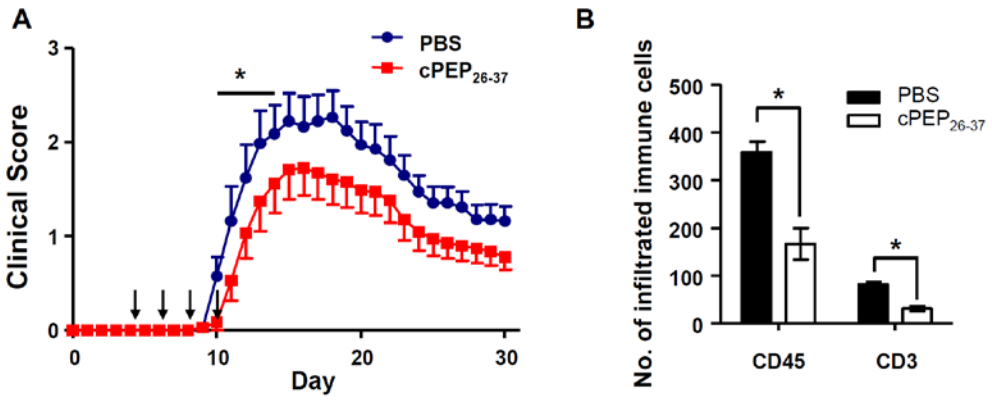

Figure 19. Functional blockage of the Ninjurin1 homophilic binding domain via cPEP$_{26-37}$ alleviates EAE susceptibility. (A) 100 µg cPEP$_{26-37}$ (n=17) per mouse was administrated intraperitoneally at days 4, 6, 8, and 10 (black arrow) after MOG$_{35-55}$ immunization. Control mice (n=17) were injected with PBS at an equivalent amount. * $p < 0.05$. (B) Accumulation of leukocyte with CD45 (pan leukocyte) and CD3 (T lymphocyte) in the spinal cord of PBS or cPEP$_{26-37}$–injected mice. The number of infiltrated immune cells in the spinal cord was counted in three mice per group: * $p < 0.05$.

8. Ninjurin1 is dominantly expressed in the actin-rich leading edges of moving cells.

To analyze the functions of Ninjurin1 on the migratory behavior of leukocyte, we established primary BMDMs which were isolated from the mouse femur and differentiated with M-CSF for 3 days. Immunostaining with the anti-F4/80 antibody, a macrophage-specific marker, shows the high purity (> 90%) of our BMDMs and the similar degrees of differentiation between WT and Ninjurin1-deficient bone-marrow macrophages having undergone treatment with M-CSF (Figure 20A). Furthermore, both immunostaining and Western blotting with $Ab_{1\text{-}15}$ in WT or Ninjurin1 KO BMDMs clearly revealed the specificity of this antibody to mouse Ninjurin1 (Figure 20B and C).

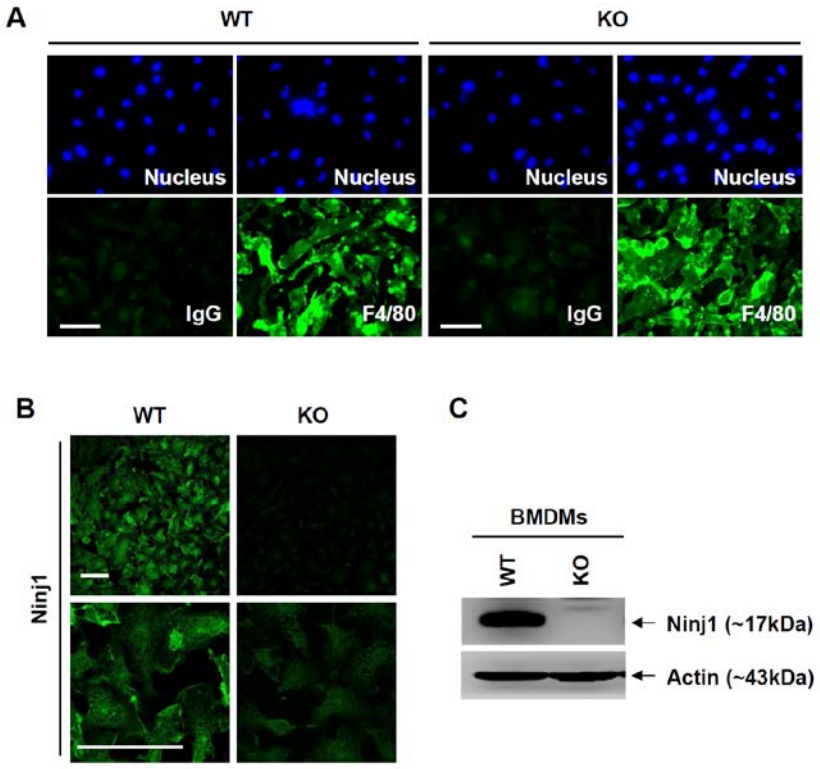

Figure 20. Primary BMDMs culture from WT or Ninjurin1 KO mice. (A) Bone marrow cells from WT and Ninjurin1-deficient BMDMs were cultured and differentiated with complete RPMI media containing 20 ng/ml M-CSF for 3 days. After 4% PFA fixation, immunostaining with anti-F4/80 antibody (green) was performed. The nucleus of BMDMs was demonstrated with Hoechst33342 (blue) staining. Scale bar = 50 μm. (B-C) BMDMs were stained and blotted with anti-Ninjurin1 antibody ($Ab_{1\text{-}15}$). Scale bar = 50 μm.

Using these primary BMDMs and $Ab_{1\text{-}15}$, we first examined the cellular distribution of Ninjurin1 in BMDMs. Double staining with $Ab_{1\text{-}15}$ and Alexa-546 phalloidin revealed that Ninjurin1 is dominantly distributed in the F-actin-rich leading edges and at the membrane ruffle of BMDMs and Raw264.7 cells (Figure 21). Consistent with this result from the mouse BMDMs, Ninjurin1 in rat BMDMs derived from SD rat femur was also abundant at the F-actin-rich leading edges and at the membrane ruffle due to the staining with the rat-specific anti-Ninjurin1 antibody (gifted from Dr. Millbrant and Dr. Araki) (Figure 22). Exogenous overexpression of GFP-mNinj1 in BMDMs and Raw264.7 cells also showed consistent localization at the F-actin-rich leading edge and membrane ruffle (Figure 23). To examine the dynamic distribution of Ninjurin1 in moving cells, GFP-mNinj1 was overexpressed in COS7 cells and time-lapse imaging under a microscope was performed. This observation clearly exhibited that GFP-mNinj1 is abundant and dynamically reorganized at the front regions of the moving cells, and contributing to their directionality (Figure 24). Together, these results suggest that Ninjurin1 is involved in cell movement via the regulation of the actin-based migratory machinery at the leading edges of moving cells.

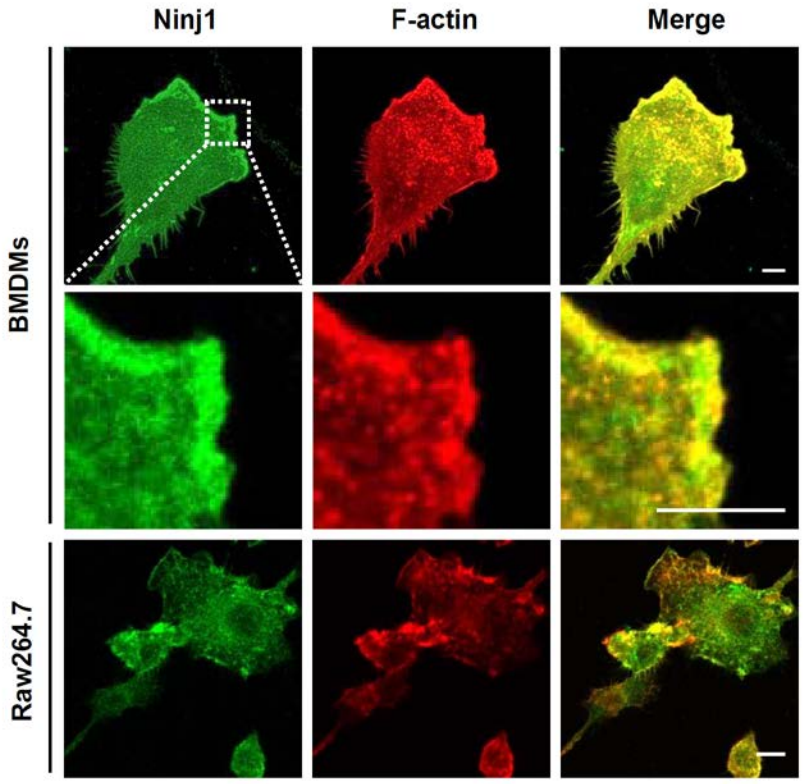

Figure 21. Endogenous Ninjurin1 is expressed at the F-actin-rich leading edge and membrane ruffle in BMDMs and Raw264.7 cells. BMDMs were cultured and differentiated with complete RPMI media containing 20 ng/ml of M-CSF for 3 days and Raw264.7 cells were cultured in complete DMEM media. After 4% PFA fixation, double immunostaining with anti-Ninjurin1 antibody ($Ab_{1\text{-}15}$, green) and Alexa-546 phalloidin (red) was performed. Dotted square boxes indicate highly magnified image of the leading edges of the moving BMDMs. Scale bar = 10 μm.

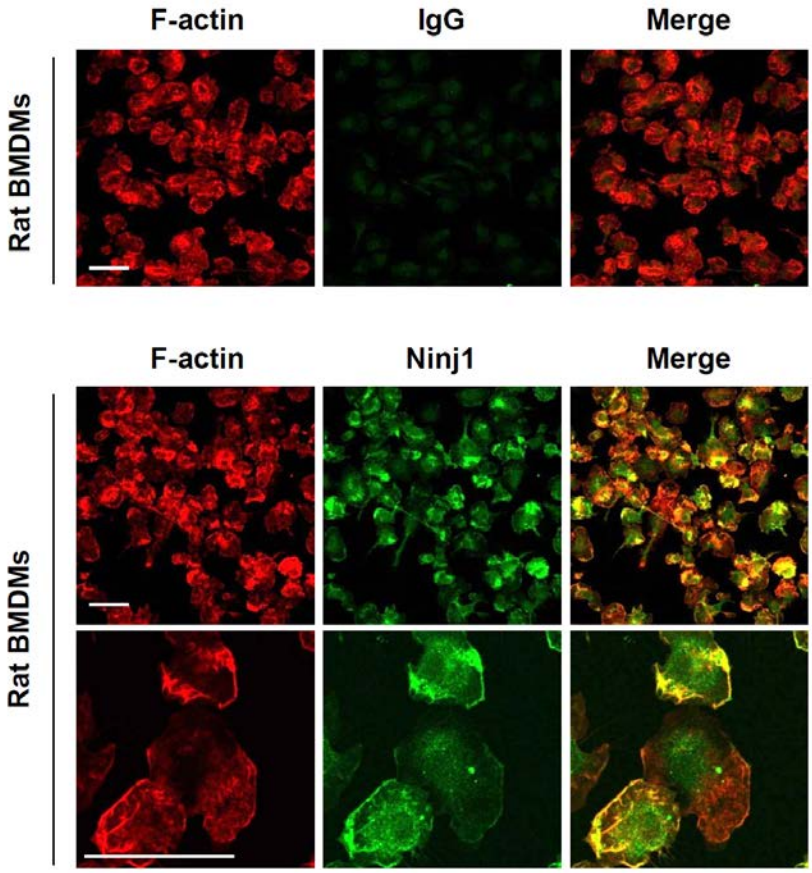

Figure 22. Expression and distribution of Ninjurin1 in rat BMDMs. Bone marrow cells from SD rat were cultured and differentiated with complete RPMI media containing 20 ng/ml M-CSF for 3 days. After 4% PFA fixation, double immunostaining of Alexa-546 phalloidin with control rabbit IgG or anti-rat Ninjurin1 antibody gifted from Dr. Millbrant and Araki (green) were performed. Scale bar = 50 μm.

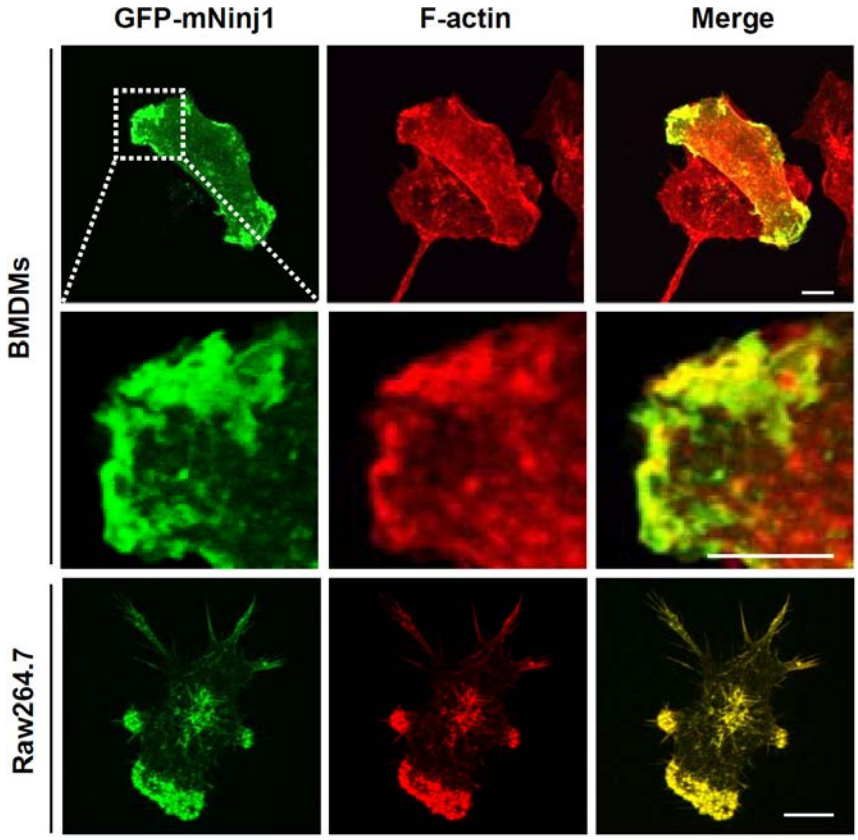

Figure 23. Exogenous Ninjurin1 is expressed at the F-actin-rich leading edge and membrane ruffle in BMDMs and Raw264.7 cells. GFP-mNinj1 (green) was transfected into BMDMs and Raw264.7 cells. After 24 hr, the BMDMs were fixed with 4% PFA and were stained with Alexa-546 phalloidin (red). Dotted square boxes indicate highly magnified image of the leading edges and membrane ruffles of moving BMDMs and Raw264.7 cells. Scale bar = 10 μm

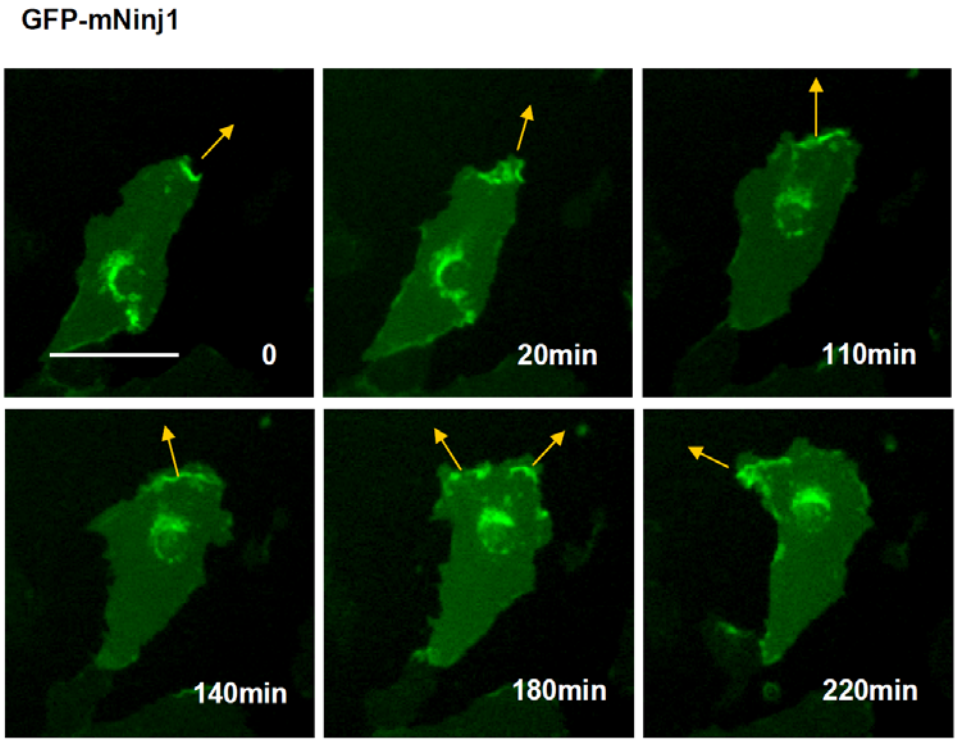

Figure 24. Ninjurin1 is expressed at the F-actin-rich leading edge and membrane ruffle in moving COS7 cells. COS7 cells were transfected with GFP-mNinj1. After 24 hr, fluorescence images were taken every 5 min for up to 5 hr. Individual frames at selected time intervals are shown. Yellow arrows indicate the direction of the moving COS7 cells. Scale bar = 50 μm.

9. Membrane protrusion formation and cell motility are reduced in Ninjurin1-deficient BMDMs and their knock-down Raw264.7 cells by RNAi.

Membrane protrusion like lamellipodia and filopodia at the leading edges are necessary for cell movement (Quast et al, 2011). Because Ninjurin1 is thought to be involved in cell migration, we compared the membrane protrusion between WT and Ninjurin1-deficient BMDMs. Interestingly, Ninjurin1-deficient BMDMs have weaker membrane protrusion properties with a smaller percentage of cells with protrusion as well as fewer protrusion per cell compared to WT BMDMs (Figure 25A and B). As membrane dynamics is also important in cell migration, we examined the membrane ruffling of WT and Ninjurin1-deficient BMDMs after M-CSF administration under high-magnified time-lapse microscopy. The membrane ruffle was weaker in the Ninjurin1-deficient BMDMs than in the WT BMDMs (Figure 25C). To prove directly whether Ninjurin1 could influence the migration of BMDMs, time-lapse observation was conducted for 6 hr under lower-magnification microscopy. As expected, the Ninjurin1-deficient BMDMs showed reduced motility with a lower velocity and shorter Euclidean distance compared to WT BMDMs (Figure 25C and D).

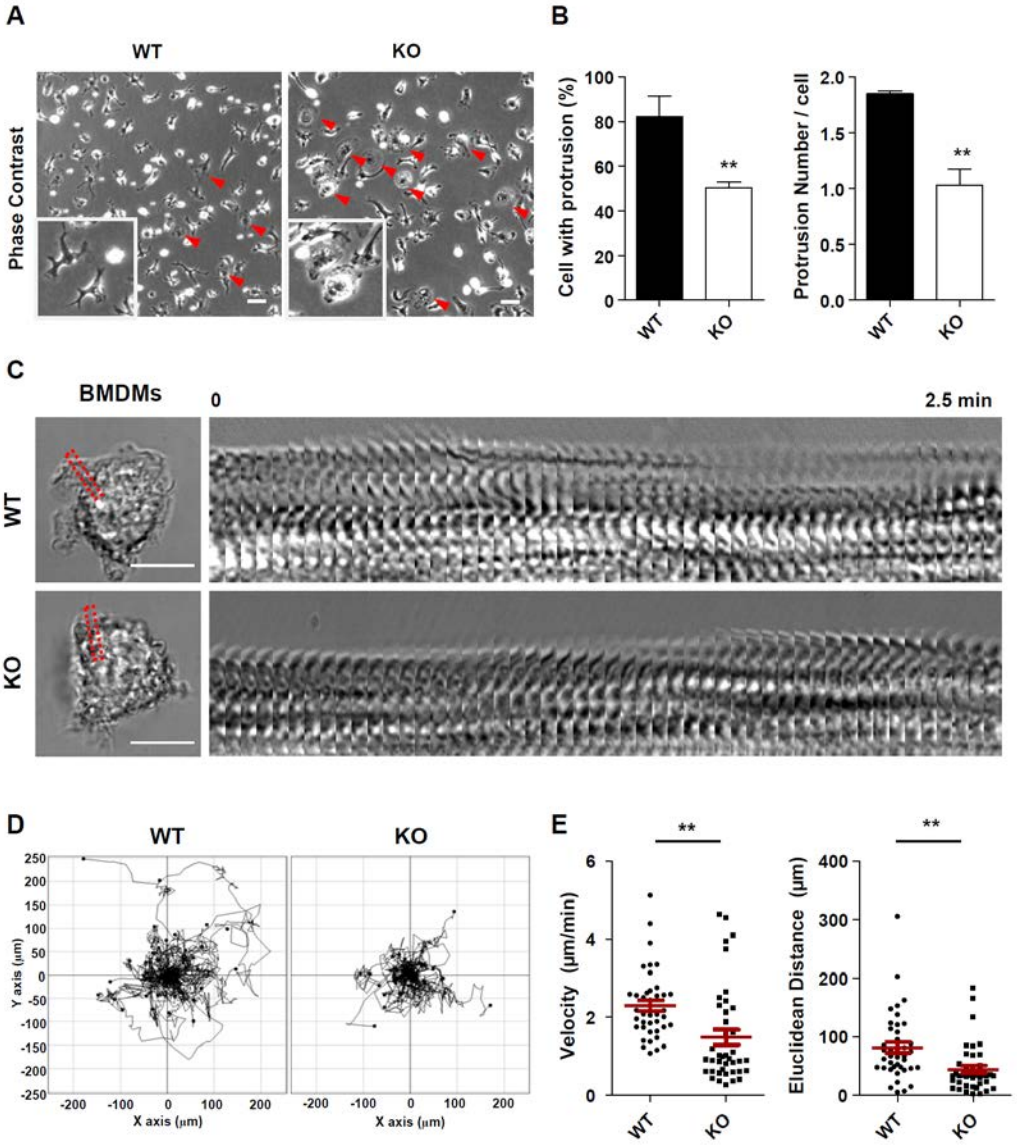
A
WT
KO
Phase Contrast
B
Cell with protrusion (%)
Protrusion Number / cell
**
WT
KO
C
BMDMs
0
2.5 min
WT
KO
D
WT
KO
Y axis (μm)
X axis (μm)
E
Velocity (μm/min)
Eluclidean Distance (μm)
**

Figure 25. Ninjurin1-deficient BMDMs and knock-down Raw264.7 cells by RNAi decrease membrane protrusion formation and cell motility. (A-B) WT and Ninjurin1-deficient BMDMs were cultured and differentiated in complete RPMI media containing 20 ng/ml of M-CSF for 3 days. (A) Representative phase contrast images are shown, in which the white squares denote high-magnification regions. Red arrows demonstrate BMDMs without membrane protrusion. Scale bar = 50 μm. (B) Values were measured from ~100 cells of four independent experiments. ** $p < 0.01$. (C) Membrane dynamics of WT or Ninjurin1-deficient BMDMs. Membrane dynamics of WT and Ninurin1-deficient BMDMs. BMDMs starved in RPMI without serum for 3 hr. After treatment with 20 ng/ml of M-CSF, DIC images were taken every 1.6 sec for 2.5 min by time-lapse microscopy, and a red square region was sequentially demonstrated. Scale bar = 10 μm. (D, E) Basal motility of WT or Ninjurin1-deficient BMDMs. Phase images of BMDMs were taken every 10 min for 6 hr in complete RPMI media containing 20 ng/ml M-CSF by time-lapse microscopy. Trajectory plot (D) and dot charts (E) of the velocity and Euclidean distance were obtained from 40 cells in two independent experiments. ** $p < 0.01$.

The results from the Ninjurin1-deficient BMDMs were confirmed by analyzing the properties of Raw264.7 cells which had undergone Ninjurin1 interference by RNAi (siNinj1). Immunostaining (Figure 26A) and Western blotting (Figure 26B) with $Ab_{1\text{-}15}$ clearly showed the knock-down efficiency of siNinj1 in Raw264.7 cells compared to the RNAi negative control (siCont). Consistent with the results from the Ninjurin1-deficient BMDMs, the siNinj1 Raw264.7 cells exhibited impaired lamellipodia- and filopodia-like protrusion (Figure 26A) with a lower proportion of cells with protrusion and with a lower average number or length per cell (Figure 26C and D). Time-lapse imaging clearly showed that the siNinjurin1 Raw264.7 cells have fewer filopodia-like protrusion and less pronounced dynamics of the protrusion than siCont Raw264.7 cells. Additionally, we observed not only the active wriggling of the cell body but also the generations of pseudopodia-like feet in the siCont Raw264.7 cells (Figure 26E). Taken together, the results with Ninjurin1-deficient BMDMs and siNinj1 Raw264.7 cells clearly demonstrate the importance of Ninjurin1 in cell motility via the formation of membrane protrusion.

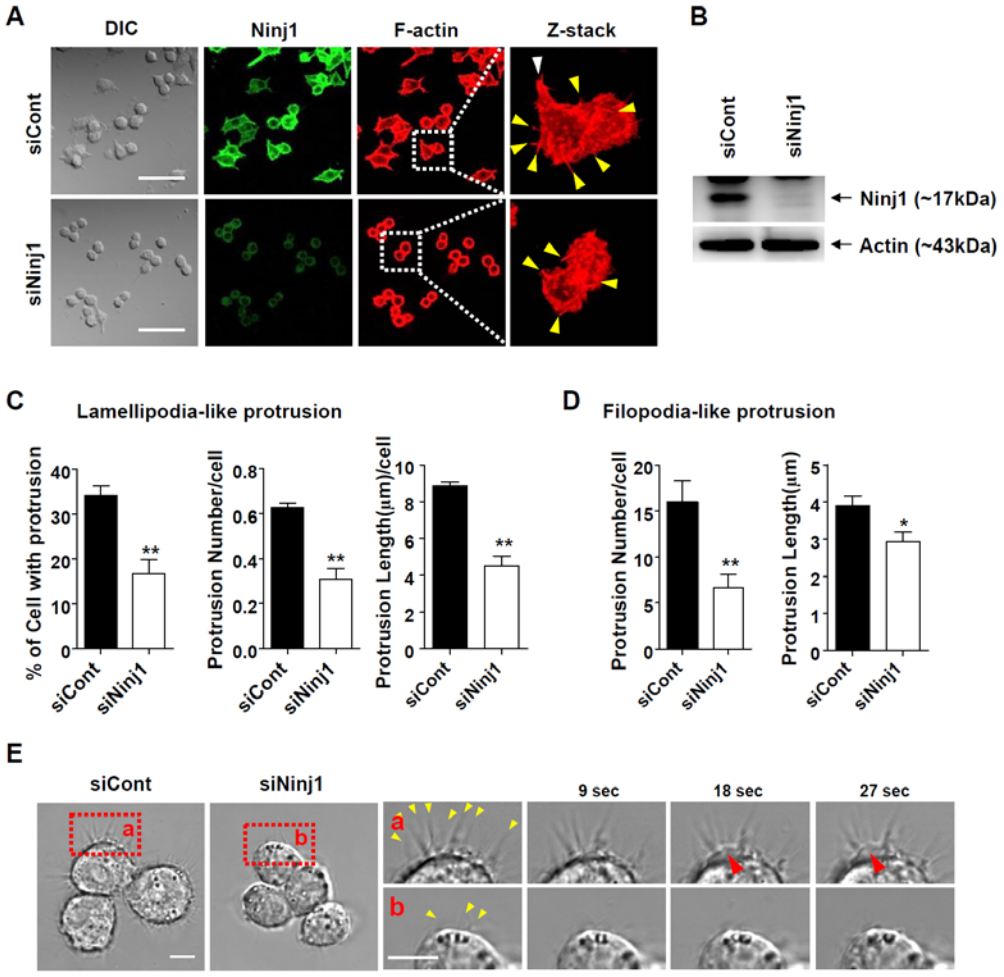
A
DIC
Ninj1
F-actin
Z-stack
siCont
siNinj1
B
siCont
siNinj1
Ninj1 (~17kDa)
Actin (~43kDa)
C
Lamellipodia-like protrusion
% of Cell with protrusion
Protrusion Number/cell
Protrusion Length(μm)/cell
siCont
siNinj1
D
Filopodia-like protrusion
Protrusion Number/cell
Protrusion Length(μm)
E
siCont
siNinj1
9 sec
18 sec
27 sec
a
b

Figure 26. Ninjurin1 knock-down Raw264.7 cells by RNAi decrease membrane protrusion formation and cell motility. (A) Control (siCont) or Ninjurin1 RNAi (siNinj1) was applied to Raw264.7 cells. After 24 hr, the Raw264.7 cells were fixed with 4% PFA and were stained with Alexa-546 phalloidin (red) and anti-Ninjurin1 antibody (Ab_{1-15}, green). Representative images are shown. Lamellipodia- or filopodia-like protrusion is denoted by white or yellow arrowheads, respectively. Scale bar = 50 μm. (B) Western blot analysis of siCont and siNinj1 Raw264.7 cells. Actin is the internal loading control. (C) Lamellipodia- (~100 cells) or (D) filopodia-like protrusion (~20 cells) was quantified with Image J software (NIH): * $p < 0.05$, ** $p < 0.01$. (E) Membrane dynamics of siCont or siNinj1 Raw264.7 cells. DIC images were taken every 1.6 sec for 3 min by time-lapse microscopy and a red square region (a and b) was sequentially demonstrated. The red arrowhead indicates a pseudopodia-like foot and the yellow arrowhead demonstrates filopodia-like protrusion. Scale bar = 10 μm.

10. Overexpression of Ninjurin1 in Raw264.7 cells enhances membrane protrusion formation and cell motility.

To examine whether the overexpression of Ninjurin1 promotes membrane protrusion formation and cell motility, we generated stable Raw264.7 cells which constitutively express GFP or GFP-mNinj1. Microscopy observation (Figure 27A) and Western blotting (Figure 27B) validated the proper molecular weight (~44 kDa) and localization to the plasma membrane of GFP-mNinj1, indicating the successful construction of stable GFP or GFP-mNinj1 Raw264.7 cells. Unlike siNinj1 Raw264.7 cells, the lamellipodia- and filopodia-like protrusive activities of stable GFP-mNinj1 Raw264.7 cells are strong with a higher proportion of cell with protrusion and a higher average number and length of the membrane protrusion (Figure 27A, C, and D). To compare the dynamics of the membrane protrusion by the overexpressed Ninjurin1, highly magnified time-lapse imaging of stable GFP- or GFP-mNinj1 Raw264.7 cells was performed. As expected, the stable GFP-mNinj1 Raw264.7 cells showed not only dynamic wriggling of the cell body and membrane protrusion but also the generation of pseudopodia-like feet (Figure 27E). Moreover, to prove directly whether the overexpressed Ninjurin1 can enhance the migration of Raw264.7 cells, time-lapse imaging was performed for 6 hr under a microscope. GFP-mNinj1 Raw264.7 cells showed increased motility

with a higher velocity and a longer Euclidean distance compared to GFP Raw264.7 cells (Figure 27F and G). In transient myc-mNinj1-overexpressed Raw264.7 cells, Ninjruin1 is located on actin-rich membrane protrusion and enhances their formation (Figure 28) that is consistent with the observations of the stable GFP-mNinj1 Raw264.7 cells. Taken together, the overexpressed-Ninjurin1 enhances the formation and dynamics of membrane protrusion to promote cell motility and movement.

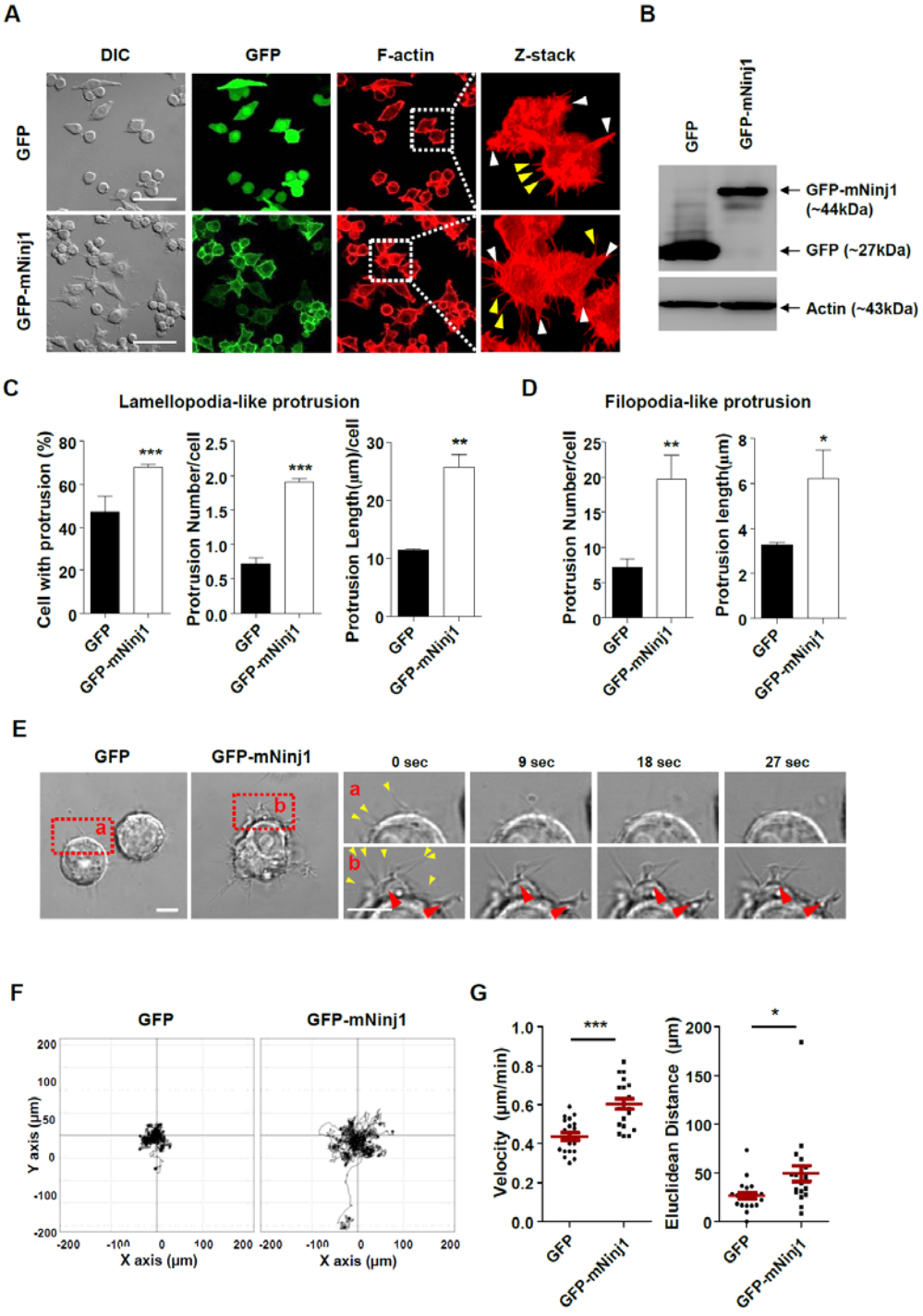
A
DIC
GFP
F-actin
Z-stack
GFP
GFP-mNinj1
B
GFP
GFP-mNinj1
GFP-mNinj1 (~44kDa)
GFP (~27kDa)
Actin (~43kDa)
C
Lamellopodia-like protrusion
Cell with protrusion (%)
Protrusion Number/cell
Protrusion Length(μm)/cell
D
Filopodia-like protrusion
Protrusion Number/cell
Protrusion length(μm)
E
GFP
GFP-mNinj1
0 sec
9 sec
18 sec
27 sec
F
GFP
GFP-mNinj1
Y axis (μm)
X axis (μm)
G
Velocity (μm/min)
Eluclidean Distance (μm)

Figure 27. Overexpression of Ninjurin1 in Raw264.7 cells increases membrane protrusion and cell motility. (A-B) The establishment of stable Raw264.7 cells to express GFP or GFP-mNinj1. Stable Raw264.7 cells fixed with 4% PFA were stained with Alexa-546 phalloidin (red). (A) Representative images are shown. Lamellipodia- or filopodia-like protrusion is depicted with white or yellow arrowheads, respectively. Scale bar = 50 μm. (B) Western blot analysis of GFP and GFP-mNinj1 Raw264.7 cells. Actin was used as an internal loading control. (C) Lamellipodia- (~100 cells) or (D) filopodia-like protrusion (~20 cells) was quantified with Image J software (NIH): * $p < 0.05$, ** $p < 0.01$, *** $p < 0.001$. (E) Membrane dynamics of GFP or GFP-mNinj1 Raw264.7 cells. DIC images were taken every 1.6 sec for 3 min by time-lapse microscopy and a red square region (a and b) was sequentially demonstrated. The red arrowhead indicates a pseudopodia-like foot and the yellow arrowhead demonstrates filopodia-like protrusion. Scale bar = 10 μm. (F and G) Basal motility of stable GFP or GFP-mNinj1 overexpressed Raw264.7 cells. Phase images of Raw264.7 cells were taken every 10 min for 6 hr by time-lapse microscopy. (F) Trajectory plot and (G) dot charts of the velocity and Euclidean distance were obtained from 30 cells. * $p < 0.05$, *** $p < 0.001$.

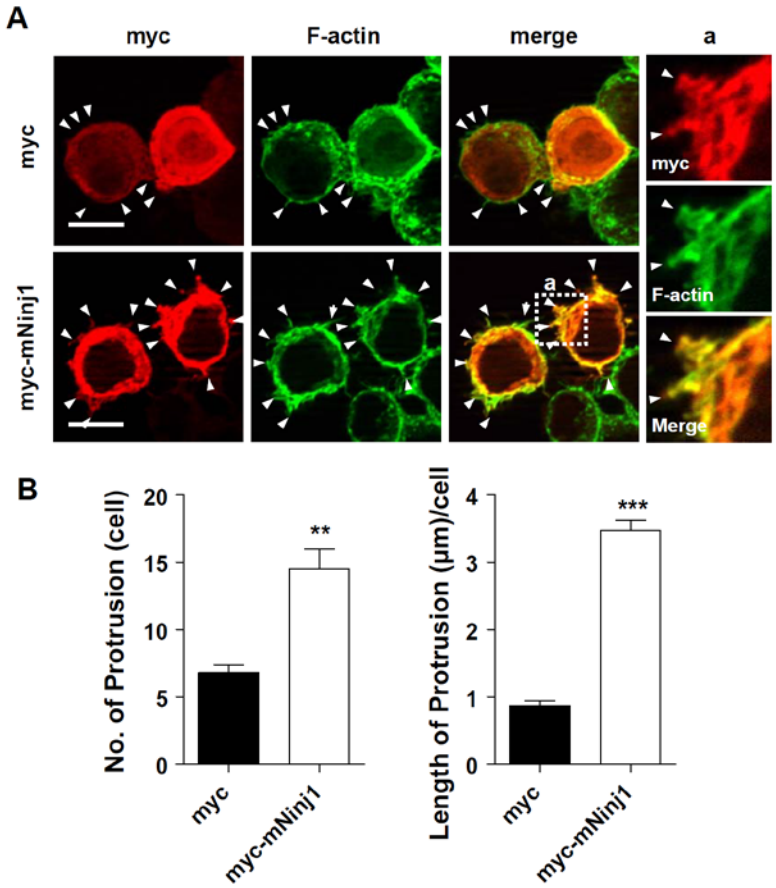

Figure 28. Formation of membrane protrusion by transient myc-mNinj1 overexpression in Raw264.7 cells. (A) Raw264.7 cells were transfected with myc-mock or myc-mNinj1. After 24 hr, double staining with FITC-phalloidin (green) and anti-myc antibody (red) was performed. White square box (a) indicate highly magnified image of the membrane protrusion region (B) The index of the number and length of protrusion (white arrow head) per cell was calculated by Image J software (NIH). Values were measured from ~40 cells. Scale bar = 10 μm. ** $p < 0.01$, *** $p < 0.001$

11. Ninjurin1 promotes adhesive and invasive protrusion toward the endothelial cell monolayer and facilitates subsequent TEM.

To precisely observe the distribution of Ninjurin1 in leukocyte when the leukocyte pass the endothelium monolayer, Raw264.7 cells transfected with myc-mNinjurin1 were added to a CSFE-labeled MBEC4 monolayer activated with TNFα and IFNγ. After 20 min of incubation, the samples were fixed with 4% paraformaldehyde (PFA) and were stained with anti-myc antibody. Highly magnified and three-dimensional Z-stack imaging allowed us to observe ameboid-shaped Raw264.7 cells passing through the MBEC4 cells monolayer with adhesive and invasive membrane protrusion (Figure 29). The overexpressed myc-mNinj1 was abundant in membrane protrusion of Raw264.7 cells (Figure 29), implying that Ninjurin1 is crucial for membrane protrusion formation with localization at the leading edge of Raw264.7 cells penetrating across the MBEC4 cell monolayer.

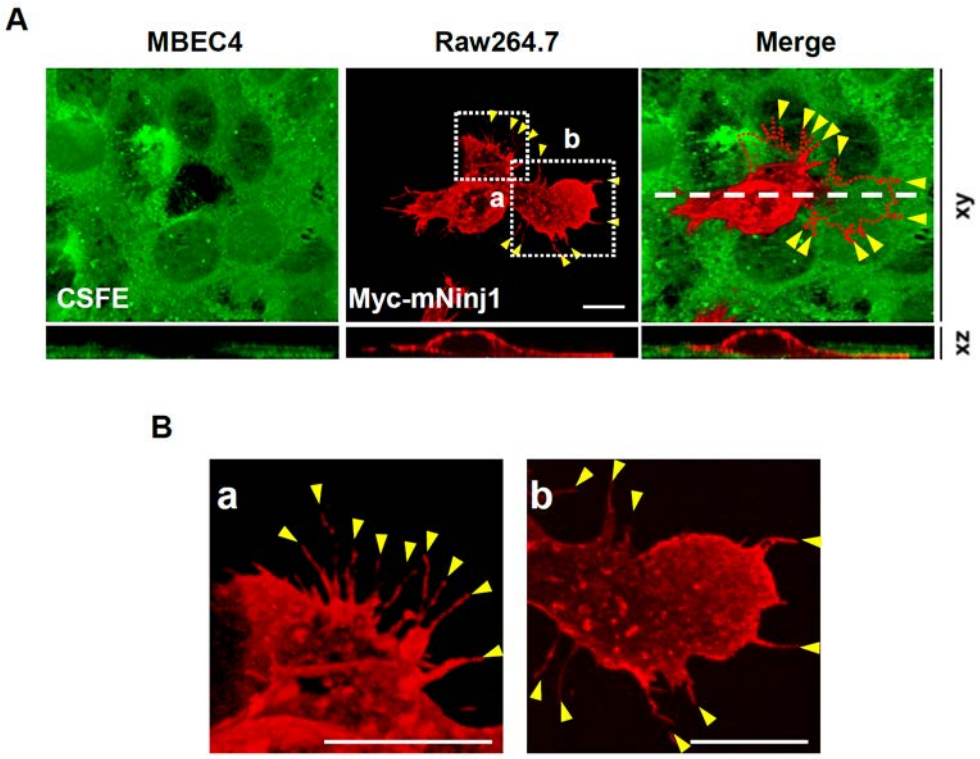

Figure 29. Ninjurin1 enhances invasive membrane protrusion across MBEC4 monolayer. Raw264.7 cells (red) transfected with myc-mNinj1 WT were added onto a 5 μM CSFE-labeled MBEC4 monolayer (green) for 20 min and Z-stack images were taken. The red dotted line (left) denotes the schematic boundary of the bottom side of the Raw264.7 cells penetrating across the MBEC4 monolayer. The white dotted line shows the sectioned region used for Z-stack imaging. Yellow arrowheads indicate Ninjurin1-rich protrusive regions. Scale bar = 10 μm.

To examine whether the ability to generate membrane protrusion is necessary for successful TEM, we used an *in vitro* modified Boyden chamber assay and compared the TEM activity levels of Ninjurin1 KO BMDMs, stable GFP-mNinj1 or RNAi Ninjurin1 knock-down Raw264.7 cells across monolayer of MBEC4 cells. The Ninjurin1-deficient BMDMs (Figure 30A) and siNinj1 Raw264.7 cells (Figure 30B) showed less TEM activity than the WT BMDMs and the siCont Raw264.7 cells, respectively. In contrast, stable GFP-mNinj1 Raw264.7 cells showed increased TEM activity compared to GFP Raw264.7 cells (Figure 30C). These results suggest that Ninjurin1 promotes membrane protrusion and, in turn, TEM across the endothelial monolayer.

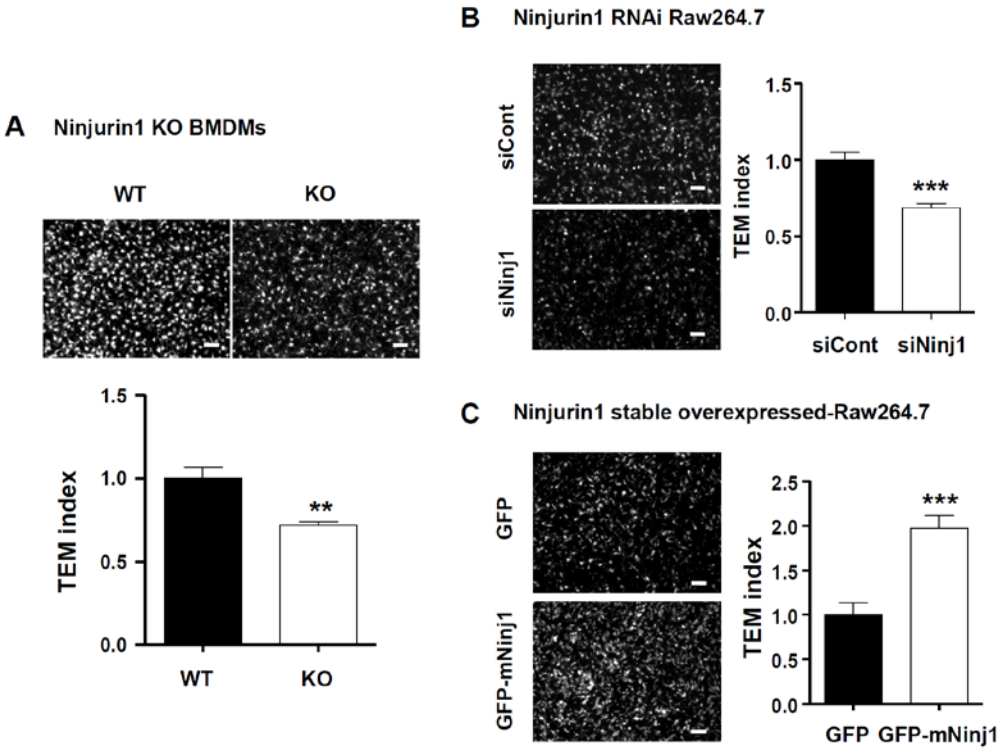

Figure 30. Ninjurin1 enhances TEM activity across MBEC4 monolayer. (A-C) TEM activity of Ninjurin1-deficient BMDMs (A), siNinj1 (B), and GFP-mNinj1 Raw264.7 cells (C) according to a modified Boyden chamber assay. Each cell, labeled with 5 μM CSFE for 5 min, was added onto the MBEC4 monolayer containing 10 ng/ml TNFα and INFγ in lower chamber. After 12 hr, the migrated cells were visualized using microscopy. Representative images are shown (top or left), and a transmigration index (bottom or right) is shown as relative to the WT BMDMs, siCont, or GFP Raw264.7 cells normalized to 100% in each case: ** $p < 0.01$, *** $p < 0.001$, Scale bar = 50 μm.

12. Ninjurin1-induced membrane protrusion formation depends not only on Rac1 activation but also on Src and PI3K pathway.

As Ninjurin1 mediates TEM by enhancing the membrane protrusions, the mechanism of how Ninjurin1 forms membrane protrusion should be explored. The Rho family of small GTPases, RhoA, Rac1, and Cdc42 regulates the cytoskeletal rearrangements underlying morphological transformations such as lamellipodia and filopodia (Heasman & Ridley, 2008). A considerable amount of evidence demonstrates that the Rho family of GTPases is also involved in leukocyte trafficking (Cernuda-Morollon & Ridley, 2006) (Figure 31). We therefore examined the basal activity of these small GTPases in stable GFP-mNinj1 or in siNinj1 Raw264.7 cells. In GFP-mNinj1 Raw264.7 cells, RhoA, Rac, and Cdc42 were significantly activated (Figure 32A) compared to the GFP Raw264.7 cells. In contrast, the Rac activity was selectively reduced in siNinj1 Raw264.7 cells, whereas RhoA and Cdc42 activity levels were similar to that of siCont Raw264.7 cells (Figure 32B). Therefore, the Rac activity can regulate the membrane protrusion formation at the downstream of Ninjurin1, which is supported in a study of NSC23766, a Rac1 specific inhibitor (Gao et al, 2004). Treatment with NSC23766 in GFP-mNinj1 Raw264.7 cells significantly decreased the protrusion properties of Ninjurin1 in terms of the percentages of cell with protrusion, the average number of cells, and the length per cell (Figure

32C and D). Taken together, Rac1 activation is required for Ninjurin1-mediated membrane protrusion formation and cell motility.

Furthermore, podosome is a specialized structure on ventral actin-rich membrane extension of cells that seems to share a common mechanism with lateral membrane protrusion. As the Src and PI3K pathway is crucial for podosome formation (Symons, 2008), we examined its contribution to Ninjurin1-mediated protrusion formation using pharmacological inhibitors. Treatment with PP2 or LY29004, a Src inhibitor and a PI3K inhibitor, respectively, significantly inhibited protrusion formation in GFP-mNinj1 Raw264.7 cells (Figure 33A and B). Collectively, Ninjurin1-induced protrusion formation relies on not only the activation of Rac1 but also on the Src and PI3K pathway.

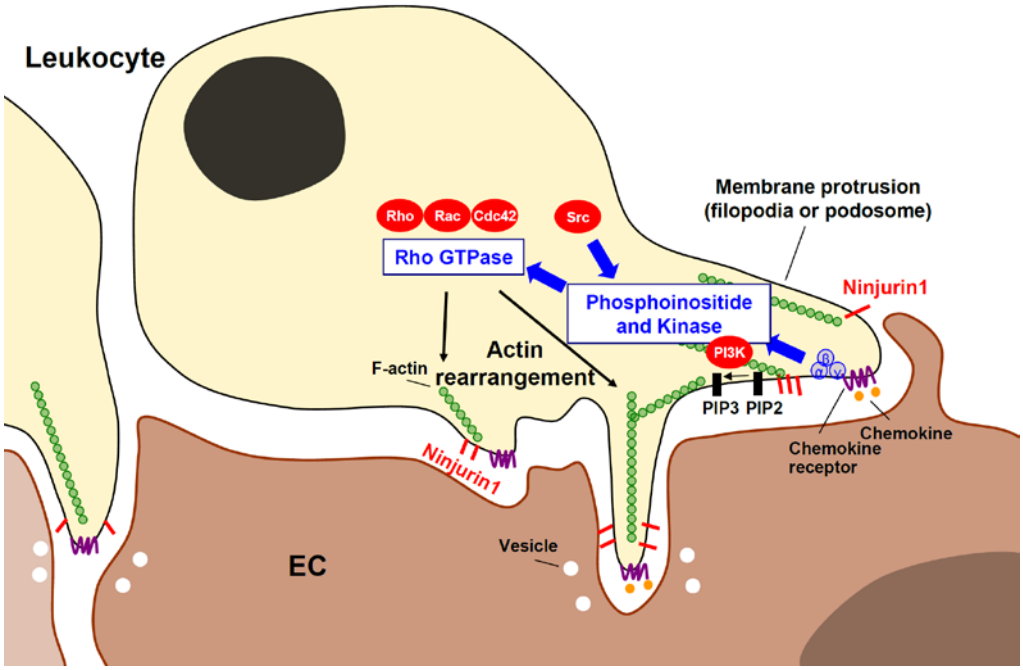

Figure 31. Molecular mechanisms of membrane protrusion formation by Ninjurin1

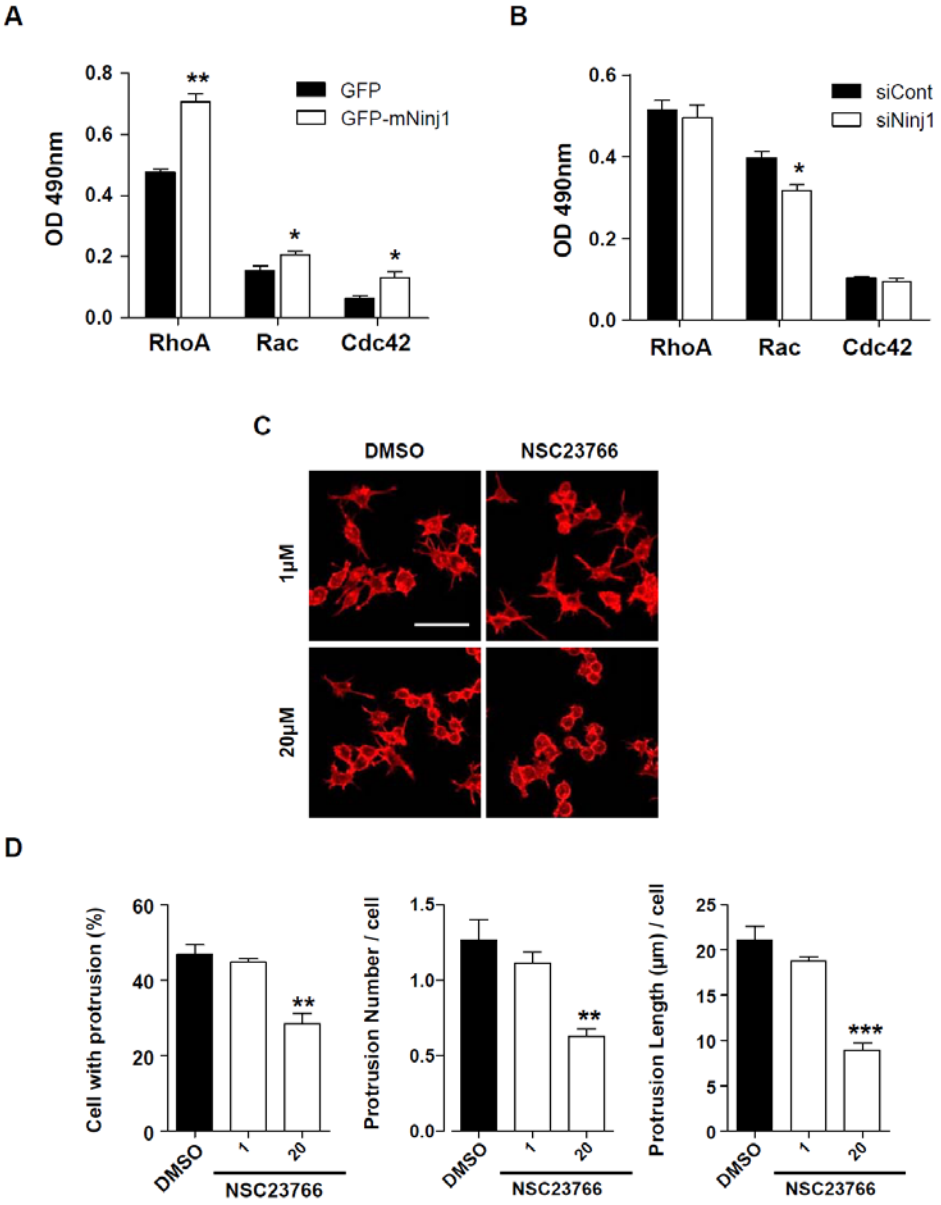
A
OD 490nm
0.8
0.6
0.4
0.2
0.0
**
*
*
GFP
GFP-mNinj1
RhoA
Rac
Cdc42
B
OD 490nm
0.6
0.4
0.2
0.0
*
siCont
siNinj1
RhoA
Rac
Cdc42
C
DMSO
NSC23766
1μM
20μM
D
Cell with protrusion (%)
60
40
20
0
**
DMSO
1
20
NSC23766
Protrusion Number / cell
1.5
1.0
0.5
0.0
**
DMSO
1
20
NSC23766
Protrusion Length (μm) / cell
25
20
15
10
5
0
***
DMSO
1
20
NSC23766

Figure 32. Rac1 activation are required for Ninjurin1-mediated membrane protrusion formation. (A-B) Analysis of the activity of small GTPases, RhoA, Rac, and Cdc42 in GFP-mNinj1 Raw264.7 cells (A) or siNinj1 (B) using an enzyme-linked assay. * $p < 0.05$, ** $p < 0.01$. (C-D) Membrane protrusion is shown in GFP-mNinj1 Raw264.7 cells after treatment with the NSC23766, a Rac1 inhibitor. NSC23766 (20 μM) and equivalent amounts of DMSO were treated to GFP-mNinj1 Raw264.7 cells for 3 hr. After fixation with 4% PFA, the cells were stained with Alexa-546 phalloidin (red). (C) Representative images are shown, and (D) values were measured from ~100 cells in three independent experiment. Scale bar = 50 μm. ** $p < 0.01$, *** $p < 0.001$.

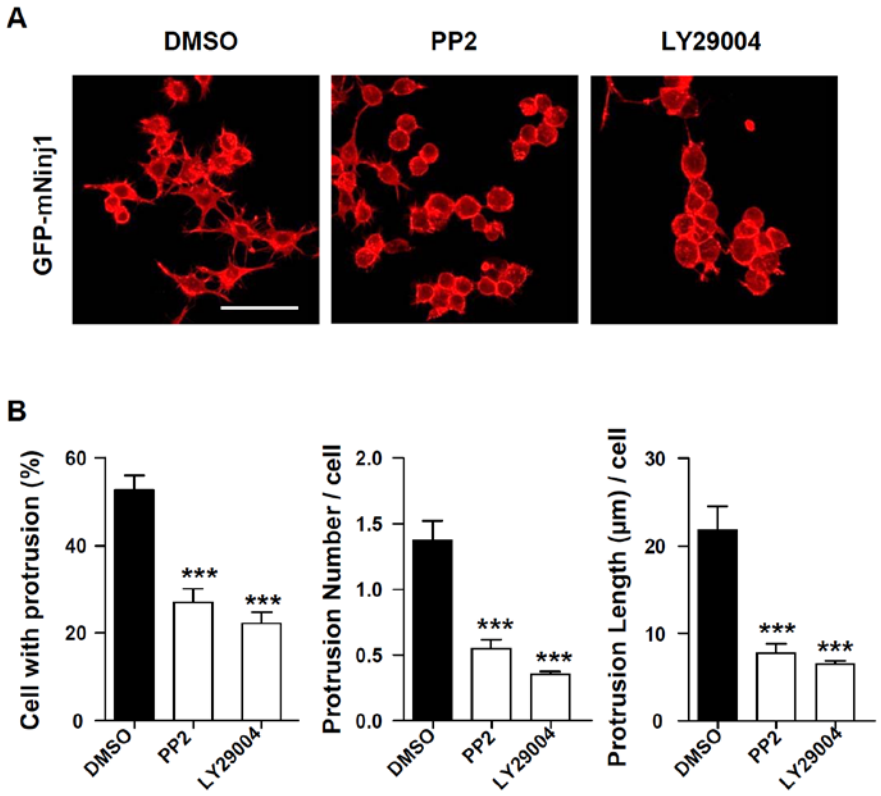

Figure **33**. **Src, PI3K pathways are required for Ninjurin1-mediated membrane protrusion formation.** The membrane protrusion formation of GFP-mNinj1 Raw264.7 is shown after treatment with PP2 (20 μM) and LY29004 (20 μM), a Src inhibitor and a PI3K inhibitor, respectively. One of the inhibitors or DMSO was added in an amount of 20 μM to GFP-mNinj1 Raw264.7 cells. After 3 hr, the Raw264.7 cells were fixed with 4% PFA and were stained with Alexa-546 phalloidin (red). (A) Representative images are shown, and (B) the values were measured from ~100 cells of three independent experiments. Scale bar = 50 μm. *** $p < 0.001$.

In this part, we defined a precise regulatory mechanism of Ninjurin1 on leukocyte trafficking. The dual functions of Ninjurin1, adhesive and protrusive activity were suggested depending on the steps of leukocyte trafficking. Ninjurin1 overexpresion is enhanced adhesion between BV2 cells and HBMECs and Ninjurin1 KO mice showed decreased adherence of leukocyte to retinal vessels in EIU (Figure 15). In addition, a custom-made antibody, $Ab_{26\text{-}37}$, and cyclic peptide, $cPEP_{26\text{-}37}$, specific to the homophilic binding domain of the N-terminal ectodomain of Ninjurin1 decreased adhesion and TEM activity *in vitro* and attenuated EAE susceptibility effectively (Figure 16-19). These results clearly demonstrated the contribution of Ninjurin1 in leukocyte-endothelium adhesion inflammatory conditions.

Furthermore, with primary cultured BMDMs, RNAi, and overexpressing Raw264.7 cells as well as time-lapse live cell imaging under high magnification, we proved the relevance to membrane protrusion formation, cell motility, and the subsequent TEM by Ninjurin1 (Figure 20-30) in a Rac1-, Src-, and PI3K-dependent manner (Figure 32 and 33). Altogether, Ninjurin1 contributes to the later crawling and transmigration stages via formation of membrane protrusion as well as to the initial rolling and adhesion stages via homophilic binding (Figure 34).

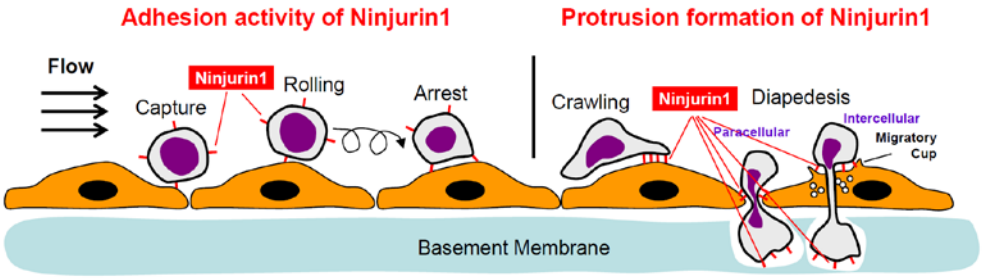

Figure 34. Schematic illustration of the stage-specific contribution of Ninjurin1 on the transmigration of leukocyte across the endothelium. Ninjurin1 plays a role in not only the initial adhesion step by its homophilic binding activity but also the later crawling and transmigration steps by membrane protrusion formation in leukocyte.

II. Posttranslational modifications of Ninjurin1

Some adhesion molecules involved in leukocyte trafficking alter their binding property by proteolytic cleavage such as CD44 (Cichy & Pure, 2003), L-selectin (Smalley & Ley, 2005), and Fractalkine (Imai et al, 1997). In *Drosophila*, the N-terminal ectodomain of Ninjurin A, having 98% homology with that of mouse Ninjurin1, can be cleaved by MMP and triggers loss of cell adhesion (Zhang et al, 2006). Glycosylation of adhesion molecules likes selectins and CD44 is involved in regulation of the immune system and is crucial for cell homing and recruitment (Bartolazzi et al, 1996; McEver & Zhu, 2010; Mitoma et al, 2007; Sperandio et al, 2009) (Figure 35). N-glycosylation of Ninjurin1 also predicted by software like NetGlyc 1.0.

In this part, therefore, we explored the proteolytic cleavage and N-glycosylation of Ninjurin1 and their biological functions in inflammation.

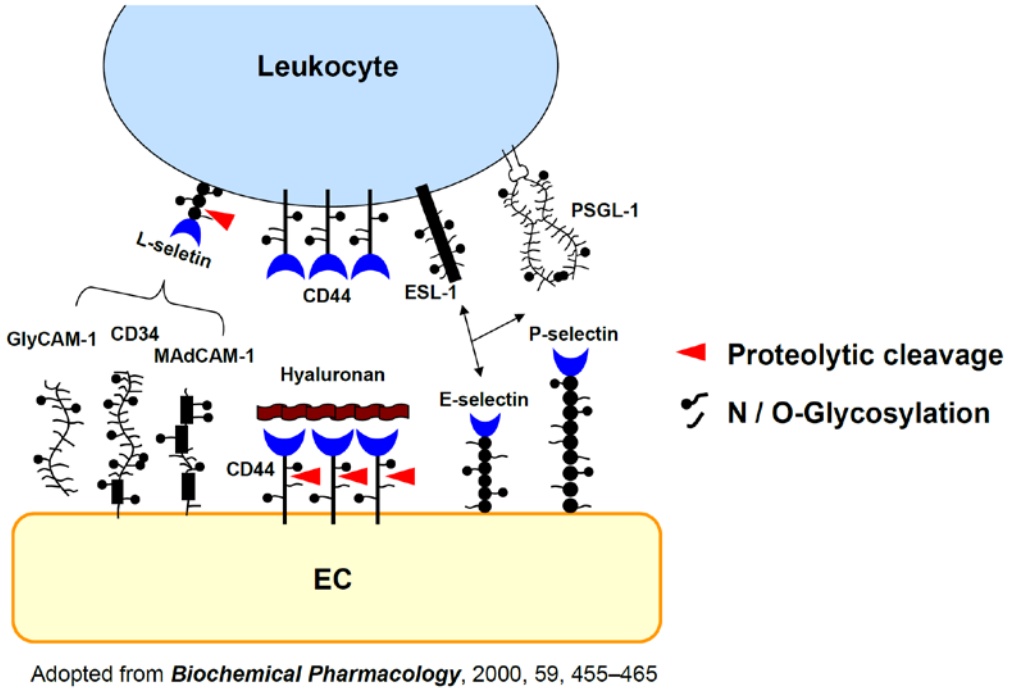

Figure 35. Posttranslational modifications, cleavage or glycosylation, of adhesion protein on the leukocyte and EC.

13. The N-terminal ectodomain of the overexpressed Ninjurin1 is cleaved *in vitro*.

To investigate whether mammalian Ninjurin1 can be cleaved, we constructed a couple of mouse Ninjurin1 plasmids tagged with Flag (Flag-mNinj1) at the N-terminus and with 3xFlag (3xFlag-mNinj1) at the C-terminus (Figure 36A). HEK293T cells overexpressed with Flag-mNinj1 produced one major band corresponding to the expected molecular weight (~ 23 kDa, black arrow) (Figure 36B), while 3xFlag-mNinjurin1 transfectants contained three additional bands (~ 15/16/19 kDa, red arrowheads) with molecular weights below the full-length (~ 21 kDa, black arrow) protein that were regarded as its cleaved fragments (Figure 34C). Interestingly, when PNGase F known as deglycosylation enzyme was treated 3xF-mNinj1 transfectants, two bands corresponding to 24 kDa and 19 kDa were disappeared, meaning them as glycosylated forms (Figure 36D). Next, we examined whether the cleaved fragments were secreted into the conditioned media (CM). After overexpressing of GFP-mNinj1 in HEK293T cells, CM was immunoprecipitated with anti-GFP antibody. Western blotting with anti-GFP antibody clearly showed the GFP-bearing fragments of Ninjurin1 in CM (Figure 36E). Collectively, these results indicate that Ninjurin1 can be cleaved at the N-terminal ectodomain and secreted into the CM *in vitro*.

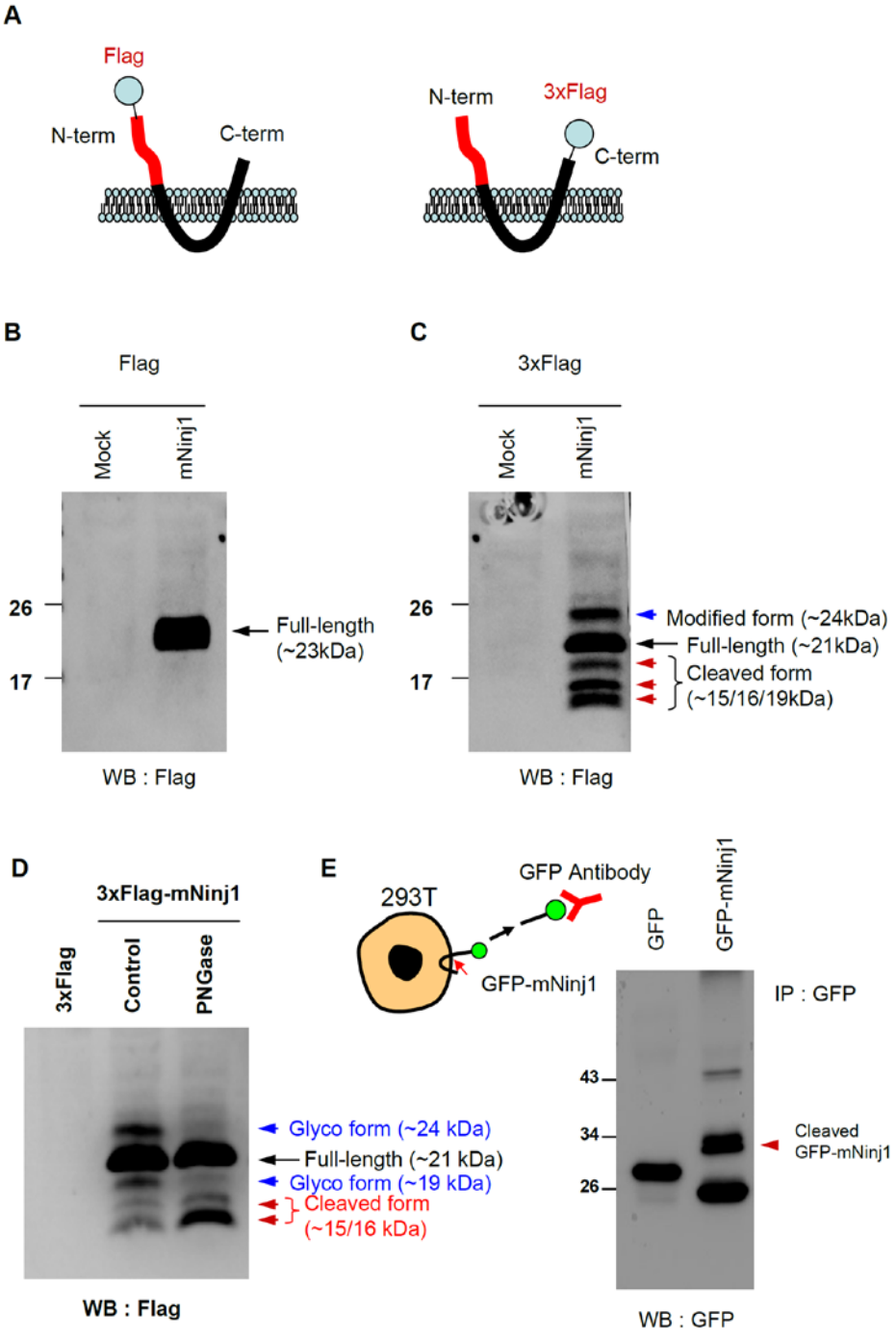
A
Flag
N-term
C-term
N-term
3xFlag
C-term
B
Flag
Mock
mNinj1
26
17
Full-length
(~23kDa)
WB : Flag
C
3xFlag
Mock
mNinj1
26
17
Modified form (~24kDa)
Full-length (~21kDa)
Cleaved form
(~15/16/19kDa)
WB : Flag
D
3xFlag-mNinj1
3xFlag
Control
PNGase
Glyco form (~24 kDa)
Full-length (~21 kDa)
Glyco form (~19 kDa)
Cleaved form
(~15/16 kDa)
WB : Flag
E
293T
GFP Antibody
GFP-mNinj1
GFP
GFP-mNinj1
IP : GFP
43
34
26
Cleaved
GFP-mNinj1
WB : GFP

Figure 36. The cleavage and glycosylation of mouse Ninjurin1 *in vitro*. (A) Schematic diagram of the two N- or C-terminus tagging mouse Ninjurin1 plasmid, Flag-mNinj1 or 3xFlag-mNinj1, respectively. (B, C) Flag-mNinj1, 3xFlag-mNinj1 or their corresponding mock plasmids were overexpressed in HEK293T cells. After 24 hr, cells were harvested and Western blotting was performed with anti-Flag antibody. (B) Black arrow (~23 kDa) depicts the full-length Flag-mNinj1. (C) Black arrow (~21 kDa) indicates the full-length 3xFlag-mNinj1 and the red arrowheads indicate the expected cleavage fragments or its modified forms (~15/16/19 kDa). The blue arrowhead (~24 kDa) indicates presumptive modified form of the full-length 3xFlag-mNinj1. (D) After 3xF-mNinj1 transfectant was incubated with PNGase F, deglycosylation enzyme, for 1hr at 37℃, Western blotting was performed with anti-Flag antibody. The blue arrowhead depicts the glycosylated form of GFP-mNinj1 or its fragments. (E) GFP or GFP-mNinj1 was transfected in HEK293T cells, and their CM were collected and immunoprecipitated with anti-GFP antibody. Western blotting was performed with anti-GFP antibody. The red arrowhead depicts the cleaved GFP-mNinj1 fragments in CM.

14. The shedding fragments of Ninjurin1 are found in the mouse liver and kidney lysates.

To test whether the fragment of Ninjurin1 exist in mouse tissue, we used two antibodies, the Ab_{1-15} or $Ab_{139-152}$ specific to N- or C-terminal domain of mouse Ninjurin1, respectively (Figure 9). With these antibodies, we performed Western blot analysis with lysates from several organs in the C57BL/6 mouse. Both antibodies recognized the endogenous full-length Ninjurin1 (~17 kDa, black arrow) with similar patterns, whereas only $Ab_{139-152}$, not Ab_{1-15}, antibody was capable of detecting one or more additional bands (~ 11/12/15 kDa, red arrowheads) below full-length Ninjurin1 in the mouse liver and kidney lysates (Figure 37A). Western blotting with the $Ab_{139-152}$ antibody after immunoprecipitation of mouse liver lysates with each antibody, IgG isotype, Ab_{1-15}, and $Ab_{139-152}$ antibody, clarified that Ninjurin1 is fragmented at the N-terminal ectodomain region (Figure 37B). Moreover, the cleaved bands in liver or kidney lyastes of Ninjurin1 KO mice were completely dissappeared that make Ninjurin1's cleavage clear (Figure 37C). Collectively, consistent with the *in vitro* observations, the fragmentations of the Ninjurin1 N-terminal ectodomain are found in the mouse liver and kidneys *in vivo*.

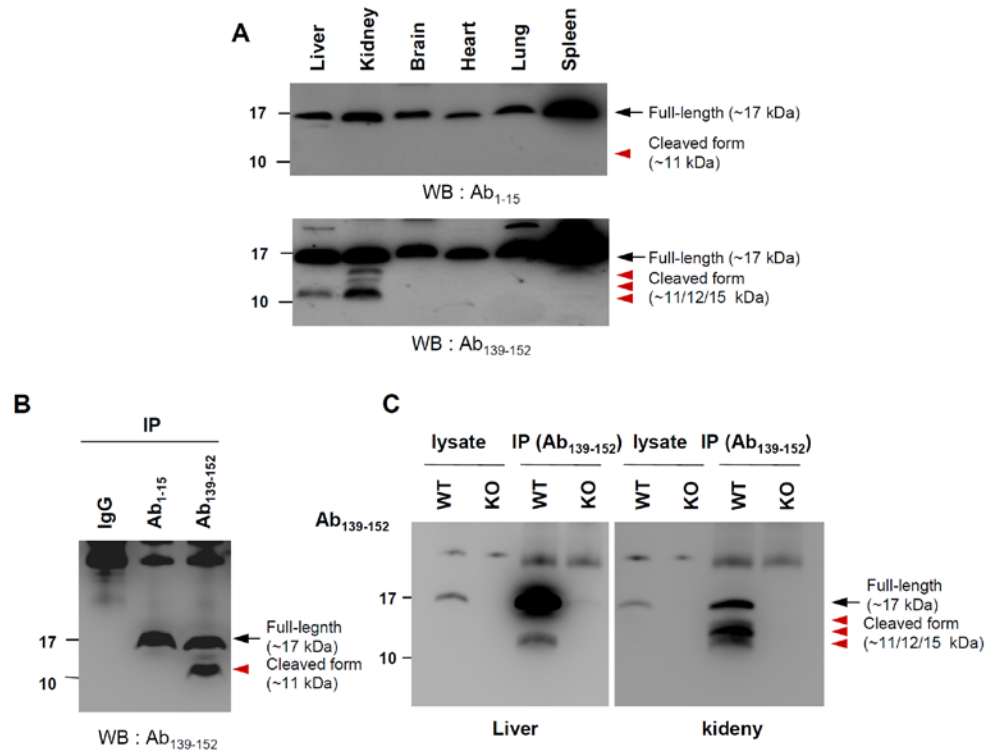

Figure 37. The cleavage of Ninjurin1 in the mouse liver and kidneys lysates.

(A) Several tissues were isolated from C57BL/6 mice and Western blot analysis was performed with $Ab_{1\text{-}15}$ or $Ab_{139\text{-}152}$. The black arrow indicates the endogenous mouse Ninjurin1 (~17 kDa) and the red arrowheads indicate bands shows its cleaved or modified forms (~11/12/15 kDa). (B) The liver lysates of mice were immunoprecipitated with normal rabbit IgG, $Ab_{1\text{-}15}$, or $Ab_{139\text{-}152}$ antibodies, and Western blot analysis was conducted with the $Ab_{139\text{-}152}$ antibody. The black arrow indicates the full-length mouse Ninjurin1 (~17 kDa) and the red arrowhead shows its cleaved form (~11 kDa). (C) Comparison of Ninjurin1 fragmentation in liver and kidney of WT and Ninjurin1 KO mice.

15. MMP9 contributes to the cleavages of Ninjurin1 in between Leu^{56} and Leu^{57}.

To elucidate which proteases might be responsible for the cleavage of Ninjurin1, we first screened putative proteases using various bioinformatics software such as Sitepredition (Verspurten et al, 2009) and MEROPS (Barrett, 2004). These softwares provided us with MMP2 and MMP9 as possible candidates (Figure 38A), and which is consistent with the report that MMP cleaves the N-terminal ectodomain of Ninjurin A in *Drosophila* (Zhang et al, 2006). Therefore, we speculated that MMP2 and/or MMP9 are able to shed mouse Ninjurin1. To prove this hypothesis, an *in vitro* MMP cleavage assay was performed as described in the *materials and methods*. MMP9 incubated with 4-aminophenylmercuric acetate (APMA), a chemical activator of MMPs, cleaved the full-length Ninjurin1 protein (~ 17 kDa, black arrow) into a smaller protein (~11 kDa, red arrowhead), while MMP2 did not (Figure 38B). Furthermore, truncated MMP9 with catalytic domain, Cat-MMP9, was able to cleave the Ninjurin1 protein, which was inhibited by treatment with GM6001, a pan-MMP inhibitor (Figure 38C), clearly demonstrating the role of MMP9 in the fragmentation of Ninjurin1.

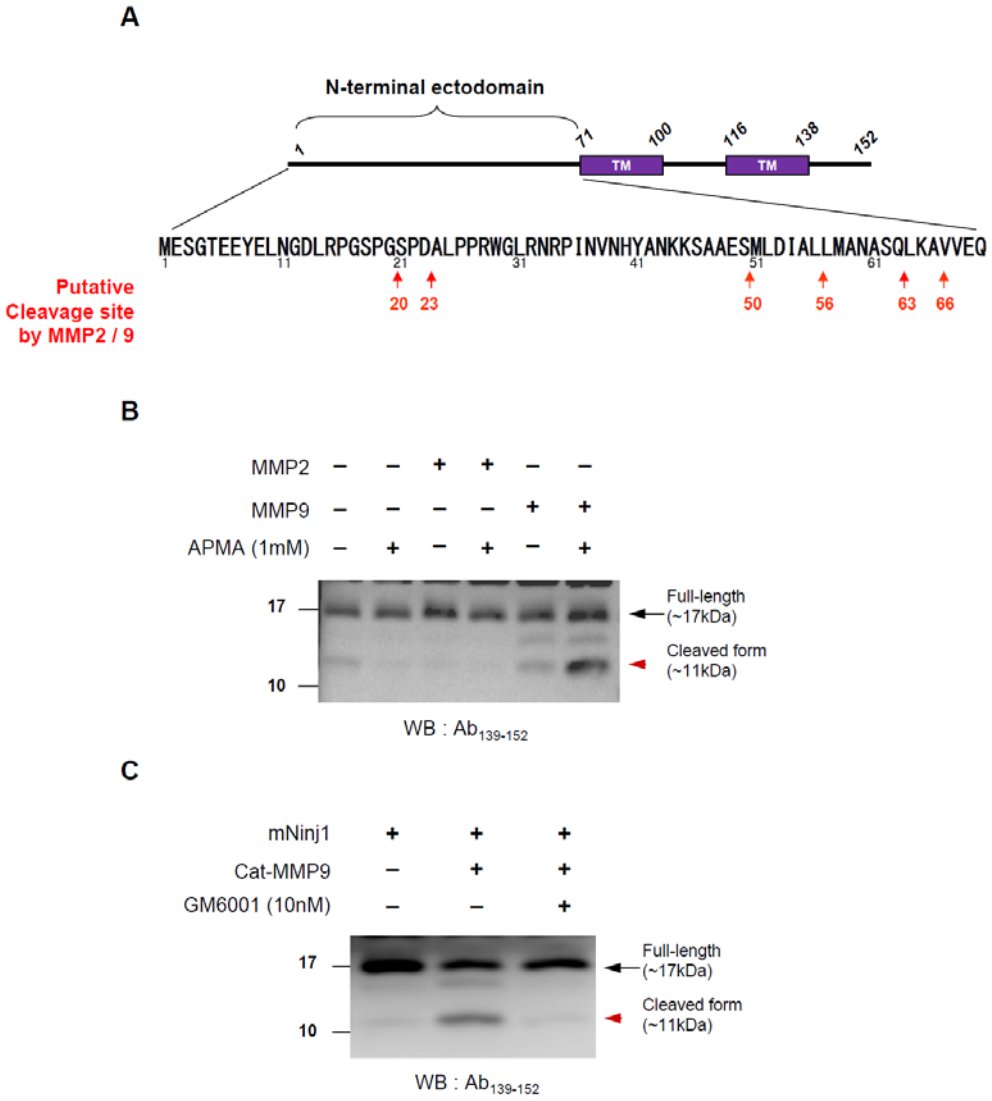
A
N-terminal ectodomain
1
71
100
116
138
152
TM
TM
MESGTEEYELNGDLRPGSPGSPDALPPRWGLRNRPINVNHYANKKSAAESMLDIALLMANASQLKAVVEQ
1
11
21
31
41
51
61
Putative
Cleavage site
by MMP2 / 9
20
23
50
56
63
66
B
MMP2 – – + + – –
MMP9 – – – – + +
APMA (1mM) – + – + – +
17
10
Full-length
(~17kDa)
Cleaved form
(~11kDa)
WB : Ab139-152
C
mNinj1 + + +
Cat-MMP9 – + +
GM6001 (10nM) – – +
17
10
Full-length
(~17kDa)
Cleaved form
(~11kDa)
WB : Ab139-152

Figure 38. Cleavage of Ninjurin1 mediated by MMP9. (A) Prediction of putative cleavage sites on mouse Ninjurin1 induced by MMP2 or MMP9. (B) The lysates from non-tagging mNinj1-overexpressed HEK293T cells were immunoprecipitated with $Ab_{1\text{-}15}$ antibody and incubated with recombinant MMP2 or MMP9 with or without p-aminophenylmercuric acetate (APMA, 1mM), a MMPs activator, for 16 hr at 37°C. The full-length mouse Ninjurin1 (black arrow, ~17 kDa) or its cleaved forms (red arrowhead, ~11 kDa) were identified by Western blotting for $Ab_{139\text{-}152}$ antibody. (C) The mouse Ninjurin1 protein immunoprecipitated with $Ab_{1\text{-}15}$ antibody from the non-tagging mNinj1 transfectants was incubated with truncated MMP9 with catalytic domain (Cat-MMP9). The cleavage of Ninjurin1 mediated Cat-MMP9 was prevented by incubation with GM6001 (10 nM), a pan-MMP inhibitor.

Next, to identify the cleavage sites on Ninjurin1 mediated by MMP9, we synthesized three kinds of peptides, PEP_{1-30}, PEP_{21-50}, and PEP_{41-70}, corresponding to the indicated region of the N-terminal ectodomain of mouse Ninjurin1 ($mNinj1_{1-70}$) (Figure 39A). After each peptide was incubated with the recombinant Cat-MMP9, the cleaved residues were determined by LC-MS analysis with Thermo Finnigan's LCQ Deca ion trap mass spectrometer. Neither PEP_{1-30} nor PEP_{21-50} was fragmented by MMP9 (Figure 39B and C). However, three additional peaks, ①, ②, and ③, were found in the ion chromatogram graph of PEP_{41-70} (Figure 39D). Mass to charge ratios (m/z) analysis revealed that each peak was matched with a cleaved fragment as follows: ② matched to PEP_{57-70} (LMANASQLKAVVEQ), ① matched to oxidized form of PEP_{57-70} at Methionine residue (ox-Met containing PEP_{57-70}), and ③ matched to PEP_{41-56}, YANKKSAAESMLDIAL) (Figure 39D). The LC-MS analysis results clearly demonstrated that the site for MMP9-mediated Ninjurin1 cleavage is in between Leu^{56} and Leu^{57} on its N-terminal ectodomain.

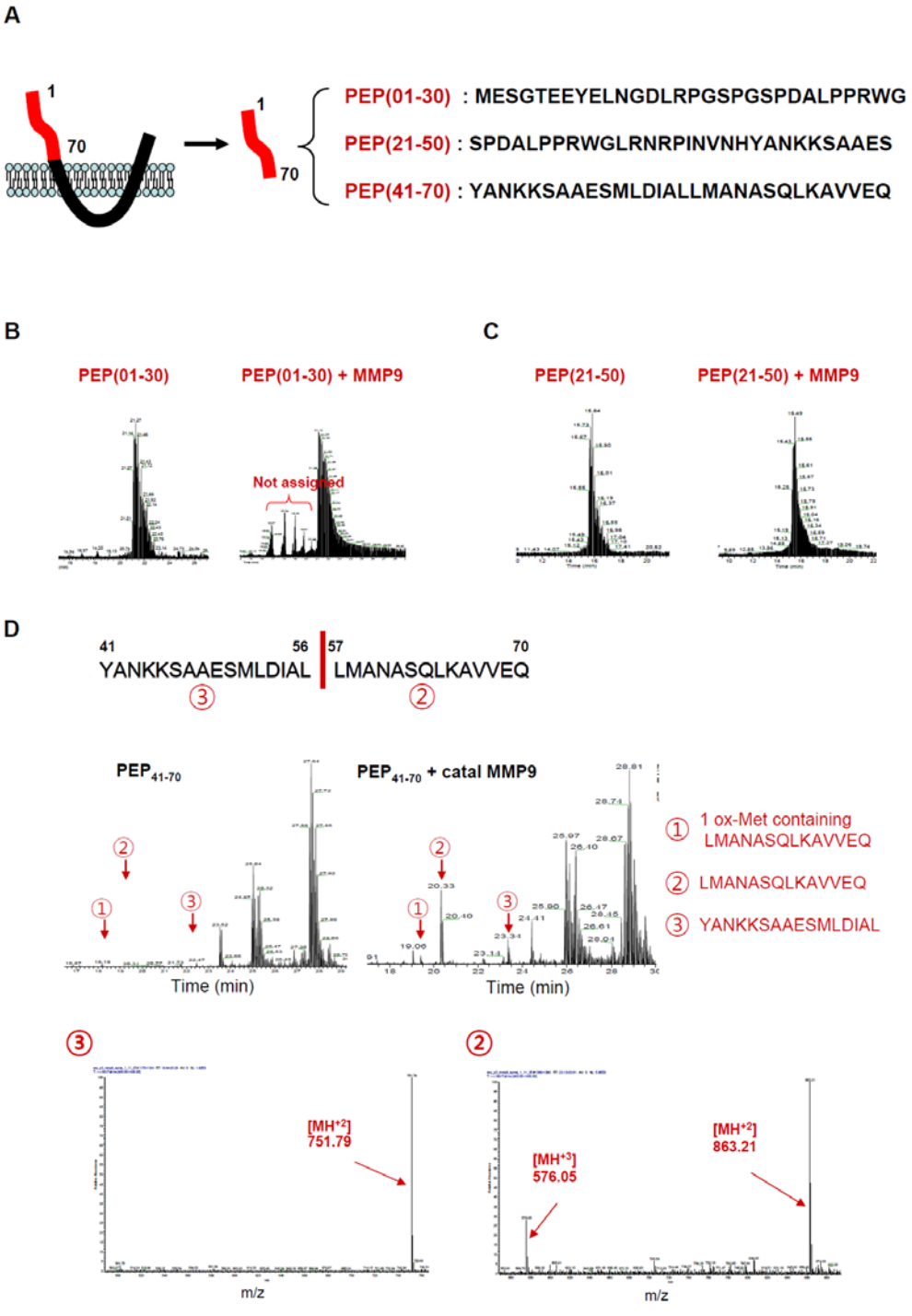
A
1
70
1
70
PEP(01-30) : MESGTEEYELNGDLRPGSPGSPDALPPRWG
PEP(21-50) : SPDALPPRWGLRNRPINVNHYANKKSAAES
PEP(41-70) : YANKKSAAESMLDIALLMANASQLKAVVEQ
B
PEP(01-30)
PEP(01-30) + MMP9
Not assigned
C
PEP(21-50)
PEP(21-50) + MMP9
D
41
56
57
70
YANKKSAAESMLDIAL
LMANASQLKAVVEQ
③
②
PEP41-70
PEP41-70 + catal MMP9
Time (min)
Time (min)
① 1 ox-Met containing LMANASQLKAVVEQ
② LMANASQLKAVVEQ
③ YANKKSAAESMLDIAL
③
[MH+2]
751.79
m/z
②
[MH+3]
576.05
[MH+2]
863.21
m/z

Figure 39. MMP9-mediated Ninjurin1 cleavage between Leu^{56} and Leu^{57}.

(A) Synthesis of three peptides corresponding with mouse Ninjurin1 ectodomain (red, aa 1~70). (B, C) LC graph after incubation of (B) PEP_{01-30} or (C) PEP_{21-50} with MMP9. (D) PEP_{41-70} corresponding to aa 41-70 on mouse $Ninjurin1_{1-70}$ was synthesized. The incubation of PEP_{41-70} with MMP9 generated three additional peaks: ①, ②, and ③. MS analysis identified each peak as the cleaved fragments of PEP_{41-70} and its modified forms: ② matched with PEP_{57-70} fragment, ① matched with the oxidized-Methionine of PEP_{57-70}, and ③ matched with PEP_{41-56}, which is the remaining portion of PEP_{57-70}.

Based on our observation, there are likely at least two or more cleavage sites in the 3xFlag-mNinj1 protein *in vitro* (Figure 36C, red arrowheads) and in the endogenous Ninjurin1 in the mouse kidney lysates (Figure 37A, red arrowheads), respectively. To determine which band corresponds with the cleavage event between Leu^{56} and Leu^{57}, an additional 3xFlag-mNinjurin$1_{57\text{-}152}$ plasmid was designed to have the remaining portion of Ninjurin1 after cleavage and was compared to the full-length 3xFlag-mNinj1 plasmid. The overexpression of 3xFlag-mNinj$1_{57\text{-}152}$ in HEK293T cells generated a band corresponding to the lowest one (red arrowhead, ~15 kDa) among the products of the full-length 3xFlag-mNinj1 (Figure 40). Altogether, these results clearly suggest that MMP9 is responsible for the cleavage of Ninjurin1 between Leu^{56} and Leu^{57}.

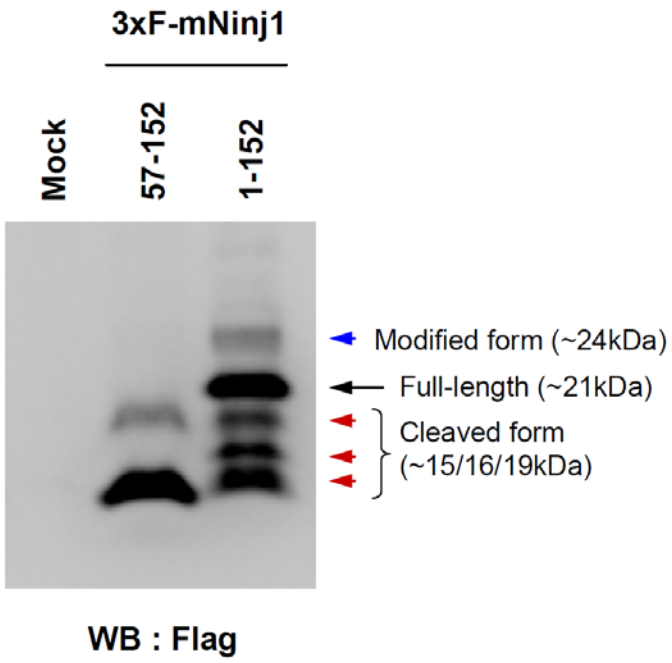

Figure 40. Identification of a product cooresponding to cleavage in between Leu[56] and Leu[57] of Ninjurin1. The 3xFlag-mNinj1$_{57\text{-}152}$, the remaining portion of the full-length 3xFlag-mNinj1 after cleavage, was transfected into HEK293T cells for 24 hr. The 3xFlag-mNinj1$_{57\text{-}152}$ generated a product corresponding to the smallest one (~ 15 kDa) among cleaved produces from the 3xFlag-mNinj1. The full-length 3xFlag-mNinj1 (~ 21 kDa), its cleaved forms (~ 15/16/19 kDa), or another modified one (~ 24 kDa) are shown with the black arrow, red arrowheads, or blue arrowhead, respectively.

16. The liberated N-terminal fragment of Ninjurin1 has chemotactic properties.

To explore the biological functions of the cleaved fragment of Ninjurin1 (mNinj1$_{1-56}$), its structural properties were estimated using computational methods: Garnier-Osguthorpe-Robson (GOR) methods for secondary structure prediction (Garnier et al, 1978) and DisEMBL database for the disordered region prediction (Linding et al, 2003). The mNinjurin1$_{1-56}$ contains the disordered N-terminal amino acids (1-11 aa), a β-sheet (15-39 aa), and a N- or C-terminal α-helix (1-10 aa and 40-56 aa) (Figure 41A). Intriguingly, several chemokines share a highly conserved tertiary structure consisting of a disordered N-terminal domain, a three-stranded anti-parallel β-sheet, and a C-terminal α-helix despite their low sequence similarity (Allen et al, 2007). Indeed, after the multiple alignments of mNinj1$_{1-56}$ with well-known chemokines including SDF-1α (Crump et al, 1997), fractalkine (Mizoue et al, 1999), and MIP-1β (Kim et al, 2001b) using T-coffee software, a consistency-based multiple sequence alignment program (Di Tommaso et al, 2011), the comparison of their secondary structures revealed a close structural similarity (Figure 41A). These results suggest that the soluble fragments of Ninjurin1 might have chemokine-like activity.

To prove the chemokine-like role of the cleaved Ninjurin1 fragment, a trans-well assay was performed. Since the GFP-mNinj1 transfectants contain the cleaved fragments in CM (Figure 36E), we examined the migration activity of Raw264.7 cells, mouse peritoneal macrophage cells, toward GFP or GFP-mNinj1 CM. Interestingly, the migration of Raw264.7 cells toward the GFP-mNinj1 CM was higher than that toward the GFP CM, and moreover, their activity was significantly decreased by neutralization of GFP-mNinj1 CM with $Ab_{1\text{-}15}$ antibody treatment (Figure 42). This result indicates that the liberated N-terminal ectodomain of Ninjurin1 could have a chemotactic activity.

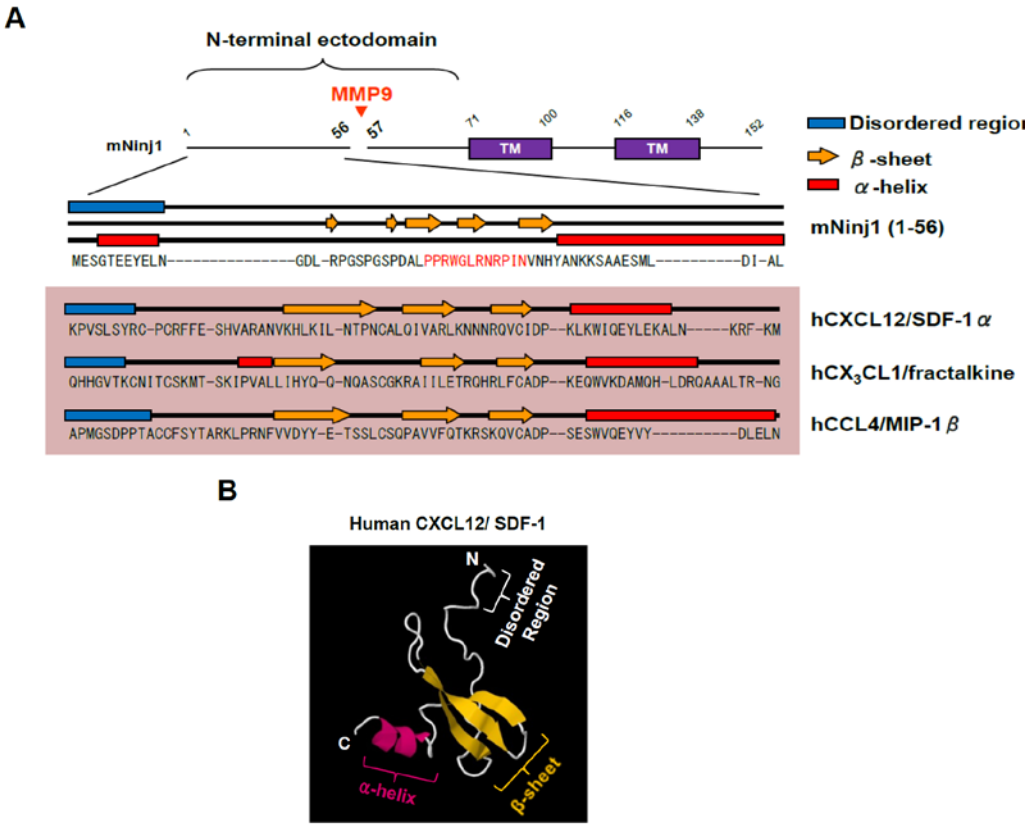
A
N-terminal ectodomain
MMP9
mNinj1
1
56
57
71
100
116
138
152
TM
TM
Disordered regio
β -sheet
α -helix
mNinj1 (1-56)
MESGTEEYELN----------GDL-RPGSPGSPDALPPRWGLRNRPINVNHYANKKSAAESML----------DI-AL
KPVSLSYRC-PCRFFE-SHVARANVKHLKIL-NTPNCALQIVARLKNNNRQVCIDP--KLKWIQEYLEKALN-----KRF-KM
hCXCL12/SDF-1 α
QHHGVTKCNITCSKMT-SKIPVALLIHYQ-Q-NQASCGKRAIILETRQHRLFCADP--KEQWVKDAMQH-LDRQAAALTR-NG
hCX3CL1/fractalkine
APMGSDPPTACCFSYTARKLPRNFVVDYY-E-TSSLCSQPAVVFQTKRSKQVCADP--SESWVQEYVY----------DLELN
hCCL4/MIP-1 β
B
Human CXCL12/ SDF-1
N
Disordered Region
C
α-helix
β-sheet

Figure 41. The fragment of Ninjurin1 has chemokine-like structure. The structural similarity of mNinj1$_{1-56}$ and well-known chemokines. (A) The disordered region, β-sheet, and α-helix are shown with blue rectangles, yellow arrows, and red rectangles, respectively. Human SDF-1α, fractalkine, MIP-1β, and mNinj1$_{1-56}$ were aligned by the program T-Coffee software (Di Tommaso et al, 2011). The structural information of each chemokines was obtained from previous NMR studies (Crump et al, 1997; Kim et al, 2001b; Mizoue et al, 1999). The structure of mNinj1$_{1-56}$ was predicted with bioinformatics software programs: Garnier-Osguthorpe-Robson method for secondary structure, DisEMBL for the disordered region, and NetNGly 1.0 for N-glycosylation site. TM; Transmembrane domain, Gly; N-glycosylation. (B) Well-known 3D structure of human CXCL12/SDF-1 α chemokine.

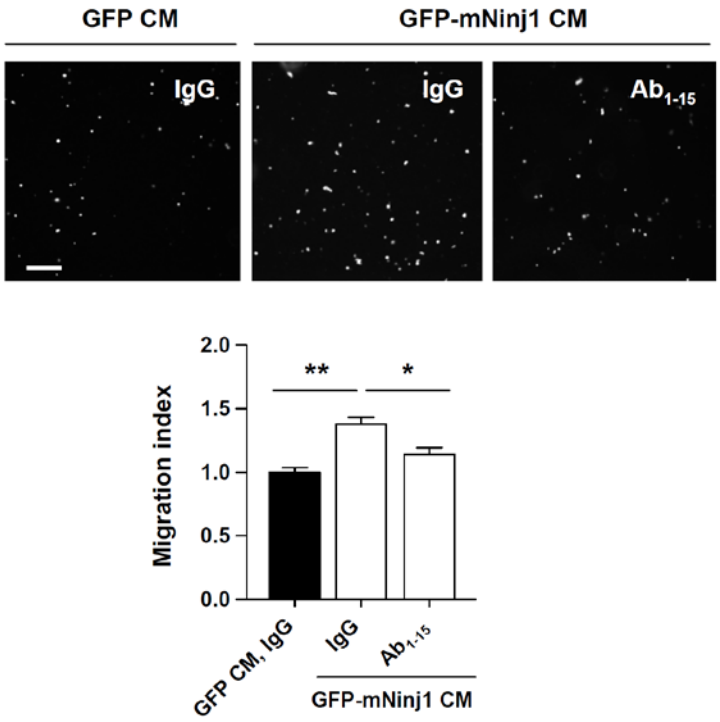

Figure 42. The liberated Ninjurin1 can attract Raw264.7 cells. The migration activity of Raw264.7 cells toward the liberated GFP-mNinj1 fragment. Raw264.7 cells labeled with CSFE (5 μM, 5 min) were added to the upper chamber of the trans-well and the CM from GFP or GFP-mNinj1 overexpressed-HEK293T cells in the slower chamber. GFP-mNinj1 CM was neutralized by incubation with either IgG isotype or Ab_{1-15} antibody (10 μg/ml). After 8 hr, the migrated cells were visualized under microscopy. Representative images are shown in (B), and the migration index (n=3) (C) is shown as a relative value to the GFP CM with IgG: * $p < 0.05$, ** $p < 0.01$, Scale bar = 100 μm.

17. N-glycosylation occurs on the Asn^{60} residues of the N-terminal ectodomain of Ninjurin1.

Glycosylation of adhesion molecules likes selectins and CD44 is involved in regulation of the immune system and is crucial for cell homing and recruitment(Bartolazzi et al, 1996; McEver & Zhu, 2010; Mitoma et al, 2007; Sperandio et al, 2009) (Figure 35). Consistent with existence of the glycosylated forms in 3xF-mNinj1 lysates (Figure 36D, blue arrowhead), myc/his-mNinj1$_{1\text{-}100}$ transfected HEK293T also showed an additional band over the full-length Ninjurin1. This band was removed by incubation with PNGase F (Figure 43A) and Tunicamycin, glycosylation inhibitor (Figure 43B), confirming the existence of N-glycosylated Ninjurin1. Since Ninjurin1 predicted to be N-glycosylated at Asn^{60} by NetNGlyc 1.0, a software of glycosylation prediction (Figure 44A), Asn^{60} was substituted to Ala^{60} (N60A). As expected, the upper band of myc/his-mNinj1$_{1\text{-}100}$ was disappeared in myc/his-mNinj1$_{1\text{-}100}$ N60A mutant transfectants (Figure 44B), indicating that Asn^{60} residue of Ninjurin1 is the site of N-glycosylation.

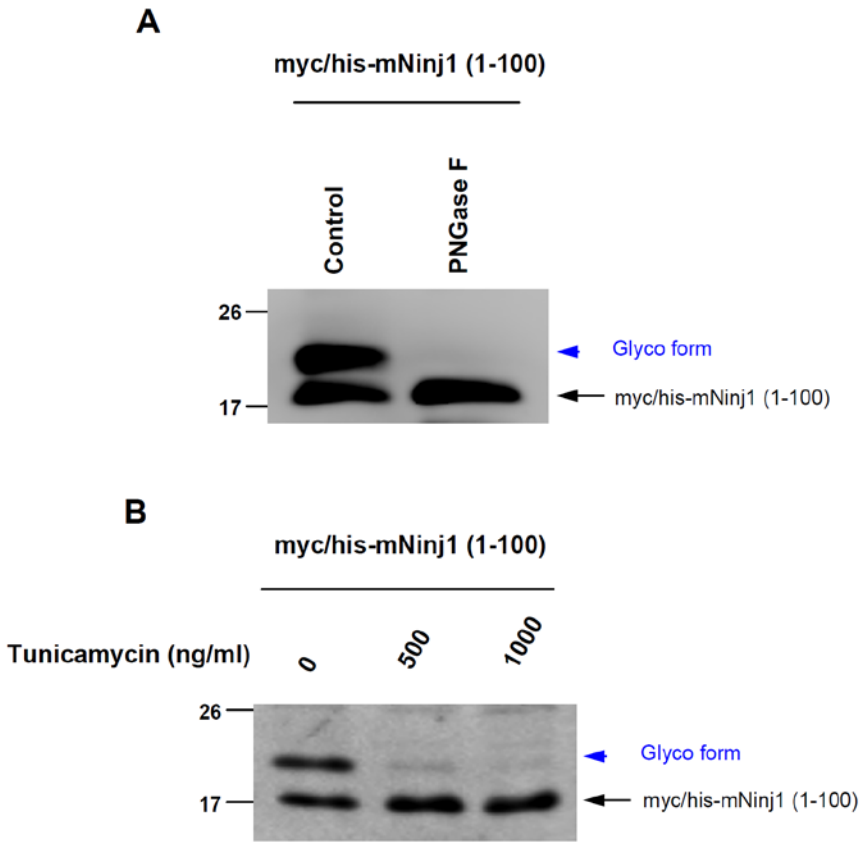

Figure 43. The existence of N-glycosylation on N-terminal ectodomain of Ninjurin1. myc/his- or myc/his-mNinj1$_{1\text{-}100}$ was transfected in HEK293T cells. After 24 hr, the lysates were analyzed by Western blotting. An additional product (blue arrowhead) was present above the full-length (black arrow) in the myc/his-mNinj1$_{1\text{-}100}$ transfectants. This band was removed by incubating with (A) PNGase F, a deglycosylation enzyme, or (B) Tunicamycin, a glycosylation inhibitor.

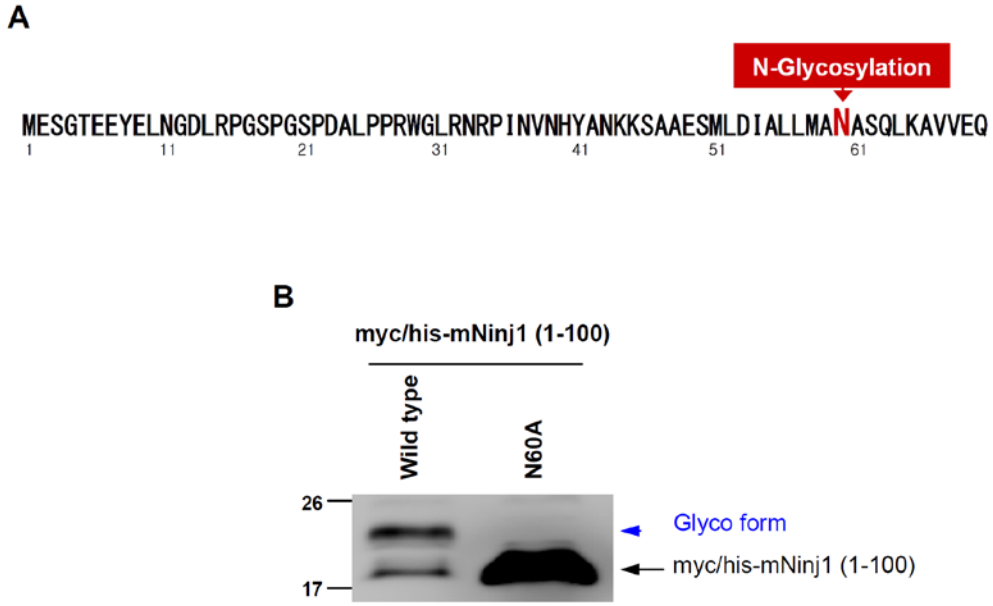

Figure 44. N-glycosylation occurs on the Asn^{60} residues of the N-terminal ectodomain of Ninjurin1. (A) The Asn^{60} residue (N, red arrow) on the mouse Ninjurin1 sequence is the putative N-glycosylation site predicted by NetNGlyc 1.0. (B) N-glycosylated myc/his-mNinj1$_{1\text{-}100}$ was disappeared in the N60A mutant transfectants which substituted Asn^{60} to Ala^{60}.

18. N-glycosylation of ninjurin1 regulates not only the formation of membrane protrusions and invadosomes but also its membrane localization and homophilic binding activity.

To explore whether N-glycosylated Ninjurin1 could alters the formation of membrane protrusions and podosomes, myc-mNinj1 WT or N60A mutant was overexpressed in Raw264.7 cells. Interestingly, the fillopodial membrane protrusions induced in the myc-mNinj1 WT transfectants were significantly reduced in myc-mNinj1 N60A mutant transfectants (Figure 45). Double staining with FITC-phalloidin showed that myc-mNinjurin1 WT was well-distributed through the region with actin-rich membrane protrusions, whereas myc-mNinj1 N60A mutants were not (Figure 45). These results suggest that the N-glycosylation of Ninjurin1 is crucial for the formation of membrane protrusions. Additionally, GFP-mNinj1 WT is efficiently targeted to the plasma membrane in HeLa cells, whereas GFP-mNinj1 N60A mutant is broadly distributed in the cytoplasm (Figure 46). Double staining with anti-calreticulin antibody, an endoplasmic reticulum (ER) marker (Figure 46A), or anti-giantin antibody, a Golgi apparatus marker (Figure 46B), revealed that GFP-mNinj1 N60A mutant is accumulated in ER and Golgi apparatus with impaired membrane localization (Figure 46A and B). Moreover, the proportion of GFP-mNinj1 WT or N60A mutant located to plasma membrane was

measured by flow cytometry. The intensity of allophycocyanin (APC) fluorescence demonstrating cell surface GFP-mNinj1 was higher in GFP-mNinj1 WT transfectant (57.6%) than in N60A mutants (33.7%) (Figure 46C).

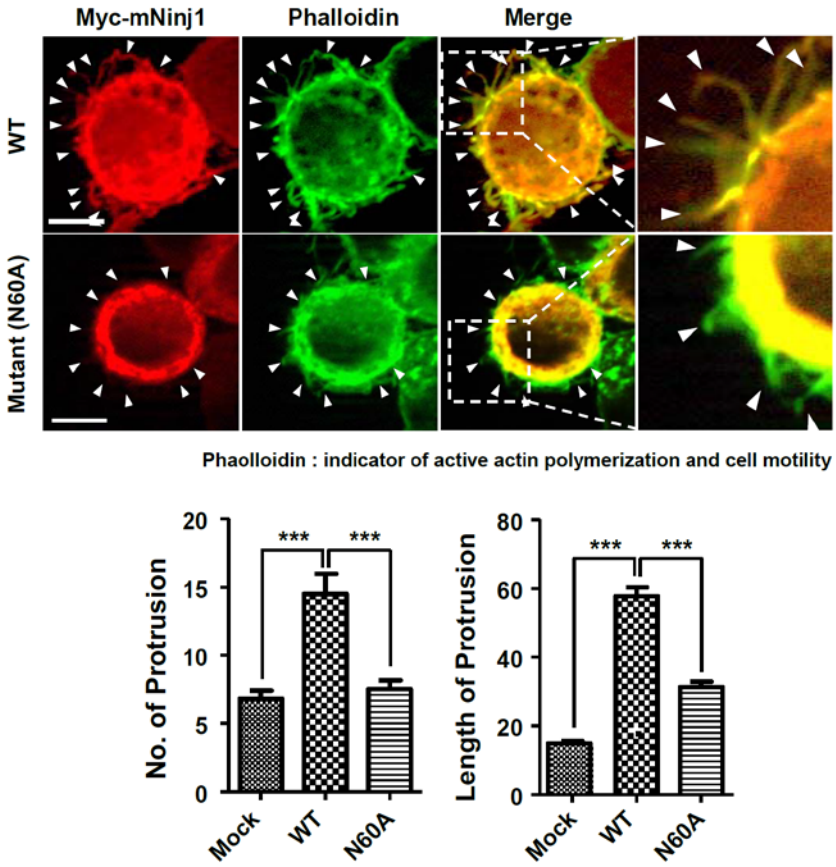

Figure 45. N-glycosylation of Ninjurin1 regulates the formation of membrane protrusions. (A) myc-mNinj1 WT or N60A mutant was overexpressed in Raw264.7 for a day and double staining with anti-myc antibody (red) and FITC-phalloidin (green) was performed. The number and length of the membrane protrusions (white arrow head) was decreased in the myc-mNinj1 N60A mutant transfectants. Values were obtained from ~40 cells from three independent experiments, **p<0.01. (B) The bar graph represents the number and length of protrusions per cell. Scale bar = 10μm.

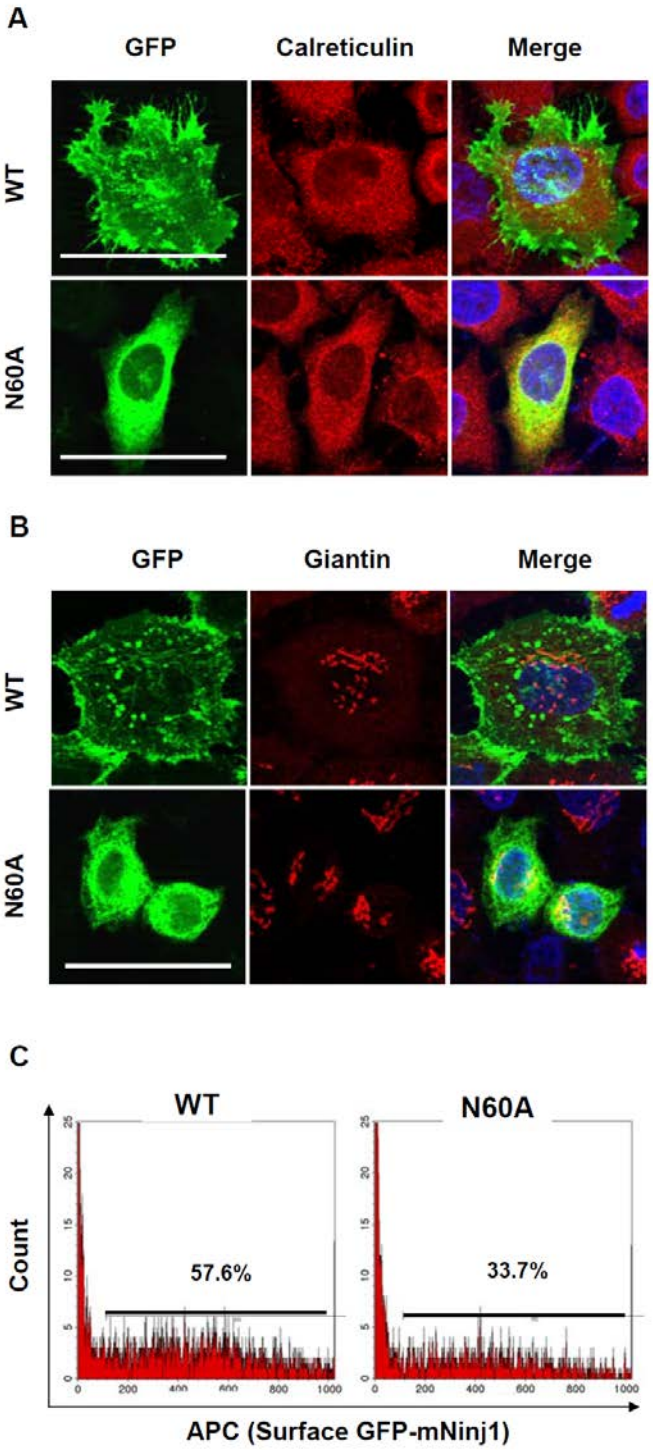
A
GFP
Calreticulin
Merge
WT
N60A
B
GFP
Giantin
Merge
WT
N60A
C
WT
N60A
Count
57.6%
33.7%
APC (Surface GFP-mNinj1)

Figure 46. N-glycosylation of Ninjurin1 regulates its membrane localization. (A, B) GFP-mNinj1 WT or N60A mutant was overexpressed in HeLa cells and double-stained with (A) anti-giantin antibody, Golgi marker, or (B) anti-calreticulin antibody, ER marker. GFP-mNinj1 N60A mutant was accumulated in the ER and Golgi apparatus. (C) GFP-mNinj1 WT or N60A mutant was transfected in HEK293T cells and the amount of GFP-mNinj1 WT or N60A mutant trafficking to the plasma membrane was determined by flow cytometry from three independent experiments.

19. N-glycosylation enhances Ninjurin1-mediated cell adhesion and TEM activity.

Additionally, we tested whether N-glycosylation might alter homophilic binding activity of Ninjurin1. Immunoprecipitation assay showed that the homophilic binding activity of Ninjurin1 was the most strongest between myc-/GFP-mNinj1 WT and WT, but was dramatically decreased between myc-/GFP-mNinj1 WT and N60A, and almost disappeared between myc-/GFP-mNinj1 N60A and N60A (Figure 47). These results suggest that N-glycosylation regulates cellular functions of ninjurin1 in two critical processes including plasma membrane trafficking and homophilic adhesion activity of Ninjurin1.

To determine direct effects of N-glycosylation of Ninjurin1 on leukocyte trafficking, we compared adhesion and TEM activity of myc-mNinj1 WT or N60A mutant-transfected Raw264.7 cells on monolayers of MBEC4 cells. The myc-mNinj1 WT-transfected Raw264.7 cells adhered more strongly to the MBEC4 cells monolayer than myc-mNinj1 N60A mutant transfectants (Figure 48A). Intriguingly, some populations of ameboid-shaped Raw264.7 cells were found on MBEC4 cells monolayer. Their number was higher in the myc-mNinj1 WT transfectants than in the myc-mNinj1 N60A mutant transfectants (Figure 48B). Furthermore, Raw264.7 cells overexpressing myc-

mNinj1 N60A mutant had weaker TEM activity across MBEC4 cells monolayer compared to that of myc-mNinj1 WT transfectants (Figure 48C).

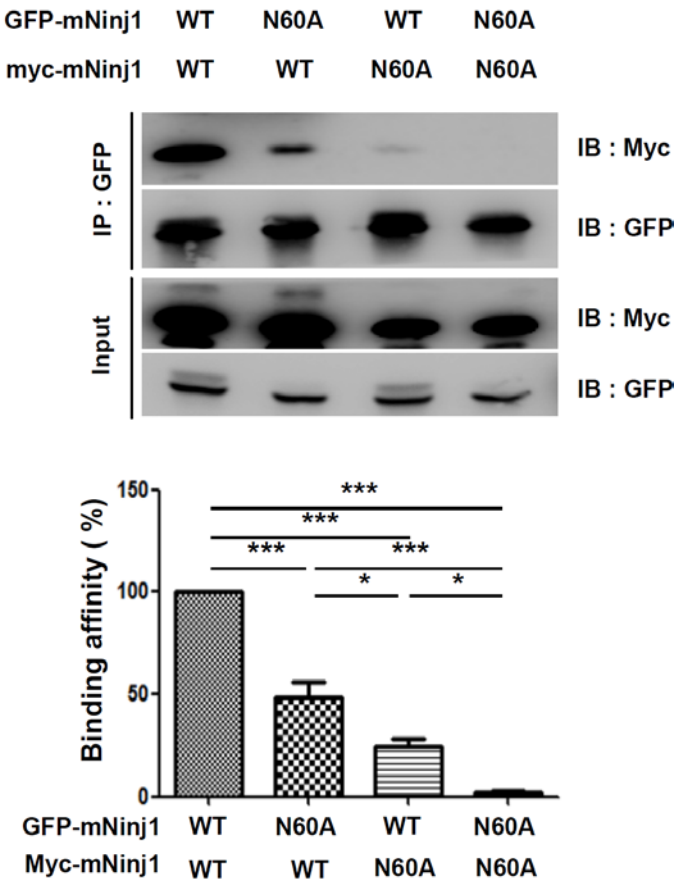

Figure 47. N-glycosylation of Ninjurin1 regulates homophilic binding activity. GFP-mNinj1 WT or N60A mutant and myc-mNinj1 WT or N60A mutant were transfected in HEK293T cells and each lysate were pull-downed with anti-GFP antibody. Binding activity is depended on the mutant property of GFP- or myc-mNinj1. *p<0.05, **p<0.01, ***p<0.001.

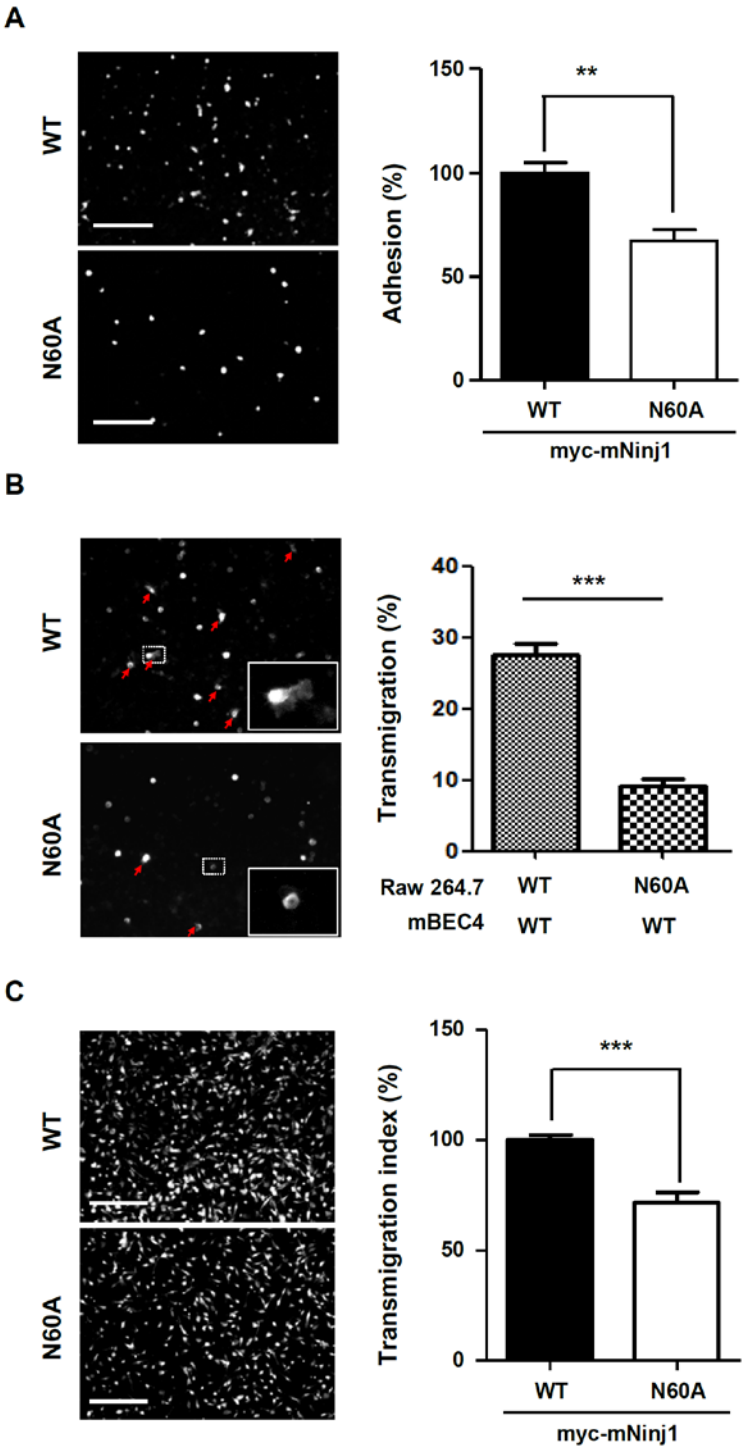
A
WT
N60A
Adhesion (%)
150
100
50
0
**
WT
N60A
myc-mNinj1
B
WT
N60A
Transmigration (%)
40
30
20
10
0
***
Raw 264.7 WT N60A
mBEC4 WT WT
C
WT
N60A
Transmigration index (%)
150
100
50
0
***
WT
N60A
myc-mNinj1

Figure 48. N-glycosylation enhances Ninjurin1-mediated cell adhesion and TEM activity. (A) Raw264.7 cells were transfected with myc-mNinj1 WT or N60A mutant and labeled with 5μM CSFE for 10min, and then, added to TNFα- and INFγ-stimulated MBEC4 monolayer for 15min, Adherent Raw264.7 cells were visualized and counted (n=3). Representative images are shown (left) and the binding index is shown as relative to the myc-mNinj1 WT transfectants, normalized to 100%. Scale bar = 50μm. **p<0.01. (B) Raw264.7 cells (red) transfected with myc-mNinj1 WT or N60A mutant were added onto CSFE-labeled MBEC4 monolayers (green) (n=3) and stained with anti-myc antibody (red). The bar graph represents the percent ratio (%) of ameboid-shaped Raw264.7 among total myc-mNinj1 WT and N60A mutant transfectants on the MBEC4 monolayer (right). Scale bar = 10μm. **p<0.01. (C) TEM activity of CSFE-labeled Raw264.7 cells transfected with myc-mNinj1 WT or N60A mutant across the MBEC4 monolayers (n=3). Representative images are shown (left) and transmigration index is shown as relative to the myc-mNinj1 WT transfectants, normalized to 100%. ***p<0.001.

To examine the *in vivo* relevance of N-glycosylation of Ninjurin1, a linear peptide ($lPEP_{26-65}$) bearing both homophilic binding domain and glycosylation residue was synthesized (Figure 49A), and then compared the blocking efficiency with $cPEP_{26-37}$. Scramble cyclic $peptide_{26-37}$ ($scPEP_{26-37}$), $cPEP_{26-37}$, and $lPEP_{26-65}$ were injected intraperitoneally at equivalent (60 nmol) amounts per mouse on 9, 10, and 11 days after EAE induction (Figure 49B). The administration of $lPEP_{26-65}$ highly alleviated EAE severity compared to $cPEP_{26-37}$, (Figure 49B), implying that N-glycosylation of ninjurin1 is probably involved in the leukocyte diapedesis. Taken together, N-glycosylation of Ninjurin1 is a novel regulator for leukocyte-endothelium adhesion and TEM that enhances leukocyte diapedesis.

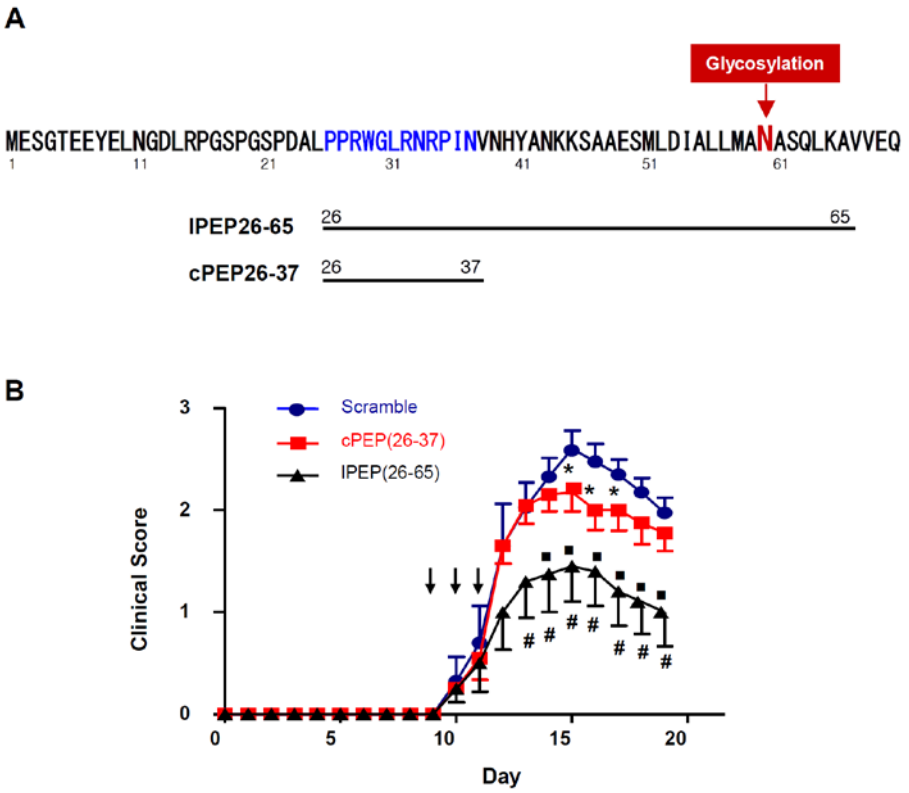

Figure 49. N-glycosylation enhances Ninjurin1-mediated EAE susceptibility. (A) Synthesis of a peptide ($lPEP_{26-65}$) bearing the residue of Asn^{60} on Ninjurin1 N-terminal ectodomain. (B) Intraperitoneal administration of 60 nmol scramble cyclic peptide ($scPEP_{26-37}$), cyclic peptide ($cPEP_{26-37}$), linear peptide ($lPEP_{26-65}$) at days 9, 10, and 11 after MOG immunization attenuated EAE clinical scores (n=10 per group). The number of infiltrated immune cells in the spinal cord was counted from three mice. *$p<0.05$ for $scPEP_{26-37}$ versus $cPEP_{26-37}$, ▪$p<0.05$ for $cPEP_{26-37}$ versus $lPEP_{26-65}$, $^{\#}p<0.05$ for $scPEP_{26-37}$ versus $lPEP_{26-65}$.

Herein, we demonstrated the cleavage of Ninjurin1 not only in a vector system *in vitro* but also in mouse tissues *in vivo*, particularly, in the liver and kidneys. Similar to the previous results in *Drosophila* (Zhang et al, 2006), MMP9 is responsible for the cleavage of mouse Ninjurin1 between Leu^{56} and Leu^{57} in its N-terminal ectodomain. Intriguingly, the liberated ectodomain of Ninjurin1 seems to have a chemotactic activity that is supported by the secondary structure similarity with well-known chemokines. In addition, we found that Ninjurin1 is glycosylated on Asn^{60} residue of N-terminal ectodomain. N60A mutant decreased the formation of membrane protrusions by impairment of their localization to plasma membrane and by loss of homophilic binding activity. Additionally, leukocyte-endothelial adhesion and TEM activity were reduced in N60A mutant transfectants. Altogether, posttranslational modifications of Ninjurin1, proteolytic cleavage and N-glycosylation probably are involved in leukocyte trafficking via chemotactic behavior and adhesive protrusion activity, respectively (Figure 50). However, their precise regulatory mechanisms should be explored further in the future

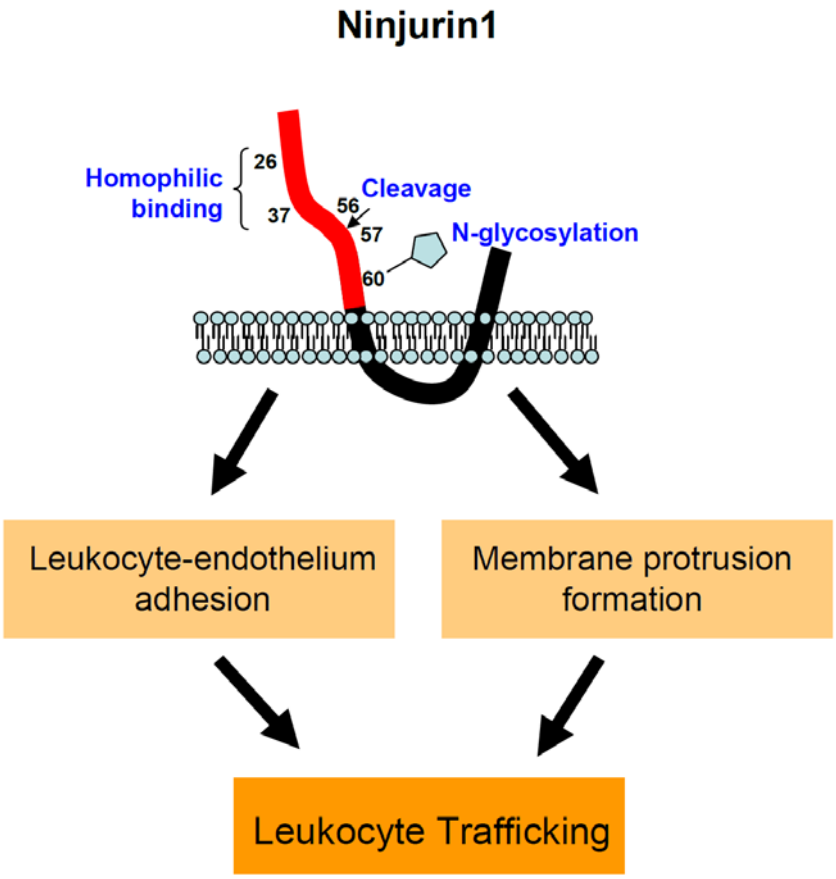

Figure 50. A proposed mechanisms of Ninjurin1-mediated leukocyte trafficking and its posttranslational modifications, proteolytic cleavage and N-glycosylation.

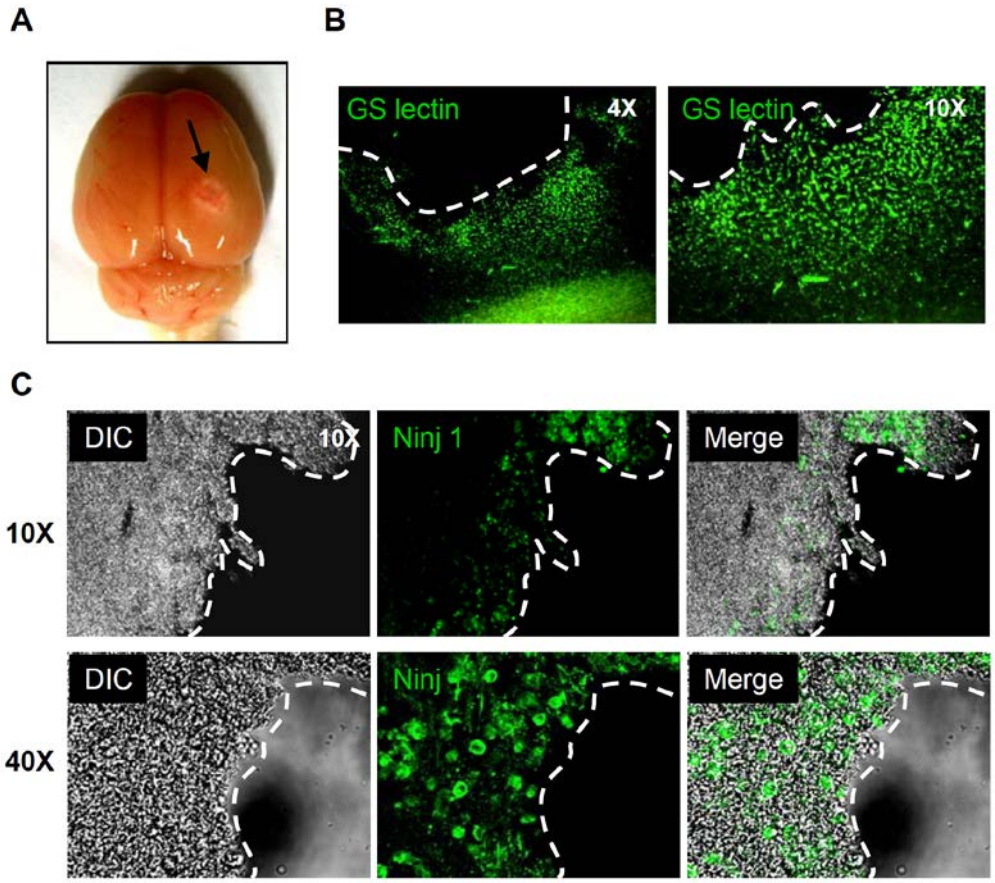

Figure 51. The expression of Ninjurin1 in lesion site of rat photothrombosis brain. (A) Photothrombosis of F344 rat (6weeks). Black arrow indicates lesion region of brain induced by photothrombosis. (B) GS lectin staining of infarct region. (C) The upregulation of Ninjurin1 (stained with anti-rat Ninjurin1 antibody from Dr. Arki) at the injured region of rat brain.

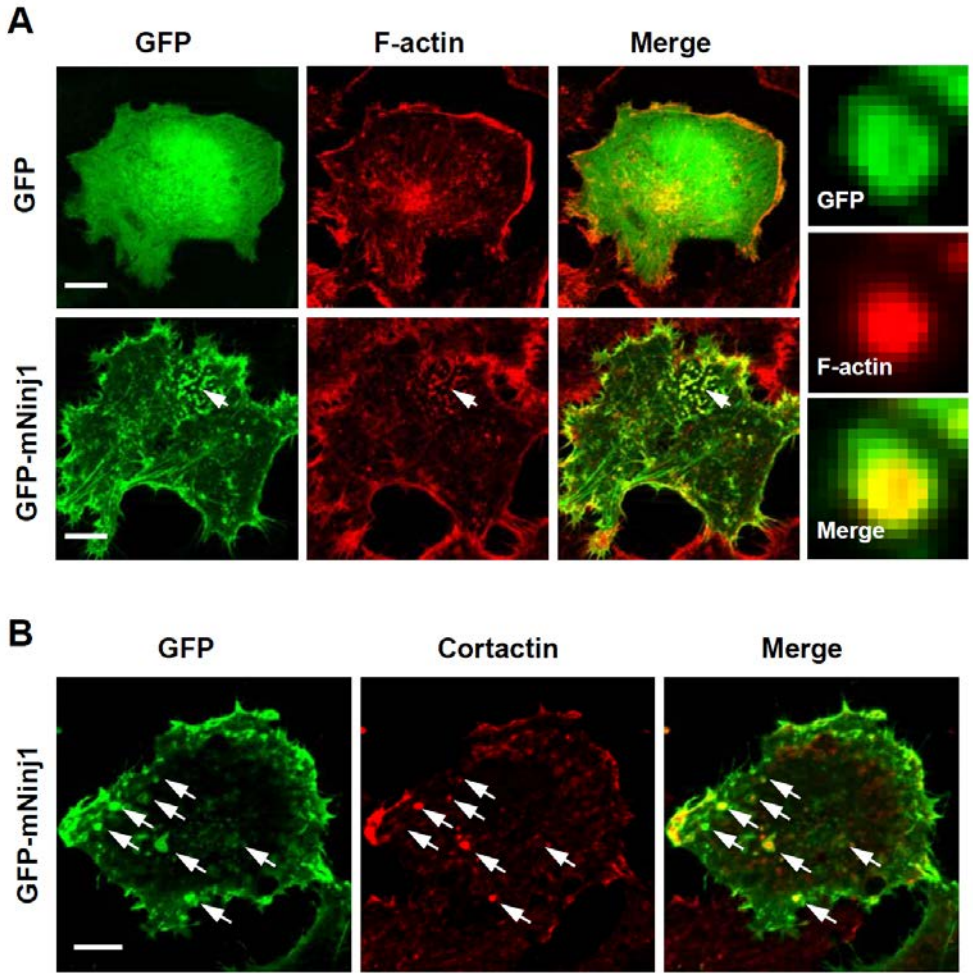

Figure 52. Localization of Ninjurin1 in the invadopodia of HeLa cells. Double staining with F-actin (A) or anti-cortactin (B), an invadopodia marker, to demonstrate the distribution of GFP-mNinj1 which is overexpressed in the HeLa cells. White arrows indicate invadopodia in where GFP-mNinj1 is localized. Scale bar = 10 μm.

DISSCUSSION

In this study, it is demonstrated that Ninjurin1 is involved in leukocyte trafficking through promigratory activity by using *in vivo* animal model and *in vitro* cell culture system. Ninjurin1 was dominantly expressed in myeloid cells (macrophages/monocytes and neutrophils) and ECs in the EAE rat brain. Both Ninjurin1 KO and antibody-neutralized mice alleviated the severity of EAE by reducing the recruitment of leukocyte into inflamed lesions, suggesting the contribution of Ninjurin1 in leukocyte trafficking *in vivo*. With *in vitro* experiments on gain or loss of Ninjurin1 activity, we proved the dual functions of Ninjurin1, adhesive and protrusive activity depending on the steps of leukocyte trafficking. Ninjurin1 contributes to the later crawling and transmigration stages via formation of membrane protrusion as well as to the initial rolling and adhesion stages via homophilic binding.

For a gene-depletion study, we used Ninjurin1 KO mice with a normal phenotype and their specifically derived BMDMs that exhibit similar hemogram and F4/80^{+} proportion to the WT counterpart, respectively. However, embryonic lethality or post-natal developmental defects are shown in some Ninjurin1 KO mice. Therefore, we can not exclude the possibility of Ninjurin1's contributions in the development of hematopoietic systems,

particularly myelopoiesis. Nevertheless, our studies of Ninjurin1 RNAi interference or stably overexpressed Raw264.7 cells coupled with primary Ninjurin1-deficient BMDMs clearly support the direct connection between Ninjurin1 and membrane protrusion, cell motility, and subsequent TEM.

The weaker inflammatory response from Ninjurin1 KO mice with EAE is thought to stem from the impairment of leukocyte-endothelium interaction. However, Ninjurin1 depletion in our KO mice is not restricted to leukocyte or endothelial cells; moreover, MOG_{35-55}-induced EAE mice show chronic inflammation which lasts for a long time (Zamvil et al, 1985). These limitations left us to debate whether the anti-inflammatory effect shown in Ninjurin1 KO mice was from specific events related to the leukocyte-endothelium interaction. To resolve this argument somewhat, we used EIU animal model which shows acute inflammation properties to induce rapid and intense leukocyte adhesion on the vessel wall of the retina within 24 hr after LPS administration (Rosenbaum et al, 1980). This short-time response in EIU mice might exclude the contributions of other effectors, except for leukocyte-endothelium interaction (Figure 15D). Therefore, our study with the EIU model supports the role of Ninjurin1 on leukocyte-endothelium interaction under inflammation.

As Ninjurin1 is known as an adhesion molecule (Araki et al, 1997), its homophilic binding properties can aptly explain how Ninjurin1 mediates the

TEM of leukocyte under inflammatory conditions. In this study, the blockage of the Ninjurin1 homophilic binding domain via $Ab_{26\text{-}37}$ or $cPEP_{26\text{-}37}$ significantly reduced not only the adhesion activity but also the TEM activity of Raw264.7 cells across the MBEC4 cell monolayer (Figure 16-19). Consistent with our results, Ifergan et al. showed that human $CD14^{+}$ monocytes pretreated with a blocking peptide specific to the homophilic binding domain of Ninjurin1 showed increased movement velocity and decreased adhesion onto human brain endothelial cells monolayer under physiological shear stress conditions. The TEM activity of the monocytes was also reduced by a treatment with this blocking peptide in a modified Boyden chamber assay (Ifergan et al, 2011). Moreover, an elegant *in vivo* observation by Odoardi et al. currently clarified the adhesive functions of Ninjurin1 during TEM. Intravenous infusion of another homophilic blocking peptide in EAE rats strongly decreased T cells crawling on the intraluminal side of CNS vessels (Odoardi et al, 2012b). These results clearly demonstrate that the homophilic binding activity of Ninjurin1 is involved not only in earlier rolling or arrest steps but also in the later crawling and transmigration of leukocyte among multistep adhesion cascades.

After their adherence to an inflamed endothelium, leukocyte produce numerous membrane protrusion to crawl on the luminal surface of the endothelium and to find potential permissive sites. Recently, two specialized

protrusive structures, podosomes or filopodia, on the ventral side of leukocyte on the EC monolayer were separately found to initiate transcellular diapedesis (Carman et al, 2007) and support millipede-like lymphocyte crawling (Shulman et al, 2009). Using highly magnified Z-stack images, we observed that myc-mNinj1 Raw264.7 cells crossing the MBEC4 cell monolayer generate intensive membrane protrusion at the front regions in which Ninjurin1 is dominantly distributed (Figure 29). This result allows us to imagine that Ninjurin1-mediated membrane protrusion formation is involved in the steps of crawling and transmigration, in addition to the well-known homophilic binding activity. Therefore, the functions of Ninjurin1, adhesive and protrusive activity, can be classified according to the stages of TEM (Figure 34). In detail, the homophilic binding activity of Ninjurin1 contributes to the rolling and adhesion of leukocyte in the initial stage when they primarily bind on the endothelium during the TEM. After their adhesions, Ninjurin1 additionally plays a role in the later crawling and transmigration steps on or across the inflamed endothelium via generating the invasive membrane protrusion (Figure 34). However, numerous adhesion molecules contribute to crawling or transmigration (Imhof & Aurrand-Lions, 2004; Ley et al, 2007; Schenkel et al, 2004) and, indeed, the adhesion activity of Ninjurin1 participates in T cell crawling (Odoardi et al, 2012b). Therefore, whether the adhesion and protrusive activities of Ninjurin1

are two independent or coordinated sequential processes requires further investigation.

According to our results, Ninjurin1 drives the formation of membrane protrusion depending on the level of Rac1 activation and on the actin-based Src or PI3K pathway, the actions of which are necessary for podosome formation (Murphy & Courtneidge, 2011; Symons, 2008), clearly demonstrating that Ninjurin1-induced membrane protrusion is a type of podosome-like structure that shares its general regulatory mechanism. In GFP-mNinj1 Raw264.7 cells, all members of the Rho family of GTPase, RhoA, Rac, and Cdc42 were activated. The contributions of the Rho family of small GTPases are diverse according to the stages of TEM (Cernuda-Morollon & Ridley, 2006). Multi-stage functions of Ninjurin1 via adhesive or protrusive activity allow several small GTPases to be involved. Furthermore, the fusogenic event of the vesicle fusing to the plasma membrane is required to supplement the source to drive the creation of membrane protrusion on moving cells (Colvin et al, 2010). As Ninjurin1 was detected in the vesicle-like structures of Raw264.7 cells or other cells in our study, Ninjurin1-mediated fusogenic activity is another potential mechanism to explain protrusion formation. This should be elucidated in the future.

Our findings by immunohistochemistry and western blotting clearly

demonstrate that Ninjurin1 is also expressed in endothelial cells and that it is upregulated under inflammatory conditions *in vitro* and in EAE spinal cord *in vivo*. In response to the protrusion formation in leukocyte, endothelial cells also generate docking structures with microvilli-like protrusion at the portions facing the penetrating leukocyte to embrace them by what is termed as a ‘migratory cup’ or ‘podoprint’ (Carman & Springer, 2004). Moreover, proteomic screening by means of mass spectrometry identified the expression of Ninjurin1 in the lipid raft membrane microdomains isolated from human brain endothelial cells (Dodelet-Devillers et al, 2009) that is localized together with the migratory cup (Carman & Springer, 2004), strongly suggesting Ninjurin1’s role in the endothelium. Therefore, whether Ninjurin1 is involved in the formation of protrusive migratory cups in endothelial cells and, if it is, how its interaction in the leukocyte-endothelium synapse regulates leukocyte diapedesis would be interesting subjects to study.

Interestingly, Ninjurin1 was partially expressed in the endothelium of injured regions of EAE rat brains. Since the infiltration of Ninjurin1^{+} leukocyte was detected in the perivascular region, we raised a possibility of heterophilic binding between Ninjurin1-expressing leukcyte and ECs via some adhesion molecules having the Ninjurin-like adhesion motif in ECs. This was coincided with the notion that some adhesion molecules mediate adhesion via

heterophilic/homophilic binding modes (Luster et al, 2005). For example, ALCAM (Activated leukocyte cell adhesion molecule), a mediator of MS, also has a role through ALCAM-CD6 heterophilic interactions or ALCAM-ALCAM homophilic interactions (Cayrol et al, 2008; van Kempen et al, 2001). Furthermore, heterophilic interactions of Ninjurin1 have already been suggested in studies of Jurket cells (Araki et al, 1997) and hyaloid vessels (Lee et al, 2009b). Therefore, the heterophilic binding partners in inflamed endothelium interacting with Ninjurin1 of leukocyte need to be identified.

Next, we investigated the contribution of posttranslational modifications of Ninjurin1, proteolytic cleavage and N-glycosylation, on the leukocyte trafficking. The fragmentations of Ninjurin1 are occurred not only in a vector system *in vitro* but also in mouse tissues *in vivo*. Similar to the previous results in *Drosophila* (Zhang et al, 2006), MMP9 is responsible for the cleavage of mouse Ninjurin1 between Leu^{56} and Leu^{57} on its N-terminal ectodomain. Intriguingly, the liberated ectodomain of Ninjurin1 have secondary structure similar to well-known chemokines and, indeed, seems to have a chemotactic activity. We also found that Ninjurin1 is glycosylated on Asn^{60} residue of N-terminal ectodomain. Mutagenesis of Asn^{60} to Ala^{60} (N60A) decreased the formation of membrane protrusions and showed impaired localization to plasma membrane and loss of its homophilic binding activity. Additionally, leukocyte-

endothelial adhesion and TEM activity were reduced in N60A mutant transfectants. Altogether, the *in vitro* and *in vivo* studies demonstrated that Ninjurin1 might regulate leukocyte trafficking via its posttranslational modifications, proteolytic cleavage or N-glycosylation.

According to our computational predictions, the liberated fragment of Ninjurin1 satisfies the structural prerequisites for a chemokine-like behavior. For the general structure of chemokines, the N-terminal disordered regions can interact with the chemokine receptors to contribute as a key signaling domain. The β-sheet and C-terminal α-helix domain can serve as binding determinants with themselves for oligomerization or with glycosaminoglycans (GAGs) for presentation on the surface of endothelial cells (Allen et al, 2007; Dyson & Wright, 2005; Mantovani et al, 2006). Interestingly, all of such structural elements are predicted in the liberated fragment of Ninjurin1. Furthermore, some chemokines act as a dimer or oligomer (Allen et al, 2007). Since Ninjurin1 binds through the homophilic binding domain, from Ala^{26} to Val^{37} (Araki et al, 1997), it is possible for the librated fragment of Ninjurin1 to dimerizes or oligomerizes with itself. Collectively, these computational studies support the structural prerequisites for the soluble fragment of Ninjurin1 to hold a chemokine-like property.

Although our study on the cleavage and N-glycosylation provides a

novel perspective to Ninjurin1-mediated leukocyte trafficking, it raises some questions to be explored in the future. First, besides the shedding between Leu^{56} and Leu^{57}, other cleavage events might exist in front of the Leu^{56} residue and thereby produce fragments corresponding with the ~16 kDa and ~19 kDa fragments of the 3xFlag-mNinj1 transfectants (Figure 36C) as well as the ~12 kDa and ~15 kDa fragments of the mouse kidneys (Figure 37A). Next, it should be determined how the N-glycosylation of Ninjurin1 can regulate their functional activity at the molecular level. Glycan-mediated conformational change of Ninjurin1 might affect its biochemical functions including homophilic binding activity and membrane targeting as well as the regulation of membrane protrusions (Marth & Grewal, 2008; Sperandio et al, 2009). Furthermore, it is interested what is the coordinated relationship between glycosylation and cleavage event? Indeed, proteolytic cleavage of some protein is finely orchestrated by their glycosylation events (Deshpande et al, 1987; Isordia-Salas et al, 2003; West et al, 2011). In this respect, structural studies of Ninjurin1 like X-ray crystallography or NMR analysis will be helpful in elucidating the structure-function relationships in the future.

Altogether, our *in vivo* animal and *in vitro* cell-based study clearly demonstrate the contributions of Ninjurin1 on leukocyte trafficking and provide the feasibility for its clinical applications coupled with consistent other group

observations (Ifergan et al, 2011; Odoardi et al, 2012a). Therefore, we strongly suggest that Ninjurin1 is a beneficial therapeutic target for modulating pathogenesis of inflamed CNS including MS.

Our preliminary study of HeLa cells, human cervical cancer cells, demonstrated that Ninjurin1 was also localized in F-actin-rich invadopodia-like structures (Figure 52), which are orthologues of podosomes in cancer cells (Murphy & Courtneidge, 2011; Symons, 2008). Furthermore, in rat photothrombosis model known as focal injury model of brain similar to stroke, the number of Ninjurin1-expressing cells in the infarct regions was increased (Figure 51). These results lead us to postulate Ninjurin1's fuctions in cancer metastasis or in other inflammatory diseases. It is notewhile that Ninjurin1 was also detected in other cell types, including neurons, oligodendrocytes, and astrocytes in the CNS (Araki & Milbrandt, 1996), an investigation of the coordinated interactions between Ninjurin1-expressing cells will be helpful when seeking to understand CNS diseases.

The growing evidence suggests that many diseases share inflammation as a convergent downstream signal after injury despite the divergent initial triggers (Lo, 2010). Therefore, our results are applicable for treatment of inflammatory CNS diseases, including atherosclerosis (Moore & Tabas, 2011), stroke (Lo, 2009), and trauma (David & Kroner, 2011) as well as other diseases

such as rheumatoid arthritis and various wounds.

REFERENCES

Allen SJ, Crown SE, Handel TM (2007) Chemokine: receptor structure, interactions, and antagonism. Annual review of immunology 25**:** 787-820

Araki T, Milbrandt J (1996) Ninjurin, a novel adhesion molecule, is induced by nerve injury and promotes axonal growth. Neuron 17**:** 353-361

Araki T, Zimonjic DB, Popescu NC, Milbrandt J (1997) Mechanism of homophilic binding mediated by ninjurin, a novel widely expressed adhesion molecule. The Journal of biological chemistry 272**:** 21373-21380

Barreiro O, Yanez-Mo M, Serrador JM, Montoya MC, Vicente-Manzanares M, Tejedor R, Furthmayr H, Sanchez-Madrid F (2002) Dynamic interaction of VCAM-1 and ICAM-1 with moesin and ezrin in a novel endothelial docking structure for adherent leukocyte. The Journal of cell biology 157**:** 1233-1245

Barrett AJ (2004) Bioinformatics of proteases in the MEROPS database. Current opinion in drug discovery & development 7**:** 334-341

Bartolazzi A, Nocks A, Aruffo A, Spring F, Stamenkovic I (1996) Glycosylation of CD44 is implicated in CD44-mediated cell adhesion to hyaluronan. J Cell Biol 132**:** 1199-1208

Cardoso CC, Martinez AN, Guimaraes PE, Mendes CT, Pacheco AG, de Oliveira RB, Teles RM, Illarramendi X, Sampaio EP, Sarno EN et al (2007) Ninjurin 1 asp110ala single nucleotide polymorphism is associated with protection in leprosy nerve damage. Journal of neuroimmunology 190**:** 131-138

Carman CV (2009) Mechanisms for transcellular diapedesis: probing and pathfinding by 'invadosome-like protrusions'. Journal of cell science 122**:** 3025-3035

Carman CV, Sage PT, Sciuto TE, de la Fuente MA, Geha RS, Ochs HD, Dvorak HF, Dvorak AM, Springer TA (2007) Transcellular diapedesis is initiated by invasive podosomes. Immunity 26**:** 784-797

Carman CV, Springer TA (2004) A transmigratory cup in leukocyte diapedesis both through individual vascular endothelial cells and between them. The Journal of cell biology 167**:** 377-388

Cayrol R, Wosik K, Berard JL, Dodelet-Devillers A, Ifergan I, Kebir H, Haqqani AS, Kreymborg K, Krug S, Moumdjian R et al (2008) Activated leukocyte cell adhesion molecule promotes leukocyte trafficking into the central nervous system. Nat Immunol 9**:** 137-145

Cernuda-Morollon E, Ridley AJ (2006) Rho GTPases and leukocyte adhesion receptor expression and function in endothelial cells. Circulation research 98**:** 757-767

Chen JS, Coustan-Smith E, Suzuki T, Neale GA, Mihara K, Pui CH, Campana D (2001) Identification of novel markers for monitoring minimal residual disease in acute lymphoblastic leukemia. Blood 97**:** 2115-2120

Cichy J, Pure E (2003) The liberation of CD44. The Journal of cell biology 161**:** 839-843

Colvin RA, Means TK, Diefenbach TJ, Moita LF, Friday RP, Sever S, Campanella GS, Abrazinski T, Manice LA, Moita C et al (2010) Synaptotagmin-mediated vesicle fusion regulates cell migration. Nature

immunology 11**:** 495-502

Constantin G, Majeed M, Giagulli C, Piccio L, Kim JY, Butcher EC, Laudanna C (2000) Chemokines trigger immediate beta2 integrin affinity and mobility changes: differential regulation and roles in lymphocyte arrest under flow. Immunity 13**:** 759-769

Crump MP, Gong JH, Loetscher P, Rajarathnam K, Amara A, Arenzana-Seisdedos F, Virelizier JL, Baggiolini M, Sykes BD, Clark-Lewis I (1997) Solution structure and basis for functional activity of stromal cell-derived factor-1; dissociation of CXCR4 activation from binding and inhibition of HIV-1. The EMBO journal 16**:** 6996-7007

David S, Kroner A (2011) Repertoire of microglial and macrophage responses after spinal cord injury. Nature reviews Neuroscience 12**:** 388-399

Deshpande KL, Fried VA, Ando M, Webster RG (1987) Glycosylation affects cleavage of an H5N2 influenza virus hemagglutinin and regulates virulence. Proceedings of the National Academy of Sciences of the United States of America 84**:** 36-40

Di Tommaso P, Moretti S, Xenarios I, Orobitg M, Montanyola A, Chang JM, Taly JF, Notredame C (2011) T-Coffee: a web server for the multiple sequence alignment of protein and RNA sequences using structural information and homology extension. Nucleic acids research 39**:** W13-17

Dodelet-Devillers A, Cayrol R, van Horssen J, Haqqani AS, de Vries HE, Engelhardt B, Greenwood J, Prat A (2009) Functions of lipid raft membrane microdomains at the blood-brain barrier. J Mol Med (Berl) 87**:** 765-774

Dyson HJ, Wright PE (2005) Intrinsically unstructured proteins and their

functions. Nature reviews Molecular cell biology 6**:** 197-208

Finger EB, Puri KD, Alon R, Lawrence MB, von Andrian UH, Springer TA (1996) Adhesion through L-selectin requires a threshold hydrodynamic shear. Nature 379**:** 266-269

Gao Y, Dickerson JB, Guo F, Zheng J, Zheng Y (2004) Rational design and characterization of a Rac GTPase-specific small molecule inhibitor. Proceedings of the National Academy of Sciences of the United States of America 101**:** 7618-7623

Garnier J, Osguthorpe DJ, Robson B (1978) Analysis of the accuracy and implications of simple methods for predicting the secondary structure of globular proteins. Journal of molecular biology 120**:** 97-120

Goverman J (2009) Autoimmune T cell responses in the central nervous system. Nature reviews Immunology 9**:** 393-407

Heasman SJ, Ridley AJ (2008) Mammalian Rho GTPases: new insights into their functions from in vivo studies. Nature reviews Molecular cell biology 9**:** 690-701

Ifergan I, Kebir H, Terouz S, Alvarez JI, Lecuyer MA, Gendron S, Bourbonniere L, Dunay IR, Bouthillier A, Moumdjian R et al (2011) Role of Ninjurin-1 in the migration of myeloid cells to central nervous system inflammatory lesions. Annals of neurology 70**:** 751-763

Imai T, Hieshima K, Haskell C, Baba M, Nagira M, Nishimura M, Kakizaki M, Takagi S, Nomiyama H, Schall TJ et al (1997) Identification and molecular characterization of fractalkine receptor CX3CR1, which mediates both leukocyte migration and adhesion. Cell 91**:** 521-530

Imhof BA, Aurrand-Lions M (2004) Adhesion mechanisms regulating the migration of monocytes. Nature reviews Immunology 4**:** 432-444

Isordia-Salas I, Pixley RA, Parekh H, Kunapuli SP, Li F, Stadnicki A, Lin Y, Sartor RB, Colman RW (2003) The mutation Ser511Asn leads to N-glycosylation and increases the cleavage of high molecular weight kininogen in rats genetically susceptible to inflammation. Blood 102**:** 2835-2842

Kim JW, Moon AR, Kim JH, Yoon SY, Oh GT, Choe YK, Choe IS (2001a) Up-Regulation of ninjurin expression in human hepatocellular carcinoma associated with cirrhosis and chronic viral hepatitis. Molecules and cells 11**:** 151-157

Kim S, Jao S, Laurence JS, LiWang PJ (2001b) Structural comparison of monomeric variants of the chemokine MIP-1beta having differing ability to bind the receptor CCR5. Biochemistry 40**:** 10782-10791

Kleinschmidt-DeMasters BK, Tyler KL (2005) Progressive multifocal leukoencephalopathy complicating treatment with natalizumab and interferon beta-1a for multiple sclerosis. The New England journal of medicine 353**:** 369-374

Lee HJ, Ahn BJ, Shin MW, Jeong JW, Kim JH, Kim KW (2009a) Ninjurin1 mediates macrophage-induced programmed cell death during early ocular development. Cell death and differentiation 16**:** 1395-1407

Lee HJ, Ahn BJ, Shin MW, Jeong JW, Kim JH, Kim KW (2009b) Ninjurin1 mediates macrophage-induced programmed cells death during early ocular development. Cell Death Differ

Ley K, Laudanna C, Cybulsky MI, Nourshargh S (2007) Getting to the site of

inflammation: the leukocyte adhesion cascade updated. Nature reviews Immunology 7**:** 678-689

Linding R, Jensen LJ, Diella F, Bork P, Gibson TJ, Russell RB (2003) Protein disorder prediction: implications for structural proteomics. Structure 11**:** 1453-1459

Lo EH (2009) T time in the brain. Nature medicine 15**:** 844-846

Lo EH (2010) Degeneration and repair in central nervous system disease. Nature medicine 16**:** 1205-1209

Lopez-Diego RS, Weiner HL (2008) Novel therapeutic strategies for multiple sclerosis--a multifaceted adversary. Nature reviews Drug discovery 7**:** 909-925

Luster AD, Alon R, von Andrian UH (2005) Immune cell migration in inflammation: present and future therapeutic targets. Nature immunology 6**:** 1182-1190

Mantovani A, Bonecchi R, Locati M (2006) Tuning inflammation and immunity by chemokine sequestration: decoys and more. Nature reviews Immunology 6**:** 907-918

Marth JD, Grewal PK (2008) Mammalian glycosylation in immunity. Nat Rev Immunol 8**:** 874-887

McEver RP, Zhu C (2010) Rolling cell adhesion. Annu Rev Cell Dev Biol 26**:** 363-396

McFarland HF, Martin R (2007) Multiple sclerosis: a complicated picture of autoimmunity. Nat Immunol 8**:** 913-919

Mitoma J, Bao X, Petryanik B, Schaerli P, Gauguet JM, Yu SY, Kawashima H, Saito H, Ohtsubo K, Marth JD et al (2007) Critical functions of N-glycans in L-selectin-mediated lymphocyte homing and recruitment. Nat Immunol 8**:** 409-418

Mizoue LS, Bazan JF, Johnson EC, Handel TM (1999) Solution structure and dynamics of the CX3C chemokine domain of fractalkine and its interaction with an N-terminal fragment of CX3CR1. Biochemistry 38**:** 1402-1414

Moore KJ, Tabas I (2011) Macrophages in the pathogenesis of atherosclerosis. Cell 145**:** 341-355

Murphy DA, Courtneidge SA (2011) The 'ins' and 'outs' of podosomes and invadopodia: characteristics, formation and function. Nature reviews Molecular cell biology 12**:** 413-426

Nourshargh S, Hordijk PL, Sixt M (2010) Breaching multiple barriers: leukocyte motility through venular walls and the interstitium. Nature reviews Molecular cell biology 11**:** 366-378

O'Brien CD, Lim P, Sun J, Albelda SM (2003) PECAM-1-dependent neutrophil transmigration is independent of monolayer PECAM-1 signaling or localization. Blood 101**:** 2816-2825

Odoardi F, Sie C, Streyl K, Ulaganathan VK, Schlager C, Lodygin D, Heckelsmiller K, Nietfeld W, Ellwart J, Klinkert WE et al (2012a) T cells become licensed in the lung to enter the central nervous system. Nature 488**:** 675-679

Odoardi F, Sie C, Streyl K, Ulaganathan VK, Schlager C, Lodygin D,

Heckelsmiller K, Nietfeld W, Ellwart J, Klinkert WE et al (2012b) T cells become licensed in the lung to enter the central nervous system. Nature

Ostermann G, Weber KS, Zernecke A, Schroder A, Weber C (2002) JAM-1 is a ligand of the beta(2) integrin LFA-1 involved in transendothelial migration of leukocyte. Nature immunology 3**:** 151-158

Ousman SS, Kubes P (2012) Immune surveillance in the central nervous system. Nature neuroscience 15**:** 1096-1101

Parsons JT, Horwitz AR, Schwartz MA (2010) Cell adhesion: integrating cytoskeletal dynamics and cellular tension. Nature reviews Molecular cell biology 11**:** 633-643

Quast T, Eppler F, Semmling V, Schild C, Homsi Y, Levy S, Lang T, Kurts C, Kolanus W (2011) CD81 is essential for the formation of membrane protrusions and regulates Rac1-activation in adhesion-dependent immune cell migration. Blood 118**:** 1818-1827

Ransohoff RM, Kivisakk P, Kidd G (2003) Three or more routes for leukocyte migration into the central nervous system. Nat Rev Immunol 3**:** 569-581

Ridley AJ, Schwartz MA, Burridge K, Firtel RA, Ginsberg MH, Borisy G, Parsons JT, Horwitz AR (2003) Cell migration: integrating signals from front to back. Science 302**:** 1704-1709

Rosenbaum JT, McDevitt HO, Guss RB, Egbert PR (1980) Endotoxin-induced uveitis in rats as a model for human disease. Nature 286**:** 611-613

Schenkel AR, Mamdouh Z, Chen X, Liebman RM, Muller WA (2002) CD99 plays a major role in the migration of monocytes through endothelial junctions.

Nature immunology 3**:** 143-150

Schenkel AR, Mamdouh Z, Muller WA (2004) Locomotion of monocytes on endothelium is a critical step during extravasation. Nature immunology 5**:** 393-400

Shulman Z, Shinder V, Klein E, Grabovsky V, Yeger O, Geron E, Montresor A, Bolomini-Vittori M, Feigelson SW, Kirchhausen T et al (2009) Lymphocyte crawling and transendothelial migration require chemokine triggering of high-affinity LFA-1 integrin. Immunity 30**:** 384-396

Smalley DM, Ley K (2005) L-selectin: mechanisms and physiological significance of ectodomain cleavage. Journal of cellular and molecular medicine 9**:** 255-266

Smith CW, Marlin SD, Rothlein R, Toman C, Anderson DC (1989) Cooperative interactions of LFA-1 and Mac-1 with intercellular adhesion molecule-1 in facilitating adherence and transendothelial migration of human neutrophils in vitro. The Journal of clinical investigation 83**:** 2008-2017

Sperandio M, Gleissner CA, Ley K (2009) Glycosylation in immune cell trafficking. Immunol Rev 230**:** 97-113

Steinman L (2005) Blocking adhesion molecules as therapy for multiple sclerosis: natalizumab. Nature reviews Drug discovery 4**:** 510-518

Steinman L (2008) Nuanced roles of cytokines in three major human brain disorders. The Journal of clinical investigation 118**:** 3557-3563

Symons M (2008) Cell biology: watching the first steps of podosome formation. Current biology : CB 18**:** R925-927

Tajouri L, Fernandez F, Griffiths LR (2007) Gene expression studies in multiple sclerosis. Curr Genomics 8**:** 181-189

van Kempen LC, Nelissen JM, Degen WG, Torensma R, Weidle UH, Bloemers HP, Figdor CG, Swart GW (2001) Molecular basis for the homophilic activated leukocyte cell adhesion molecule (ALCAM)-ALCAM interaction. J Biol Chem 276**:** 25783-25790

Verspurten J, Gevaert K, Declercq W, Vandenabeele P (2009) SitePredicting the cleavage of proteinase substrates. Trends in biochemical sciences 34**:** 319-323

Weber C, Springer TA (1998) Interaction of very late antigen-4 with VCAM-1 supports transendothelial chemotaxis of monocytes by facilitating lateral migration. J Immunol 161**:** 6825-6834

West MB, Wickham S, Quinalty LM, Pavlovicz RE, Li C, Hanigan MH (2011) Autocatalytic cleavage of human gamma-glutamyl transpeptidase is highly dependent on N-glycosylation at asparagine 95. The Journal of biological chemistry 286**:** 28876-28888

Zamvil S, Nelson P, Trotter J, Mitchell D, Knobler R, Fritz R, Steinman L (1985) T-cell clones specific for myelin basic protein induce chronic relapsing paralysis and demyelination. Nature 317**:** 355-358

Zhang S, Dailey GM, Kwan E, Glasheen BM, Sroga GE, Page-McCaw A (2006) An MMP liberates the Ninjurin A ectodomain to signal a loss of cell adhesion. Genes & development 20**:** 1899-1910

국문 초록

닌주린1 (Ninjurin1)은 세포의 상호작용에 중요한 결합 단백질이다. 하지만 염증성 중추신경계 질환 발병 과정에 대한 닌주린의 병태생리학적 기능과 그 자세한 조절 기전에 대한 연구는 매우 미미한 실정이다. 따라서 본 연구를 통해 닌주린1 단백질 및 그 전사 후 변형과정, 즉 단편화와 당화 과정에 의한 염증 조절 기전에 대해 연구하였다. 다발성경화증 (Multiple sclerosis)의 동물 모델인 Experimental autoimmune encephalomyelitis (EAE) 랫트 뇌에서, 닌주린은 대식세포, 단핵구, 또는 호중구와 같은 혈액유래 면역세포 뿐만아니라 혈관내피세포에서 주로 관찰이된다. Ninjurin1 유전자를 제거하였거나 항체를 주입하여 그 활성을 저해한 후 EAE를 유발하였을 경우, 손상 조직내로 침투하는 면역세포의 수가 감소하였으며, 결국 EAE에 대한 감수성이 줄어들었다. 이러한 결과를 통해 닌주린1이 면역 세포을 이동을 조절하여 염증 반응을 매개함을 확인하였으며, 세포생물학적 방법을 통해 그 조절 기전을 시기별로 자세히 연구하였다. 면역세포 이동 초기 과정 중 닌주린1은 혈관내피세포와 면역세포의 부착을 유도하고, 부착된 면역세포의 세포막 미세 돌기를 형성시켜 혈관 관통을 매개하는 것을 규명하였다. 다음으로 닌주린1의 단편화 (cleavage)와 당화 (glycosylation)가 면역세포의 이동에 미치는 영향을

연구하였다. 닌주린1 벡터를 과발현시킨 세포와 생쥐의 간 또는 신장 조직에서 단편화된 닌주린1이 관찰되며, 질량 분석 방법을 통해 MMP9이 닌주린1의 Leu^{56} 과 Leu^{57} 아미노산 잔기 사이를 자르는 것으로 확인되었다. 잘려진 닌주린1 단편은 기존 알려진 케모카인들과 유사한 구조를 가지며, 실제로 면역세포의 이동을 조절한다. 또한 닌주린1은 Asn^{60} 아미노산 잔기에 당화가 일어나며 이를 통해 면역 세포와 혈관내피세포의 결합이 유도되며 세포막의 미세 돌기의 형성이 증가하여, 결국 손상조직 내로 면역세포의 이동을 매개한다. 따라서 본 연구는 닌주린1이 면역세포의 손상조직 내로의 이동을 증진한다는 것과 그 자세한 작용 기전을 규명하여 중추신경계 염증 질환 치료제 발굴을 위한 주요한 후보 단백질이 될 수 있음을 제안하였다.

Keywords : **Experimental autoimmune encephalomyelitis (EAE) / Leukocyte trafficking / Ninjurin1 / Membrane protrusion formation / Posttranslational modifications**

Student Number : **2007-30469**